Chapter 7

Simulation and Empirical Analysis

This chapter contains an empirical study of the performance of the five multi-objective ant colony optimisation algorithms presented in this thesis, and an analysis of the influence of various algorithmic features on performance. The five algorithms are compared to each other and also to a state-of-the-art, multi-objective evolutionary algorithm, the NSGA-II, which was adapted in this thesis (refer to Section 6.7) for the multi-objective, power-aware routing problem. This chapter refers to the adapted NSGA-II as the NSGA-II-MPA. Several numeric simulations are presented and discussed with the goal of validating the algorithms which have been implemented.

The remainder of this chapter is organised as follows: Section 7.1 describes the experimental procedure which was followed in order to test the five algorithms. Section 7.2 presents the empirical analysis of control parameters. Section 7.3 discusses parameter settings for NSGA-II-MPA. Section 7.4 compares the implemented algorithms, while Section 7.5 concludes the chapter.

7.1 Experimental Procedure

Different network configurations (scenarios) are tested for each algorithm and the Pareto fronts are obtained for each of the algorithms. The following subsections describe the different network scenarios, the simulation environment, and the performance measures used to compare the different Pareto fronts.

7.1.1 Network Scenarios

A number of different network scenarios were considered, where the characteristics of each scenario differ in the number of nodes, N_G, pause time, T_{sm}, and the global range of the mobility model, R_g. Table 7.1 illustrates the different values for N_G, T_{sm} and R_g, from which a total of 54 scenarios have been generated as listed in Table 7.2.

Table 7.1: Different simulation parameters used to generate network scenarios

	N_G	T_{sm}	R_g
value 1	30	1 sec	300 m
value 2	100	2 sec	500 m
value 3	300	3 sec	800 m
value 4		4 sec	
value 5		5 sec	
value 6		6 sec	

Table 7.2: List of scenarios for comparing the algorithms

Scenario Name	Configuration	Scenario Name	Configuration
scenario 1a	$N_G = 30$, $R_g = 300$ m, $T_{sm} = 1$ sec	scenario 6a	$N_G = 100$, $R_g = 800$, $T_{sm} = 1$ sec
scenario 1b	$N_G = 30$, $R_g = 300$ m, $T_{sm} = 2$ sec	scenario 6b	$N_G = 100$, $R_g = 800$, $T_{sm} = 2$ sec
scenario 1c	$N_G = 30$, $R_g = 300$ m, $T_{sm} = 3$ sec	scenario 6c	$N_G = 100$, $R_g = 800$, $T_{sm} = 3$ sec
scenario 1d	$N_G = 30$, $R_g = 300$ m, $T_{sm} = 4$ sec	scenario 6d	$N_G = 100$, $R_g = 800$, $T_{sm} = 4$ sec
scenario 1e	$N_G = 30$, $R_g = 300$ m, $T_{sm} = 5$ sec	scenario 6e	$N_G = 100$, $R_g = 800$, $T_{sm} = 5$ sec
scenario 1f	$N_G = 30$, $R_g = 300$ m, $T_{sm} = 6$ sec	scenario 6f	$N_G = 100$, $R_g = 800$, $T_{sm} = 6$ sec
scenario 2a	$N_G = 30$, $R_g = 500$ m, $T_{sm} = 1$ sec	scenario 7a	$N_G = 300$, $R_g = 300$, $T_{sm} = 1$ sec
scenario 2b	$N_G = 30$, $R_g = 500$ m, $T_{sm} = 2$ sec	scenario 7b	$N_G = 300$, $R_g = 300$, $T_{sm} = 2$ sec
scenario 2c	$N_G = 30$, $R_g = 500$ m, $T_{sm} = 3$ sec	scenario 7c	$N_G = 300$, $R_g = 300$, $T_{sm} = 3$ sec
scenario 2d	$N_G = 30$, $R_g = 500$ m, $T_{sm} = 4$ sec	scenario 7d	$N_G = 300$, $R_g = 300$, $T_{sm} = 4$ sec
scenario 2e	$N_G = 30$, $R_g = 500$ m, $T_{sm} = 5$ sec	scenario 7e	$N_G = 300$, $R_g = 300$, $T_{sm} = 5$ sec
scenario 2f	$N_G = 30$, $R_g = 500$ m, $T_{sm} = 6$ sec	scenario 7f	$N_G = 300$, $R_g = 300$, $T_{sm} = 6$ sec
scenario 3a	$N_G = 30$, $R_g = 800$ m, $T_{sm} = 1$ sec	scenario 8a	$N_G = 300$, $R_g = 500$, $T_{sm} = 1$ sec
scenario 3b	$N_G = 30$, $R_g = 800$ m, $T_{sm} = 2$ sec	scenario 8b	$N_G = 300$, $R_g = 500$, $T_{sm} = 2$ sec
scenario 3c	$N_G = 30$, $R_g = 800$ m, $T_{sm} = 3$ sec	scenario 8c	$N_G = 300$, $R_g = 500$, $T_{sm} = 3$ sec
scenario 3d	$N_G = 30$, $R_g = 800$ m, $T_{sm} = 4$ sec	scenario 8d	$N_G = 300$, $R_g = 500$, $T_{sm} = 4$ sec
scenario 3e	$N_G = 30$, $R_g = 800$ m, $T_{sm} = 5$ sec	scenario 8e	$N_G = 300$, $R_g = 500$, $T_{sm} = 5$ sec
scenario 3f	$N_G = 30$, $R_g = 800$ m, $T_{sm} = 6$ sec	scenario 8f	$N_G = 300$, $R_g = 500$, $T_{sm} = 6$ sec
scenario 4a	$N_G = 100$, $R_g = 300$ m, $T_{sm} = 1$ sec	scenario 9a	$N_G = 300$, $R_g = 800$, $T_{sm} = 1$ sec
scenario 4b	$N_G = 100$, $R_g = 300$ m, $T_{sm} = 2$ sec	scenario 9b	$N_G = 300$, $R_g = 800$, $T_{sm} = 2$ sec
scenario 4c	$N_G = 100$, $R_g = 300$ m, $T_{sm} = 3$ sec	scenario 9c	$N_G = 300$, $R_g = 800$, $T_{sm} = 3$ sec
scenario 4d	$N_G = 100$, $R_g = 300$ m, $T_{sm} = 4$ sec	scenario 9d	$N_G = 300$, $R_g = 800$, $T_{sm} = 4$ sec
scenario 4e	$N_G = 100$, $R_g = 300$ m, $T_{sm} = 5$ sec	scenario 9e	$N_G = 300$, $R_g = 800$, $T_{sm} = 5$ sec
scenario 4f	$N_G = 100$, $R_g = 300$ m, $T_{sm} = 6$ sec	scenario 9f	$N_G = 300$, $R_g = 800$, $T_{sm} = 6$ sec
scenario 5a	$N_G = 100$, $R_g = 500$ m, $T_{sm} = 1$ sec	scenario 5d	$N_G = 100$, $R_g = 500$, $T_{sm} = 4$ sec
scenario 5b	$N_G = 100$, $R_g = 500$ m, $T_{sm} = 2$ sec	scenario 5e	$N_G = 100$, $R_g = 500$, $T_{sm} = 5$ sec
scenario 5c	$N_G = 100$, $R_g = 500$ m, $T_{sm} = 3$ sec	scenario 5f	$N_G = 100$, $R_g = 500$, $T_{sm} = 6$ sec

Values of N_G from 30 to 300 represent a small to large network which enables a scalability analysis of the algorithms. Values of T_{sm} from 1 sec to 6 sec determine how often the environment changes and represent high to low change frequencies. Values of R_g from 300 meters to 800 meters determine the amount of displacement of the current location of the optimum and represent low to high change severities.

The performance of each algorithm was tested under all 54 scenarios. For each of the scenarios 30 independent simulations have been executed and results are reported as averages over these simulations. Both the comparative results and the empirical results of the impact of the parameters in terms of the performance of each algorithm are reported in Section 7.4.

In order to test the quality of the solutions, a high initial energy of 400 energy units was used for each node.

7.1.2 Simulation Environment

The simulation environment generates a network topology consisting of a number of nodes. Initial placement of nodes was made randomly within the simulation environment, which is a circular area with a diameter of 300m, 500m, or 800m. Nodes move within this area according to the RPGM model (refer to Section 6.5). The centre of the circular area is also mobile, and its motion follows the RWP model (refer to Section 2.4).

All the nodes have a resting period of T_{sm} seconds. T_{sm} determines the change frequency. The performance of each algorithm was checked for $T_{sm} = 1$, $T_{sm} = 2$, $T_{sm} = 3$, $T_{sm} = 4$, $T_{sm} = 5$, and $T_{sm} = 6$ seconds. After the resting period all the nodes moved in accordance with the RWP mobility model. This process repeated itself throughout the simulation, thus bringing about continuous changes in the topology of the underlying network. The number of changes for each simulation is $S_{T_{tot}} \ / \ T_{sm}$, where $S_{T_{tot}}$ is the total simulation time.

Before the topology changes, a number of iterations of the multi-objective optimisation algorithm had taken place and, at each iteration, each ant had calculated a solution, T, evaluated the solution and, if non-dominated, inserted the solution into the Pareto set, P_s. Thereafter, the solutions in P_s which were dominated by T were deleted from P_s. Before the mobility model was applied again, a packet was sent from the source node to the destination node using a random route, T_s, from the Pareto set list and the ApplyMobilityChanges procedure was executed (refer to Algorithm 12).

7.1.3 Performance Measures

The five proposed algorithms and the NSGA-II-MPA algorithm each produced an estimated Pareto front, $\mathcal{PF}$ ($P_{EEMACOMP}$, $P_{EEMACOMH}$, $P_{EEMMASMP}$, $P_{EEMMASMH}$, $P_{EEMACOMC}$, and $P_{NSGA-II-MPA}$). Each $\mathcal{PF}$ was evaluated using three quantitative metrics, discussed in Section 4.7.2:

- **The ND metric**: The number of non-dominated solutions is computed, noted as $\bar{n}_{alg}$ in the result tables.
- **The spread metric**: The diversity of solutions in each Pareto front is computed using the spread metric, noted $\bar{\varrho}$ in the result tables.
- **The hypervolume measure**: The size of the dominated space is computed using the hypervolume measure, noted $\bar{\xi}$ in the result tables.

Simulation of the five algorithms presented the following practical problems. Firstly, due to mobility, different independent runs of the algorithms produced results that differed significantly. To overcome this high variability, performance measures were calculated as averages over 30 independent runs for each of the algorithms. For each scenario, each algorithm is therefore executed thirty times, with each execution starting from different initial conditions. For each run of an algorithm a Pareto-optimal set of solutions, $\mathcal{PF}$, was computed, one for each network topology. The number of times that one algorithm has a better n_{alg}, ϱ, and ξ average than all the other algorithms before each change, is counted and referred to as n^w_{alg}, ϱ^w, and ξ^w respectively. The total average for all iterations before a change to the environment occurs, further averaged over 30 simulations is calculated for each metric and referred to as $\bar{n}_{alg}$, $\bar{\varrho}$, and $\bar{\xi}$. The standard deviation, and a 95% confidence interval, CI, is provided next to each value.

Secondly, when simulating the algorithms the network topology changes after the mobility model is applied. For fair comparison among the different algorithms, it is important that the algorithms are tested on the same sequence of topology changes. Therefore, based on the mobility model used, a sequence of node changes is determined for each of the 30 runs. All algorithms are then evaluated on these change sequences.

The objective of the experiments is to analyse and compare the performance of the six algorithms according to the metrics listed above.

7.1.4 Sending a Packet

A network initialised with random or uniform pheromone tables will not contain any useful information about good routes. After a short time has elapsed, the largest probabilities in the pheromone tables of each node will define relatively optimal routes. For example, after 500 time steps or 5 seconds, the algorithm will converge on typically good routes in relation to the five objectives, and a packet may be sent from the source to the destination. Therefore, each algorithm runs for the allowed pause time, T_{sm}, before sending a packet.

7.2 Empirical Analysis of the Ant-Based Algorithms Control Parameters

The space of possible control parameter settings for the five ant algorithms is large, including parameters r_0, ρ_l, ρ_g, α, β_ν, β_ξ, β_π, β_ϱ, β_ς, λ_E, λ_ν, λ_ξ, λ_π, λ_ϱ, λ_ς, and P_{as}.

The objective of this section is to perform a sensitivity analysis of these parameters in order to derive suggestions of how the parameters should be initialized for best performance. For each parameter, a number of values were tested while all the other parameters were held constant. The default value of the parameters is: $\beta_\nu = 3.0$, $\beta_\xi = 3.0$, $\beta_\pi = 3.0$, $\beta_\varrho = 3.0$, $\beta_\varsigma = 3.0$, $S_{T_{tot}}$=120sec, $r_0 = 0.5$, $\rho_l = 0.5$, $\rho_g = 0.5$, $\alpha = 1.0$, $\lambda_E = 6$, $\lambda_\nu = 0.2$, $\lambda_\xi = 0.2$, $\lambda_\pi = 0.2$, $\lambda_\varrho = 0.2$, $\lambda_\varsigma = 0.2$, $P_{as} = 100$. These values were obtained using a trial-and-error process for finding preliminary best parameter settings. For each parameter value the Pareto front, $\mathcal{PF}$, was obtained using the process described in Section 7.1.3. The performance metrics listed in Section 7.1.3 were computed for each of these Pareto fronts and used to determine the best values for each control parameter. Due to space limitations, the influence of parameter values is only presented for a 30 nodes network.

The results of the empirical analysis of the ant-based algorithms control parameters are illustrated in Tables D.1-D.18 in Appendix D. Graphs of the performance metrics as a function of the different control parameters, T_{sm} and R_g, based on Tables D.1-D.18, are presented in Appendix E using the FluxViz software [1]. Relations between the different performance metrics and the parameter values with reference to different change frequencies are illustrated in two dimension figures. Each value is the average of

the three change severities. Relations between the different performance metrics and the parameter values with reference to different change severities are also illustrated in two dimension figures, where each value is the average of the six change frequencies.

The following subsections perform an empirical analysis of the sensitivity of the algorithms to the above parameters.

7.2.1 Heuristics vs Pheromone Parameters

Parameters β_ν, β_ξ, β_π, β_ϱ, and β_ς set the relative importance of heuristic versus pheromone information. In the transition rules for the developed algorithms (refer to equations (6.20), (6.31), (6.42), (6.48), and (6.54)), parameters β_ψ, where ψ represents either ν, ξ, π, ϱ, or ς depending on the sub-objective, are the exponents of heuristics, $\eta_{\psi_{ij}}$, which are defined as in equations (6.13)-(6.17). Heuristic values ranged between 0 (high link cost) and 1 (small link cost).

The larger the value of β_ψ, the smaller the emphasis on heuristic information, and learned desirability discovered by pheromone trails is favored. In this case, ants may choose non-optimal paths too quickly. On the other hand, a small value for β_ψ gives higher priority to heuristic information over pheromone and the algorithm becomes more greedy and leads to increased exploration.

In order to find the best value for all β_ψ parameters, values for these parameters were randomly selected from the range $[1, 7]$. The values $(\beta_\nu, \beta_\xi, \beta_\pi, \beta_\varrho, \beta_\varsigma) \in \{(1,1,1,1,1), (3,3,3,3,3), (3.5,4,4.5,4,5), (4.5,5,3.5,4,4), (5,5,5,5,5), (7,7,7,7,7)\}$ were selected and tested. For this study the rest of the parameter values were fixed as in Section 7.2.

Tables D.1-D.3 in appendix D summarise the empirical results for β_ψ using the $\bar{n}_{alg}$, $\bar{\varrho}$ and $\bar{\xi}$ metrics. These results are visualised using the FluxViz software in Figures E.1-E.15 in appendix E. These figures highlights the best results with blue indicating the best values for the $\bar{n}_{alg}$, $\bar{\varrho}$ and $\bar{\xi}$ metrics. Relations between the different performance metrics and the β_ψ values with reference to different change frequencies are illustrated in Figures 7.1-7.3. Relations between the different performance metrics and the β_ψ values with reference to different change severities are illustrated in Figures 7.4-7.6. The β_ψ axis represents the combination of the parameters $(\beta_\nu, \beta_\xi, \beta_\pi, \beta_\varrho, \beta_\varsigma)$ used in the experiments. Axis values of β_ψ=1, 2, 3, 4, 5, 6 respectively refer to parameter combinations $(1,1,1,1,1)$, $(3,3,3,3,3)$, $(3.5,4,4.5,4,5)$, $(4.5,5,3.5,4,4)$, $(5,5,5,5,5)$, and $(7,7,7,7,7)$.

The larger the number of non-dominated solutions, $\bar{n}_{alg}$, the better the effectiveness

of the MOO algorithm in generating desired solutions. A value of zero for $\bar{\varrho}$ indicates that all members of the Pareto front are equidistantly spaced. A higher value of $\bar{\xi}$ indicates that the obtained Pareto front is closer to the true Pareto front.

For each β_ψ parameter combination, referred to as an experiment, six different change frequencies (with $T_{sm} \in \{1, 2, 3, 4, 5, 6\}$) and three different change severities (with $R_g \in \{300, 500, 800\}$) were used. The same applies with the rest of the sections for the empirical analysis of the ant-based algorithms control parameters.

The rest of this section discusses the results obtained from the experiments with regards to the influence of β_ψ on the performance metrics.

1. **Influence of β_ψ on the number of non-dominated solutions, $\bar{n}_{alg}$.**

   Irrespective of the change frequency and change severity, for $(\beta_\nu, \beta_\xi, \beta_\pi, \beta_\varrho, \beta_\varsigma) \in \{(1, 1, 1, 1, 1), (3, 3, 3, 3, 3)\}$ all the algorithms produced a very low number of non-dominated solutions (refer to Figures E.1, E.4, E.7, E.10, E.13, 7.1, 7.4). For values of $(\beta_\nu, \beta_\xi, \beta_\pi, \beta_\varrho, \beta_\varsigma) = (3.5, 4, 4.5, 4, 5)$, $(\beta_\nu, \beta_\xi, \beta_\pi, \beta_\varrho, \beta_\varsigma) = (4.5, 5, 3.5, 4, 4)$, and $(\beta_\nu, \beta_\xi, \beta_\pi, \beta_\varrho, \beta_\varsigma) = (5, 5, 5, 5, 5)$ the best values of $\bar{n}_{alg}$ were obtained. Therefore, β_ψ should be large enough in order to have a strong focus on pheromone information.

   For all the experiments, $\bar{n}_{alg}$ decreased with increase in change frequency, T_{sm} (refer to Figure 7.1), which is expected. As frequency of change increases, the time available for adaptation becomes shorter and it becomes more difficult to find optimum solutions.

   Also, $\bar{n}_{alg}$ decreased with increase in change severity, R_g (refer to Figure 7.4), which is also expected. With high change severity there is a large displacement of the current location of the optimum and it is more difficult to adapt and to find optimal solutions.

2. **Influence of β_ψ on the spread metric, $\bar{\varrho}$.**

   Irrespective of the change frequency and change severity, for $(\beta_\nu, \beta_\xi, \beta_\pi, \beta_\varrho, \beta_\varsigma) \in \{(1, 1, 1, 1, 1), (3, 3, 3, 3, 3)\}$ all the algorithms displayed a higher value for $\bar{\varrho}$ which means less uniformly distributed solutions (refer to Figures E.2, E.5, E.8, E.11, E.14). For all values of $(\beta_\nu, \beta_\xi, \beta_\pi, \beta_\varrho, \beta_\varsigma) \in \{(3.5, 4, 4.5, 4, 5), (4.5, 5, 3.5, 4, 4), (5, 5, 5, 5, 5), (7, 7, 7, 7, 7)\}$ lower values of $\bar{\varrho}$ (more uniformly dis-

tributed solutions) were obtained. Higher values of β_ψ, and therefore a strong focus on pheromone information, produced a better solution spread.

A decrease in change frequency, T_{sm}, leads to more uniformly distributed solutions (refer to Figure 7.2), which is expected. As the change frequency decreases, the time left for adaptation gets larger and there are more iterations available to track the optima. The archive is more likely to become full several times, and each time the crowding distance is used in selecting which solution in the archive will be replaced with a new solution. This promotes diversity among the stored solutions in the archive since those solutions which are in the most crowded areas are most likely to be replaced by a new solution. At the end the archive will contain more non-dominated solutions which are in the least crowded area in the objective space, therefore, maintaining a good spread of non-dominated solutions.

The value of $\bar{\varrho}$ increased with increase in change severity, R_g (refer to Figure 7.5), which is also expected. When R_g increases, more iterations are needed to track the optima after the change occurred and therefore the distribution of solutions decreases correspondingly.

3. **Influence of β_ψ on the hypervolume metric, $\bar{\xi}$.**

   For $(\beta_\nu,\ \beta_\xi,\ \beta_\pi,\ \beta_\varrho,\ \beta_\varsigma) \in \{(1,1,1,1,1),(3,3,3,3,3)\}$ all the algorithms displayed a lower value of the $\bar{\xi}$ metric (refer to Figures E.3, E.6, E.9, E.12, E.15). For all values of $(\beta_\nu,\ \beta_\xi,\ \beta_\pi,\ \beta_\varrho,\ \beta_\varsigma) \in \{(3.5,4,4.5,4,5),(4.5,5,3.5,4,4),(5,5,5,5,5)\}$ the best values of $\bar{\xi}$ were obtained. For $(\beta_\nu,\ \beta_\xi,\ \beta_\pi,\ \beta_\varrho,\ \beta_\varsigma) = (7,7,7,7,7)$ all the algorithms presented a decline in value of the $\bar{\xi}$ metric (refer to Figures 7.3, 7.6) which shows that too much exploitation is not good. These observations are true for all change frequencies (refer to Figure 7.3) and all change severities (refer to Figure 7.6).

   The graphs indicate an increase in $\bar{\xi}$ with decrease in change frequency (refer to Figure 7.3). This result is expected since low change frequency gives more iterations, and theoretically is supposed to produce a uniform distribution of the solutions and closeness of the solutions to the optimal Pareto set, thus increasing the size of the dominated space (hypervolume measure). Also, the graphs indicate an increase of hypervolume, $\bar{\xi}$, with decrease in change severity (refer to Figure 7.6). It is intuitive to assume that smaller change severities are easier to adapt to, primar-

ily by transferring solutions from the past optimisation problem which may help to accelerate the rate of convergence to the optima, after a change has occurred. Therefore the closeness of the solutions to the optimal Pareto set should be getting worse as the change severity increases.

For the values of $(\beta_\nu, \beta_\xi, \beta_\pi, \beta_\varrho, \beta_\varsigma) \in \{(3.5, 4, 4.5, 4, 5), (4.5, 5, 3.5, 4, 4), (5, 5, 5, 5, 5)\}$, all algorithms displayed the best value, with reference to all three metrics. Accordingly, the value of $(\beta_\nu, \beta_\xi, \beta_\pi, \beta_\varrho, \beta_\varsigma) = (3, 4, 4.5, 4, 5)$ was adopted for the remainder of the simulations.

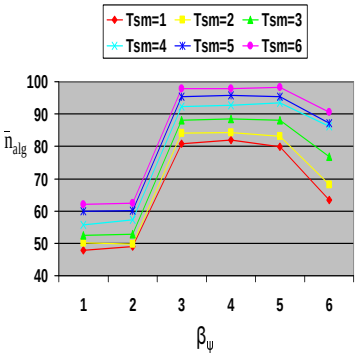

(a) EEMACOMP

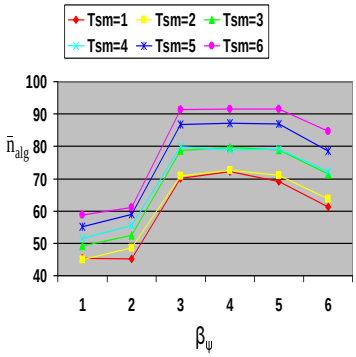

(b) EEMACOMH

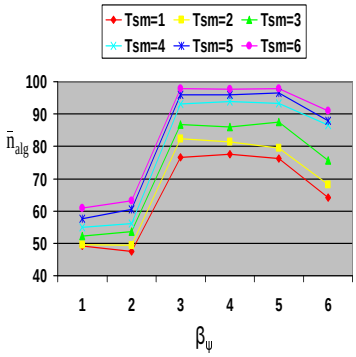

(c) EEMMASMP

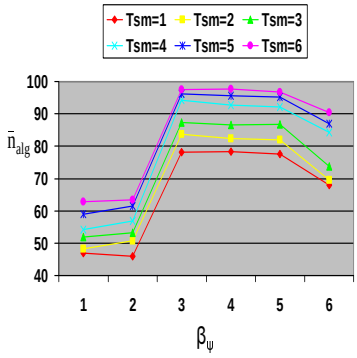

(d) EEMMASMH

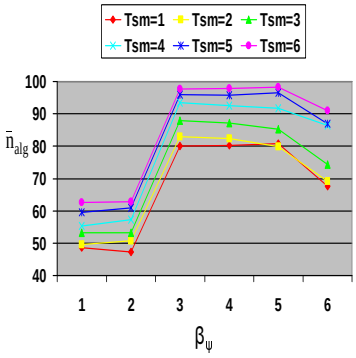

(e) EEMACOMC

Figure 7.1: Influence of β_ψ on $\bar{n}_{alg}$ metric, for different change frequencies, T_{sm}

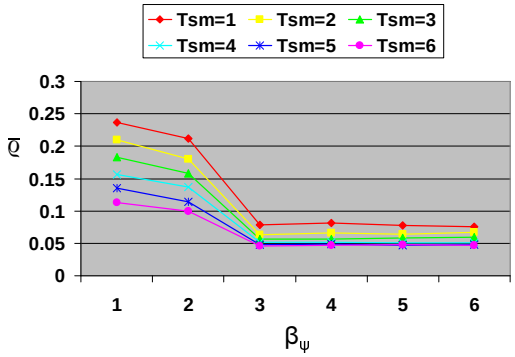

(a) EEMACOMP

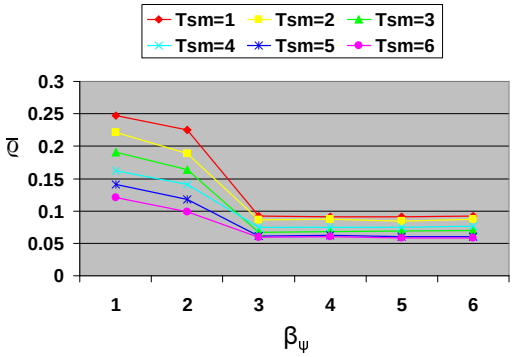

(b) EEMACOMH

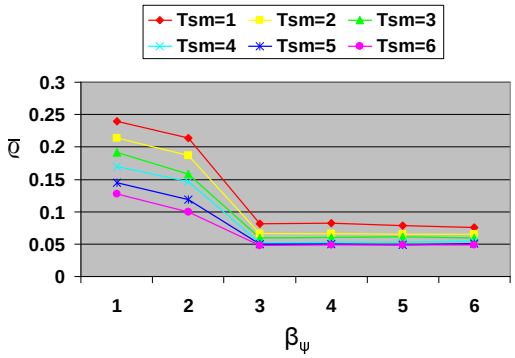

(c) EEMMASMP

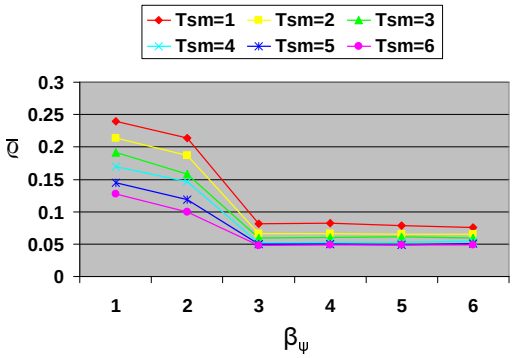

(d) EEMMASMH

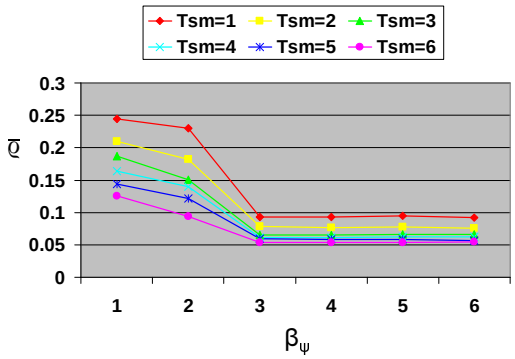

(e) EEMACOMC

Figure 7.2: Influence of β_ψ on $\bar{\varrho}$ metric, for different change frequencies, T_{sm}

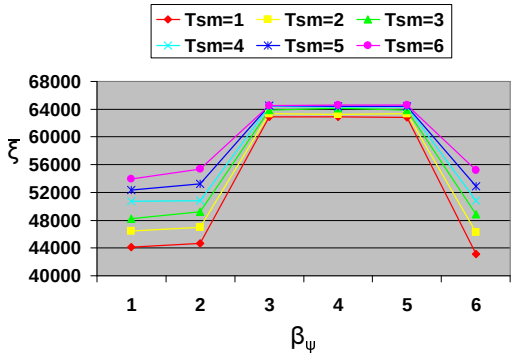

(a) EEMACOMP

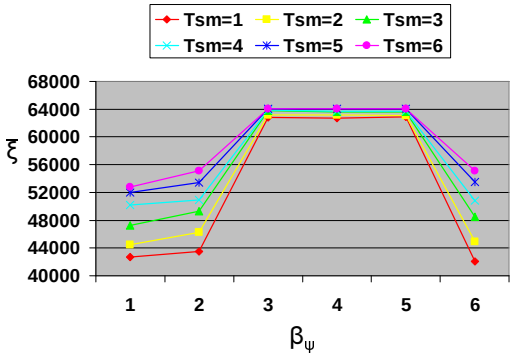

(b) EEMACOMH

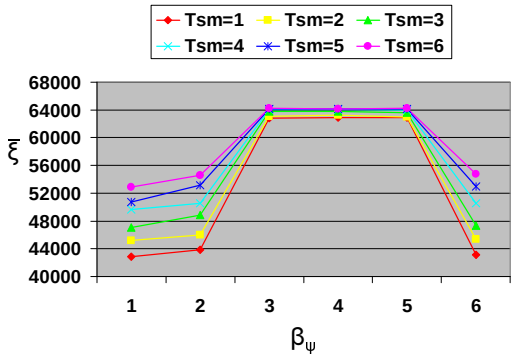

(c) EEMMASMP

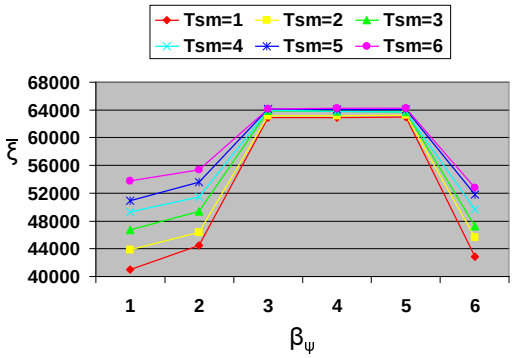

(d) EEMMASMH

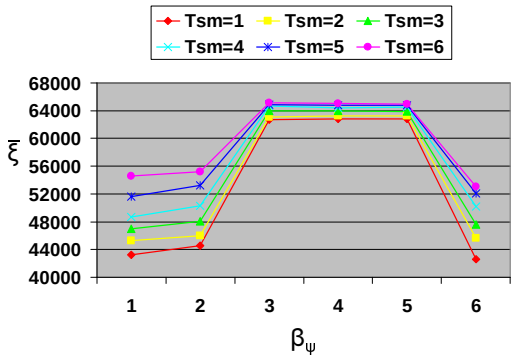

(e) EEMACOMC

Figure 7.3: Influence of β_ψ on $\bar{\xi}$ metric, for different change frequencies, T_{sm}

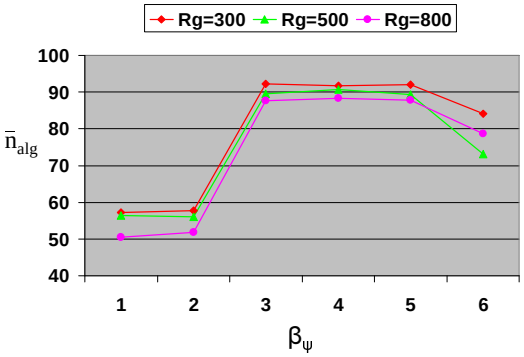

(a) EEMACOMP

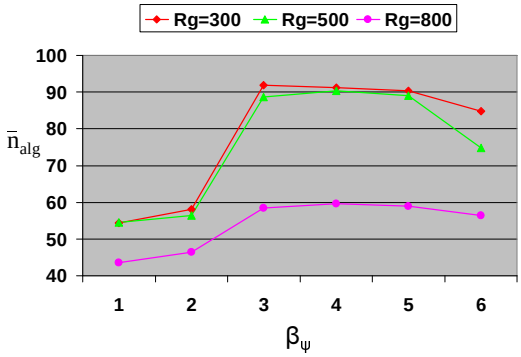

(b) EEMACOMH

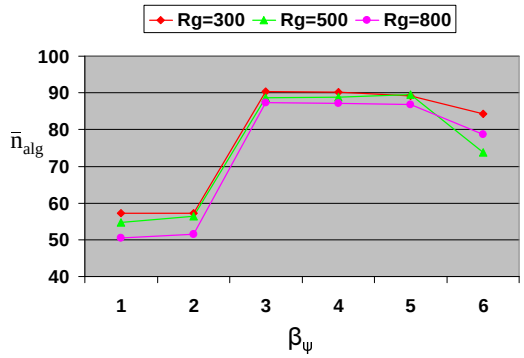

(c) EEMMASMP

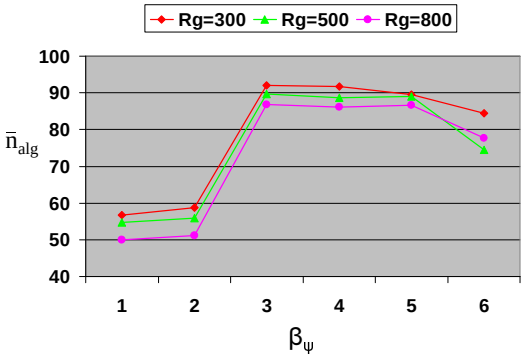

(d) EEMMASMH

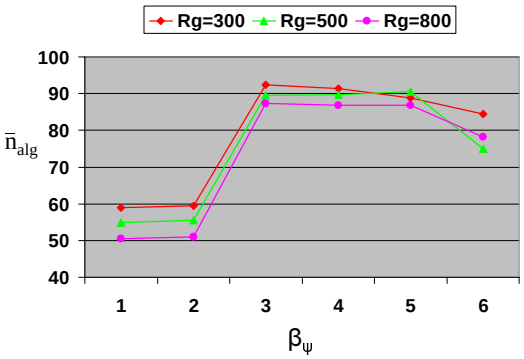

(e) EEMACOMC

Figure 7.4: Influence of β_ψ on $\bar{n}_{alg}$ metric, for different change severities, R_g

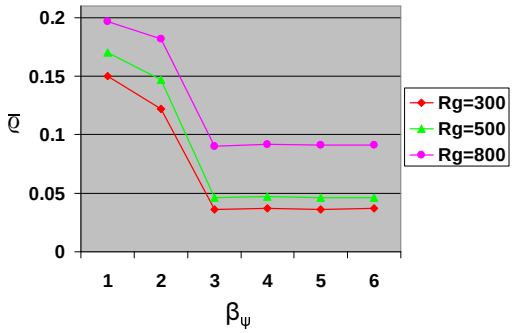

(a) EEMACOMP

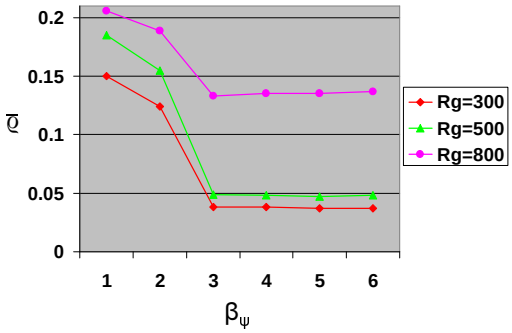

(b) EEMACOMH

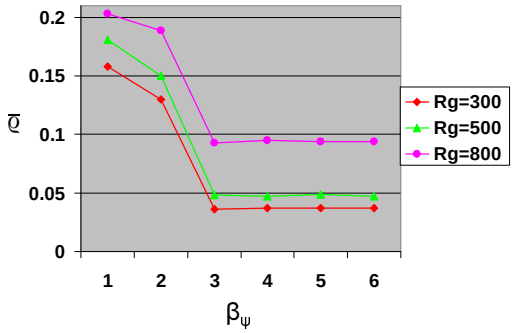

(c) EEMMASMP

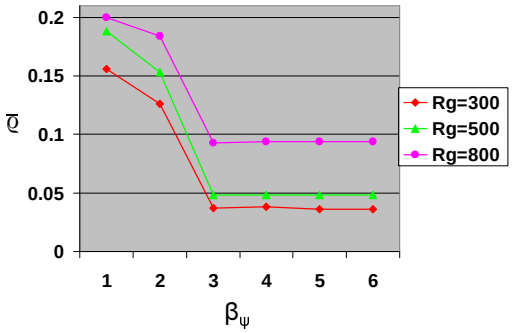

(d) EEMMASMH

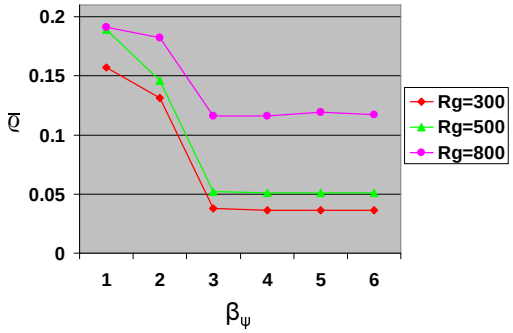

(e) EEMACOMC

Figure 7.5: Influence of β_ψ on $\bar{\varrho}$ metric, for different change severities, R_g

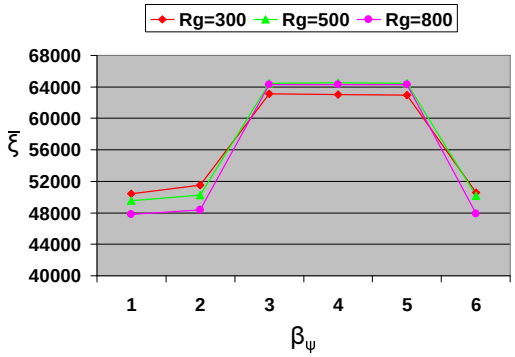

(a) EEMACOMP

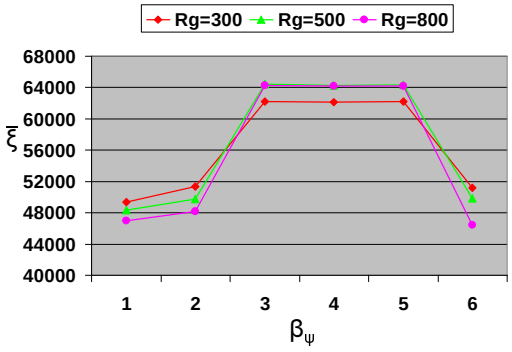

(b) EEMACOMH

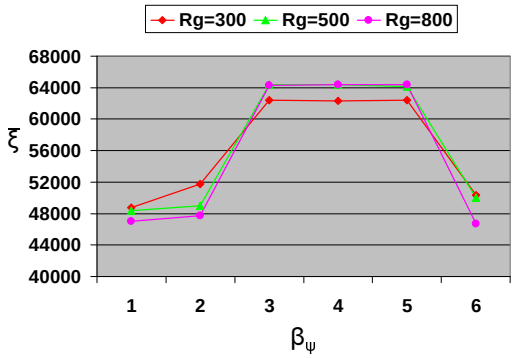

(c) EEMMASMP

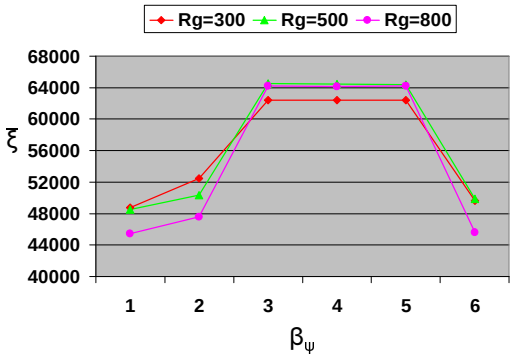

(d) EEMMASMH

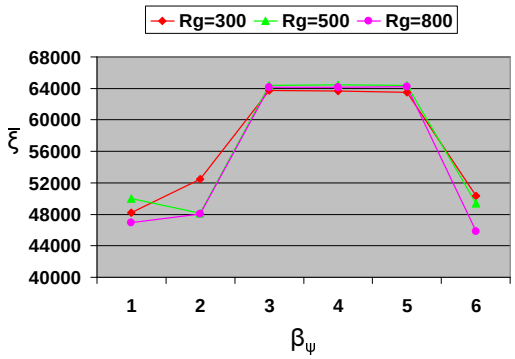

(e) EEMACOMC

Figure 7.6: Influence of β_ψ on $\bar{\xi}$ metric, for different change severities, R_g

7.2.2 Exploration Vs Exploitation Parameter, r_0

The parameter, r_0, is used in the ACS transition rule (refer to equations (6.20), (6.31), (6.54)) to control the balance between exploration and exploitation of the search space. Parameter r_0 takes values within the interval $[0, 1]$. When r_0 approaches zero, exploration is favoured. More focus can be given on exploitation instead of exploration by increasing the value of r_0.

In order to find the best value for r_0, five values were considered, namely $r_0 \in \{0.1,\ 0.3,\ 0.5,\ 0.7,\ 0.9\}$.

Since r_0 is an ACS specific parameter, the influence of r_0 is investigated only for the EEMACOMP, EEMACOMH and EEMACOMC algorithms, as these make use of the ACS equation to compute the transition probability (see equations (6.20), (6.31), (6.54)).

Tables D.4-D.6 summarise the empirical results for r_0 using the $\bar{n}_{alg}$, $\bar{\varrho}$ and $\bar{\xi}$ metrics. Results are visualised in Figures E.16-E.24. Relations between the different performance metrics and the r_0 values with reference to different change frequencies are illustrated in Figures 7.7-7.9. Relations between the different performance metrics and the r_0 values with reference to different change severities are illustrated in Figures 7.10-7.12.

The following parameter values were used based on the result of the previous section: $\beta_\nu = 3.5$, $\beta_\xi = 4.0$, $\beta_\pi = 4.5$, $\beta_\varrho = 4.5$, and $\beta_\varsigma = 5.0$. The rest of the parameter values were fixed as in Section 7.2.

The rest of this section discusses the results obtained from the experiments with regards to the influence of r_0 on the performance metrics.

1. **Influence of r_0 on the number of non-dominated solutions, $\bar{n}_{alg}$.**

   For the values of $r_0 \in \{0.5,\ 0.7,\ 0.9\}$ all the algorithms produced the largest $\bar{n}_{alg}$ irrespective of change frequencies and change severities. For $r_0 = 0.1$ and $r_0 = 0.3$ results are similar to the values of $r_0 \in \{0.5,\ 0.7,\ 0.9\}$ for lower change frequencies ($T_{sm} \in \{3, 4, 5, 6\}$). For $r_0 = 0.1$ and $r_0 = 0.3$ and higher change frequencies ($T_{sm} = 1$ and $T_{sm} = 2$) all the algorithms produced a very low number of non-dominated solutions compared to larger values of T_{sm} (refer to Figure 7.7). This result is expected because for $r_0 = 0.1$ and $r_0 = 0.3$ there is a high exploration of the search space and if the change frequency is too high environment changes may occur before convergence. That is, high exploration negatively affected the

number of non-dominated solutions for high change frequencies. For the values of $r_0 \in \{0.5,\ 0.7,\ 0.9\}$ all the algorithms produced the largest $\bar{n}_{alg}$ for high change frequencies which indicates that exploitation should be preferred under high change frequencies.

For all the experiments, $\bar{n}_{alg}$ increased with decrease in change frequency, T_{sm} (refer to Figure 7.7). This result is expected as low change frequencies provides more time to explore the search space, thereby finding more solutions.

The EEMACOMH algorithm produced the lowest number of non-dominated solutions for $R_g = 800$, for all values of r_0 (refer to Figure 7.10(b)).

Independent of change frequency and change severity, the best values for r_0 are $r_0 \in \{0.5,\ 0.7,\ 0.9\}$ (refer to Tables D.4-D.6 and Figures E.16, E.19, E.22).

2. **Influence of r_0 on the spread metric, $\bar{\varrho}$.**

   For values of $r_0 \in \{0.5,\ 0.7,\ 0.9\}$ all the algorithms produced a lower spread metric value producing more uniformly distributed solutions.

   Values of $r_0 = 0.1$ and $r_0 = 0.3$ produced the largest spread metric value with high change frequencies ($T_{sm} = 1$ and $T_{sm} = 2$). That is, high exploration negatively affected the solution spread for high change frequencies. The values of $r_0 = 0.1$ and $r_0 = 0.3$ produced a low spread metric value with low change frequencies ($T_{sm} \in \{3, 4, 5, 6\}$), for all ACO algorithms.

   The graphs indicate an increase in $\bar{\varrho}$ (i.e. deterioration in the solution spread) with increase in change severity (refer to Figure 7.11). When R_g increases, more iterations are needed to track the optima after the change occurred and therefore less time is available to reach a good distribution of solutions.

   The best values for the solution spread are produced with $r_0 = 0.5$, irrespective of change frequencies and change severities (refer to Tables D.4-D.6 and Figures E.17, E.20, E.23).

3. **Influence of r_0 on the hypervolume metric, $\bar{\xi}$.**

   For all change frequencies and all change severities the values of $r_0 = 0.1$ and $r_0 = 0.3$ produced the worst results for the hypervolume metric (refer to Figures E.18, E.21, E.24). That is, high exploration negatively affected the $\bar{\xi}$ metric. This is

related to the fact that the computational load of the hypervolume calculation sharply increases, the more criteria are considered (when the number of objectives increases). Combined with a high exploration of the search space, environment changes may occur before convergence thus affecting the hypervolume.

The graphs indicate an increase in $\bar{\xi}$ with decrease in change frequency (refer to Figure 7.9). Also, the graphs indicate an increase in $\bar{\xi}$, with decrease in change severity (refer to Figure 7.12).

The best values for the hypervolume were produced with $r_0 = 0.5$, for all change frequencies and all change severities.

A value of $r_0 = 0.5$ offers the best trade-off between metrics $\bar{n}_{alg}$, $\bar{\varrho}$ and $\bar{\xi}$ for all change frequencies and all change severities. Therefore, a value of 0.5 for r_0 was adopted for the remainder of the simulations.

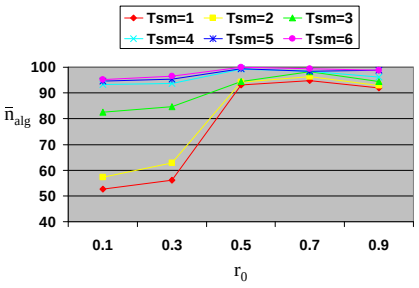

(a) EEMACOMP

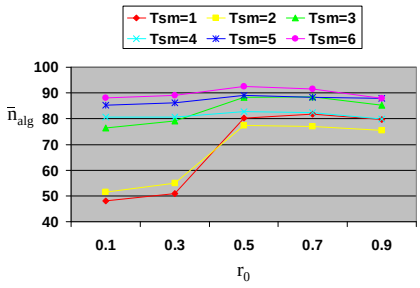

(b) EEMACOMH

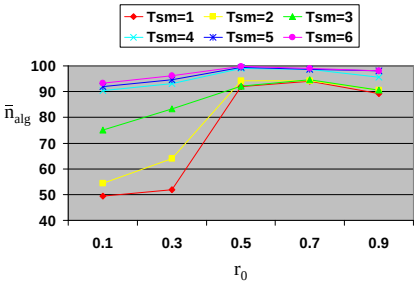

(c) EEMACOMC

Figure 7.7: Influence of r_0 on $\bar{n}_{alg}$ metric, for different change frequencies, T_{sm}

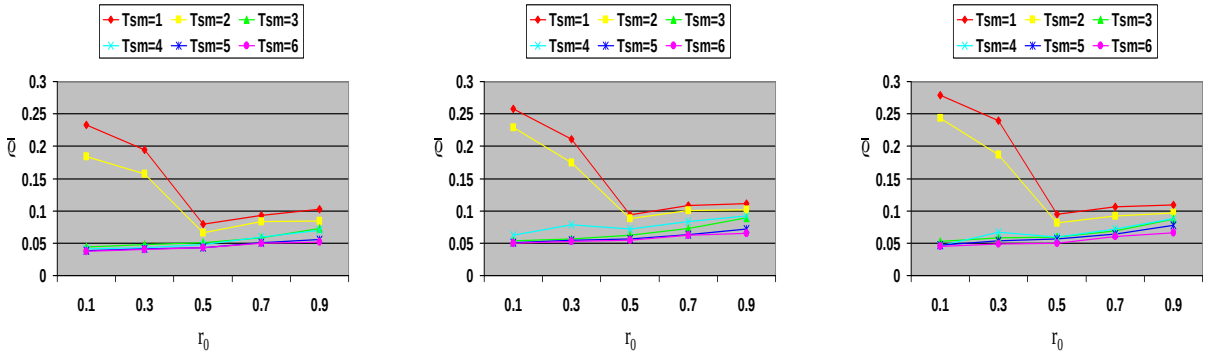

(a) EEMACOMP (b) EEMACOMH (c) EEMACOMC

Figure 7.8: Influence of r_0 on $\bar{\varrho}$ metric, for different change frequencies, T_{sm}

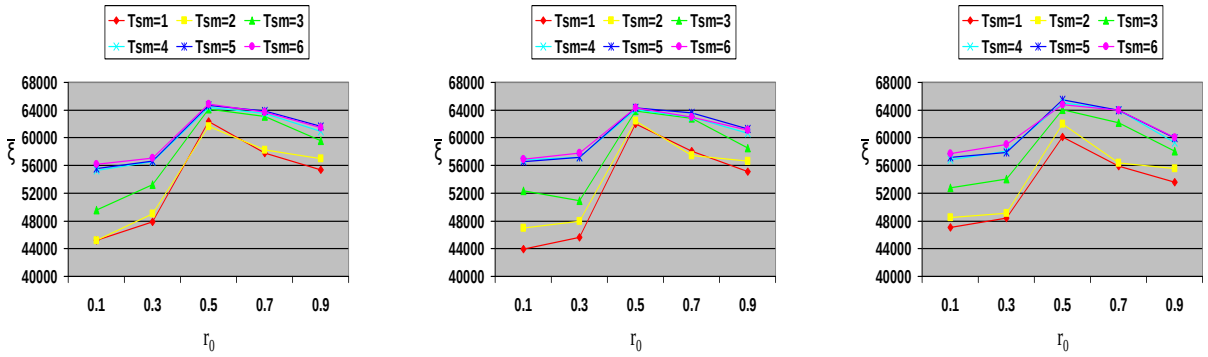

(a) EEMACOMP (b) EEMACOMH (c) EEMACOMC

Figure 7.9: Influence of r_0 on $\bar{\xi}$ metric, for different change frequencies, T_{sm}

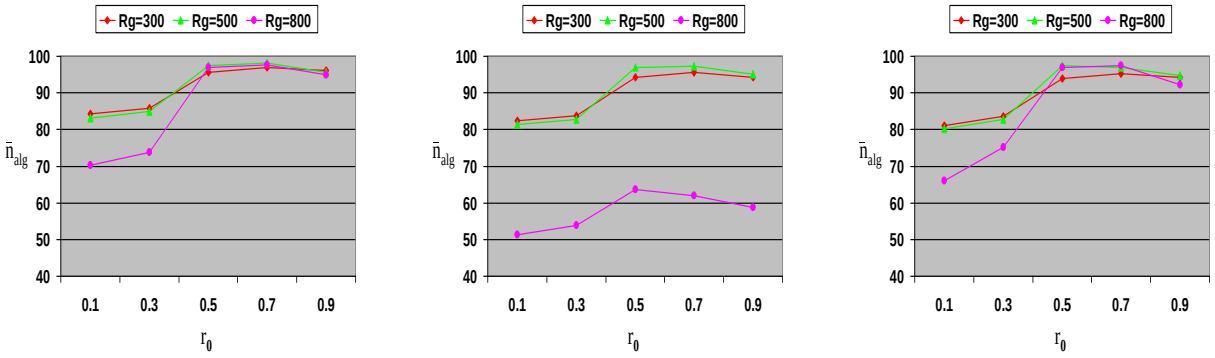

(a) EEMACOMP (b) EEMACOMH (c) EEMACOMC

Figure 7.10: Influence of r_0 on $\bar{n}_{alg}$ metric, for different change severities, R_g

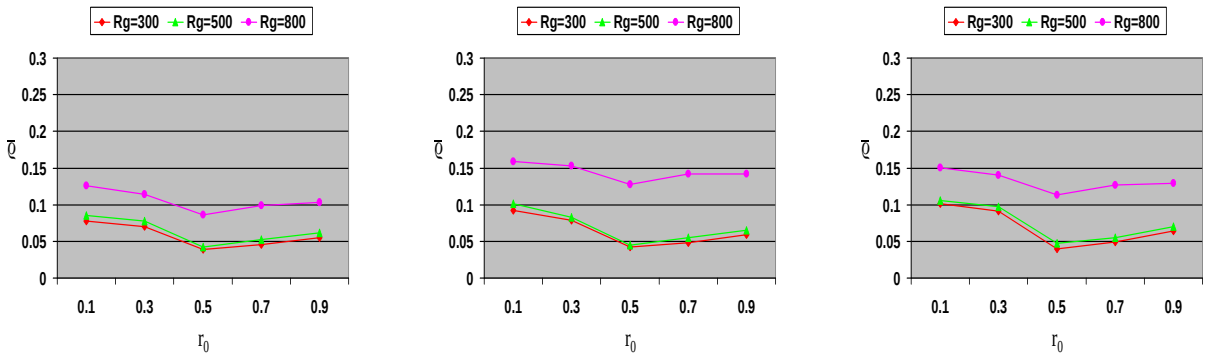

(a) EEMACOMP (b) EEMACOMH (c) EEMACOMC

Figure 7.11: Influence of r_0 on $\bar{\varrho}$ metric, for different change severities, R_g

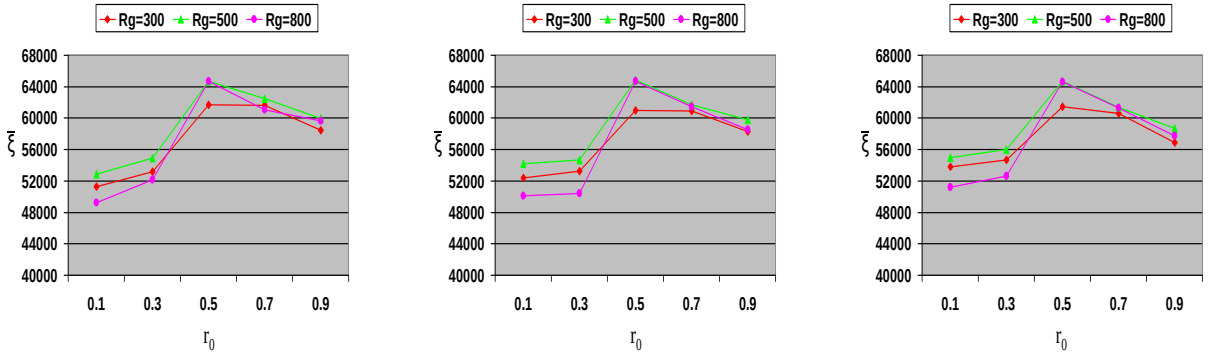

(a) EEMACOMP (b) EEMACOMH (c) EEMACOMC

Figure 7.12: Influence of r_0 on $\bar{\xi}$ metric, for different change severities, R_g

7.2.3 Local Decay Parameter, ρ_l

After each solution construction step, the local updating rule is applied for all the ACS based algorithms (refer to equations (6.26) and (6.37)). The local decay parameter, ρ_l, determines the rate at which pheromone on all the paths are evaporated after each step. Parameter ρ_l has values within the interval $[0, 1]$. A high value of ρ_l leaves less pheromone at each step. Consequently, the ants have less information on other ants' paths, and the

search is less focused, favouring exploration. More focus can be given on exploitation instead of exploration by decreasing the value of ρ_l.

In order to find the best value for ρ_l, five values for ρ_l were considered, namely $\rho_l \in \{0.1,\ 0.3,\ 0.5,\ 0.7,\ 0.9\}$. Since ρ_l is an ACS parameter, the influence of ρ_l is investigated only for the EEMACOMP, EEMACOMH and EEMACOMC algorithms, as these make use of the ACS local update rule. The following parameter values were used based on the result of sections 7.2.1-7.2.2: $\beta_\nu = 3.5$, $\beta_\xi = 4.0$, $\beta_\pi = 4.5$, $\beta_\varrho = 4.5$, $\beta_\varsigma = 5.0$, and $r_0 = 0.5$. The rest of the parameter values were fixed as in Section 7.2.

Tables D.7-D.9 summarise the empirical results for control parameter ρ_l using the $\bar{n}_{alg}$, $\bar{\varrho}$ and $\bar{\xi}$ performance metrics. Results are visualised in Figures E.25-E.33 and 7.13-7.18.

The rest of this subsection discusses the results obtained from the experiments with regards to the influence of ρ_l on the performance metrics.

1. **Influence of ρ_l on the number of non-dominated solutions, $\bar{n}_{alg}$.**

   All the algorithms produced high values for $\bar{n}_{alg}$ for all values of ρ_l and low change frequencies ($T_{sm} \in \{5, 6\}$). For values of $\rho_l = 0.1$ and $\rho_l = 0.3$ and high change frequencies ($T_{sm} \in \{1, 2, 3, 4\}$) (refer to Figure 7.13) all the algorithms struggled to find many non-dominated solutions. It is clear that too much exploitation (small ρ_l) is not good under high change frequency with regard to $\bar{n}_{alg}$. In fact, this observation is true for change frequencies $T_{sm} \in \{1, 2, 3, 4\}$ and all change severities (refer to Figures E.25, E.28, E.31, 7.13, 7.16).

   For all the experiments, $\bar{n}_{alg}$ decreased with increase in change frequency (refer to Figure 7.13). This result is expected since, as frequency of change increases, the time available for adaptation becomes shorter and it becomes more difficult to find optimum solutions.

   Results for $R_g = 800$ show that the EEMACOMH algorithm produced the lowest number of non-dominated solutions (refer to Figure 7.16(b)).

   The best results for the $\bar{n}_{alg}$ metric were obtained with $\rho_l \in \{0.5, 0.7\}$, irrespective of change frequencies and change severities (refer to Tables D.7-D.9 and Figures E.25, E.28, E.31, 7.13, 7.16).

2. **Influence of ρ_l on the spread metric, $\bar{\varrho}$.**

Results for $\rho_l = 0.1$ and $\rho_l = 0.3$ show that all the algorithms failed in obtaining a good spread in the found non-dominated solutions (refer to Figures E.26, E.29, E.32), irrespective of change severities and for change frequencies $T_{sm} \in \{1, 2, 3, 4\}$. The spacing metric for $\rho_l = 0.9$ is also higher (obtaining less uniformly distributed solutions) than the spacing metric obtained with $\rho_l \in \{0.5, 0.7\}$. It is also clear that too much exploration (very large ρ_l) and too much exploitation (small ρ_l) is not good (refer to Figures 7.14 and 7.17). In fact this observation is true for all change frequencies and all change severities. A balance of exploration and exploitation is needed, which is achieved with a $\rho_l \in \{0.5, 0.7\}$ (refer to Tables D.7-D.9 and Figures 7.14 and 7.17).

The graphs indicate a deterioration in the solution spread with increase in change frequency (refer to Figure 7.14). A decrease in change frequency leads to more uniformly distributed solutions, which is expected (refer to Section 7.2.1 on page 160).

The graphs indicate a deterioration in the solution spread with increase in change severity (refer to Figure 7.17). That is, high change severity negatively affected the solution spread.

3. **Influence of ρ_l on the hypervolume metric, $\bar{\xi}$.**

   Irrespective of the change frequency and change severity, all algorithms succeeded in obtaining good performance with respect to the hypervolume metric (refer to Figures E.27, E.30, E.33). A general trend that is observed over all values of T_{sm} and R_g is that performance peaks at $\rho_l = 0.5$ and $\rho_l = 0.7$. Again this indicates that a balance between exploration and exploitation is best for this dynamic environment, since a high value of ρ_l which favours exploration and a low value of ρ_l which favours exploitation produced the lowest values for the hypervolume (refer to Figures 7.15 and 7.18).

   The graphs indicate in most cases an increase in $\bar{\xi}$ with decrease in change frequency (refer to Figure 7.15). This result is expected, since low change frequency gives more time for adaptation and is supposed to produce a uniform distribution of the solutions and closeness of the solutions to the optimal Pareto set.

A value of $\rho_l = 0.5$ and $\rho_l = 0.7$ offers the best trade-off between metrics $\bar{n}_{alg}$, $\bar{\varrho}$ and $\bar{\xi}$ for all change frequencies and all change severities. Accordingly, the value of 0.5 for ρ_l

was adopted for the remainder of the simulations.

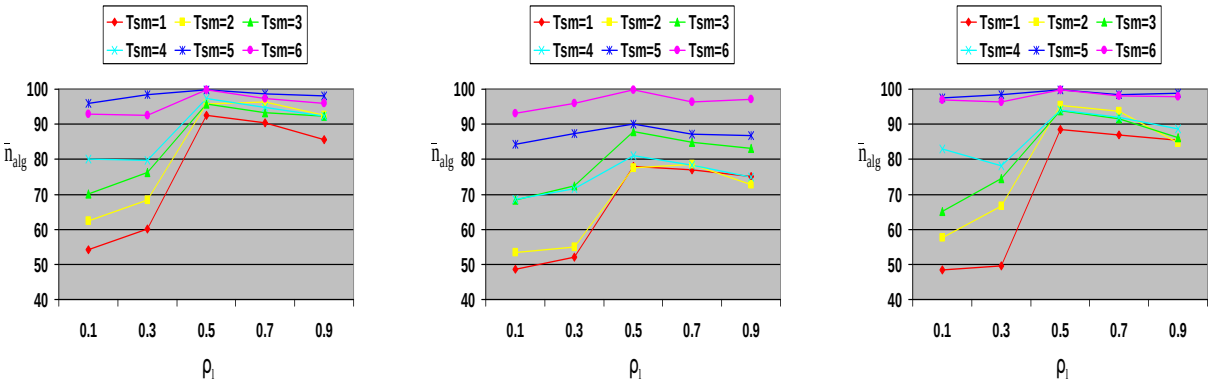

(a) EEMACOMP (b) EEMACOMH (c) EEMACOMC

Figure 7.13: Influence of r_l on $\bar{n}_{alg}$ metric, for different change frequencies, T_{sm}

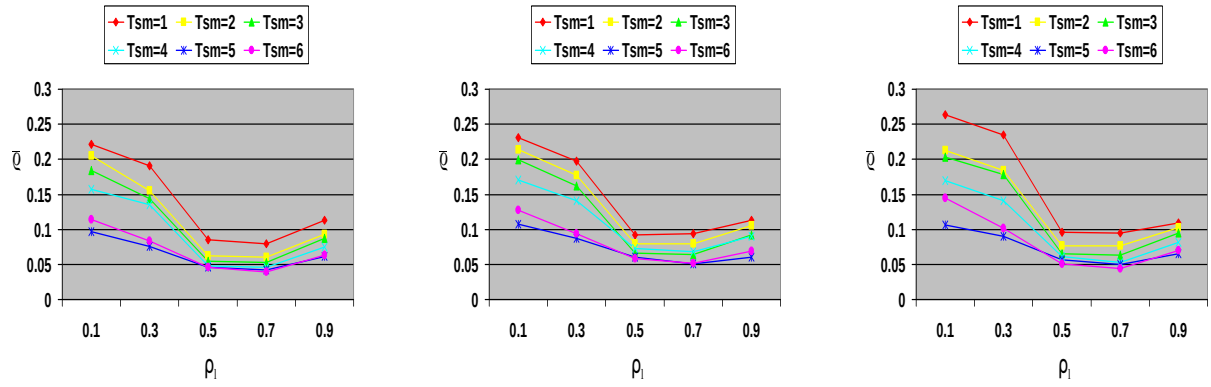

(a) EEMACOMP (b) EEMACOMH (c) EEMACOMC

Figure 7.14: Influence of r_l on $\bar{\varrho}$ metric, for different change frequencies, T_{sm}

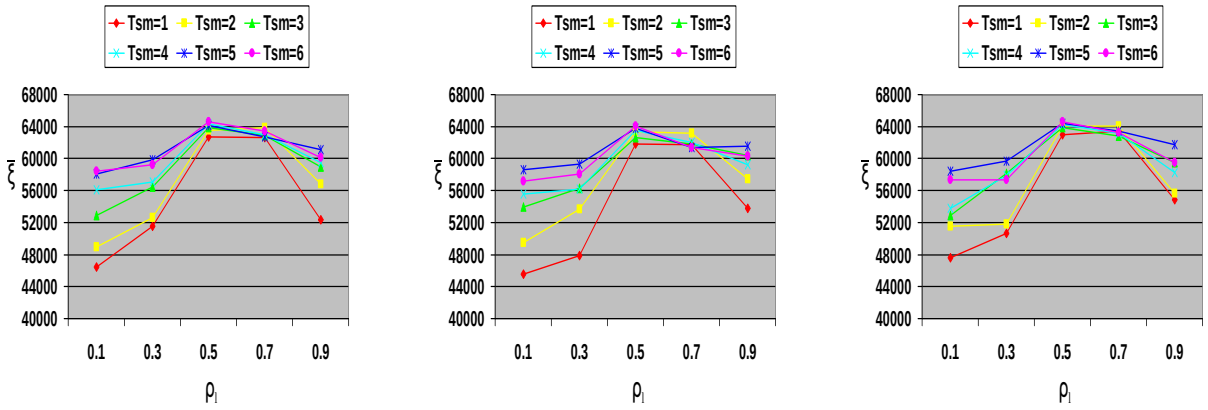

(a) EEMACOMP (b) EEMACOMH (c) EEMACOMC

Figure 7.15: Influence of r_l on $\bar{\xi}$ metric, for different change frequencies, T_{sm}

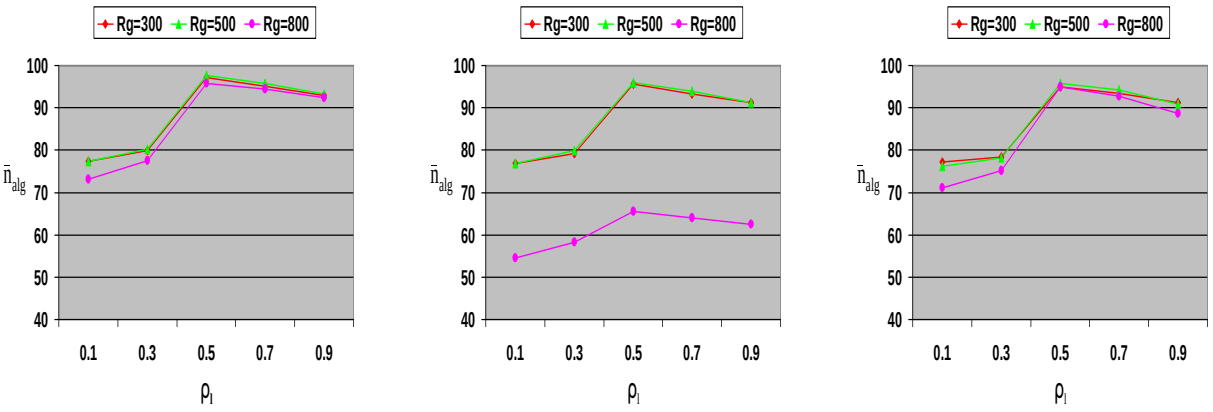

(a) EEMACOMP (b) EEMACOMH (c) EEMACOMC

Figure 7.16: Influence of r_l on $\bar{n}_{alg}$ metric, for different change severities, R_g

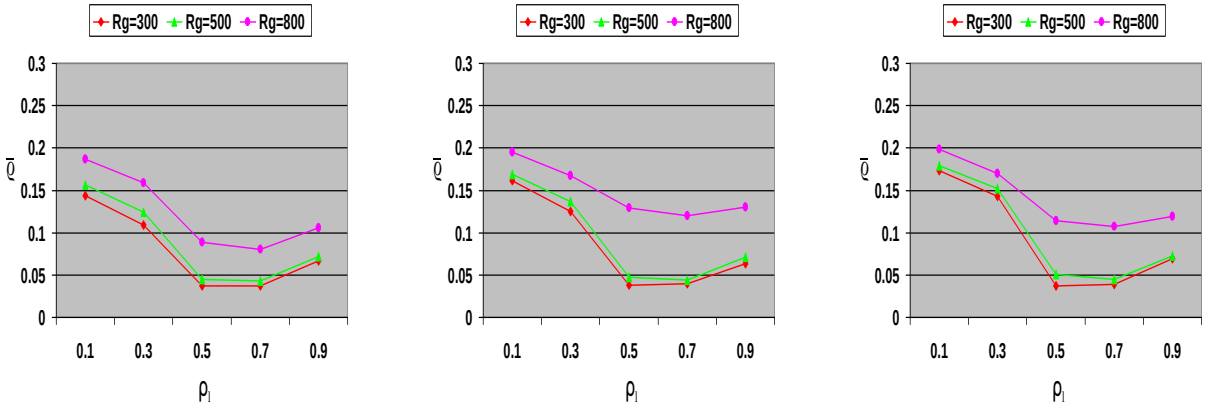

(a) EEMACOMP (b) EEMACOMH (c) EEMACOMC

Figure 7.17: Influence of r_l on $\bar{\varrho}$ metric, for different change severities, R_g

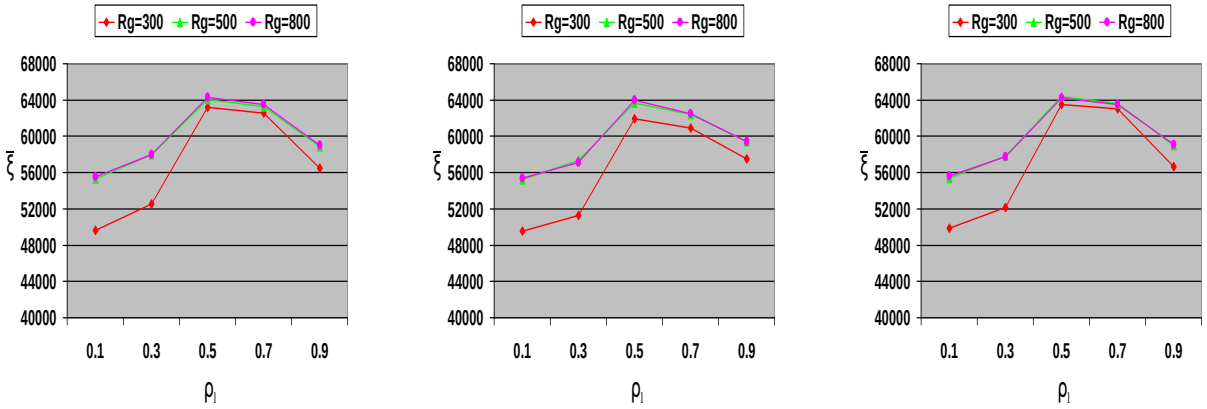

(a) EEMACOMP (b) EEMACOMH (c) EEMACOMC

Figure 7.18: Influence of r_l on $\bar{\xi}$ metric, for different change severities, R_g

7.2.4 Global Decay Parameter, ρ_g

After each iteration, all ants found a solution and the global updating rule is applied (refer to equations (6.24), (6.35), and (6.56). The global decay or global evaporation parameter, ρ_g, sets the amount of pheromone that evaporate on the paths after each loop, as for ρ_l. A high value of ρ_g will help finding more solutions instead of focusing on a specific solution.

In order to find the best value for ρ_g, five values were considered, namely $\rho_g \in \{0.1, 0.3, 0.5, 0.7, 0.9\}$. The influence of ρ_g was investigated for all five algorithms.

The following parameter values were used based on the result of sections 7.2.1-7.2.3: $\beta_\nu = 3.5$, $\beta_\xi = 4.0$, $\beta_\pi = 4.5$, $\beta_\varrho = 4.5$, $\beta_\varsigma = 5.0$, $r_0 = 0.5$, and $\rho_l = 0.5$. The rest of the parameter values were fixed as in Section 7.2.

Tables D.10-D.12 summarise the empirical results for control parameter ρ_g using the $\bar{n}_{alg}$, $\bar{\varrho}$ and $\bar{\xi}$ metrics. Results are visualised in Figures E.34-E.48 and 7.19-7.24.

The rest of this subsection discusses the results obtained from the experiments.

1. **Influence of ρ_g on the number of non-dominated solutions, $\bar{n}_{alg}$.**

   Parameter ρ_g follows similar trends as for ρ_l with reference to $\bar{n}_{alg}$, except that there is no real trend between $\bar{n}_{alg}$ and the change frequency (refer to Figures E.25, E.28, E.31, E.34, E.37, E.40, E.43, E.46). Values of $\rho_g \in \{0.5, 0.7\}$ performed the best for all change frequencies (refer to Figure 7.19) and for all change severities (refer to Figure 7.22).

2. **Influence of ρ_g on the spread metric, $\bar{\varrho}$.**

   Results for $\rho_g = 0.1$ and $\rho_g = 0.3$ show that all the algorithms failed in obtaining a good spread in the found non-dominated solutions (refer to Figures E.35, E.38, E.41, E.44, E.47), irrespective of change severities and change frequencies. For $\rho_g = 0.9$, the spread metric is higher than the spread metric obtained with $\rho_g \in \{0.5, 0.7\}$. It seems to be a general trend for all results thus far that too much exploration (very large ρ_g) and too much exploitation (small ρ_g) is not good. For $\rho_g = 0.9$ there is high pheromone evaporation and the search is very random. Consequently, it takes more time for the algorithms to converge to a solution. That explains the high value of $\bar{\varrho}$. For $\rho_g = 0.1$ and $\rho_g = 0.3$ there is high pheromone concentration and ants tend to converge to the same solution. There is a too early convergence to sub-optimal solutions, which again explains the high value of $\bar{\varrho}$.

Again, parameter ρ_g follows the same trends as for ρ_l with reference to $\bar{\varrho}$. Values of $\rho_g \in \{0.5, 0.7\}$ performed the best (refer to Tables D.10-D.12 and Figures 7.20 and 7.23).

3. **Influence of ρ_g on the hypervolume metric, $\bar{\xi}$.**

   Parameter ρ_g follows the same trends as for ρ_l with reference to $\bar{\xi}$ (refer to Figures E.27, E.30, E.33, E.36, E.39, E.42, E.45, E.48).

   A general trend that was observed over all values of T_{sm} and R_g is that performance peaks at $\rho_g = 0.5$ and $\rho_g = 0.7$ (refer to Figures 7.21 and 7.24). Again this indicates that a balance between exploration and exploitation is best for this dynamic environment.

A value of $\rho_g = 0.5$ and $\rho_g = 0.7$ offered the best trade-off between metrics $\bar{n}_{alg}$, $\bar{\varrho}$ and $\bar{\xi}$ for all change frequencies and all change severities. Accordingly, the value of $\rho_g = 0.7$ was adopted for the remainder of the simulations.

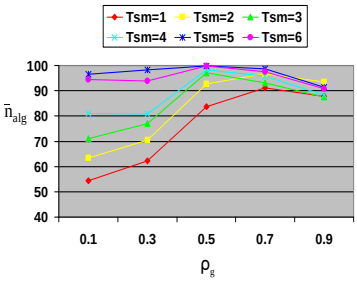

(a) EEMACOMP

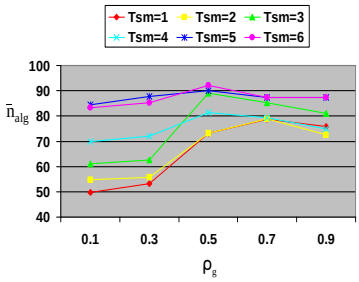

(b) EEMACOMH

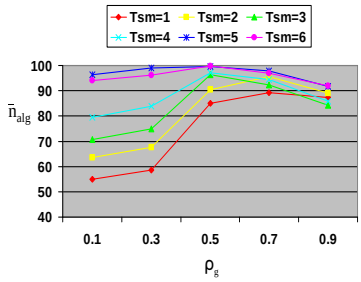

(c) EEMMASMP

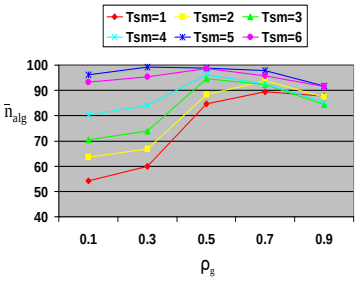

(d) EEMMASMH

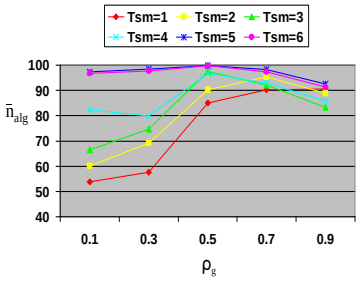

(e) EEMACOMC

Figure 7.19: Influence of ρ_g on $\bar{n}_{alg}$ metric, for different change frequencies, T_{sm}

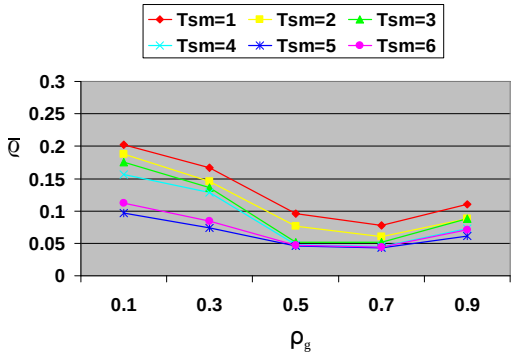

(a) EEMACOMP

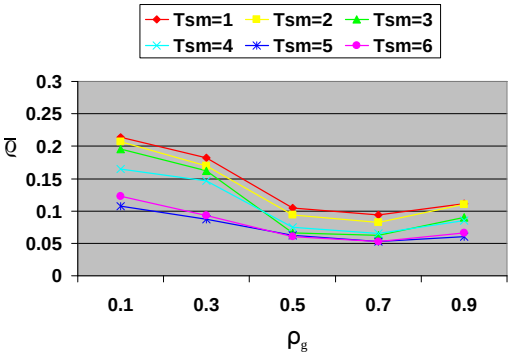

(b) EEMACOMH

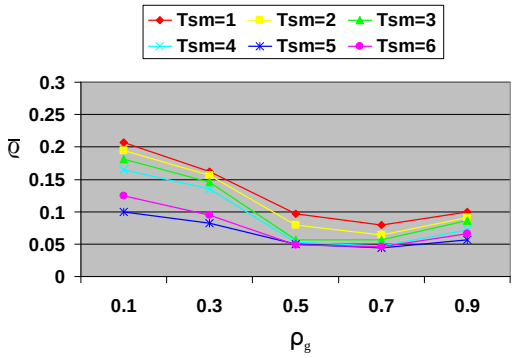

(c) EEMMASMP

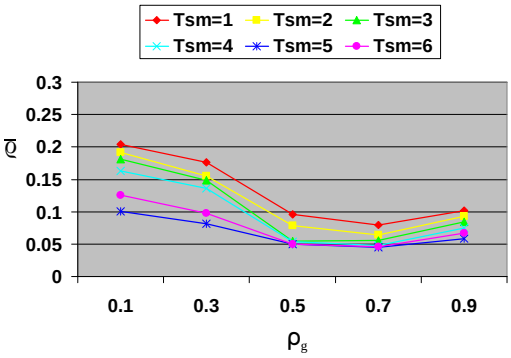

(d) EEMMASMH

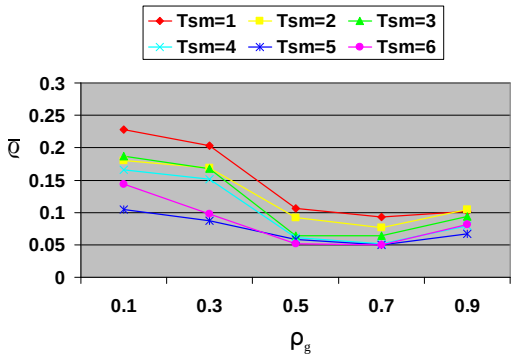

(e) EEMACOMC

Figure 7.20: Influence of ρ_g on $\bar{\varrho}$ metric, for different change frequencies, T_{sm}

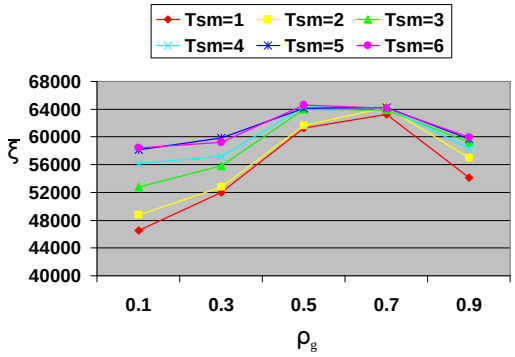

(a) EEMACOMP

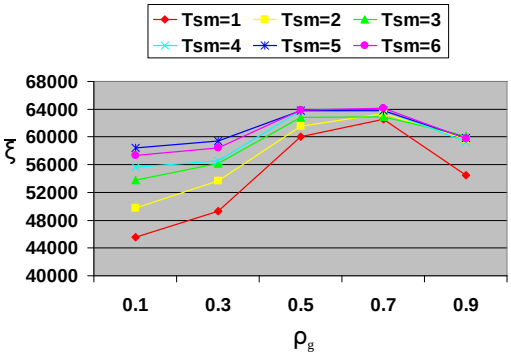

(b) EEMACOMH

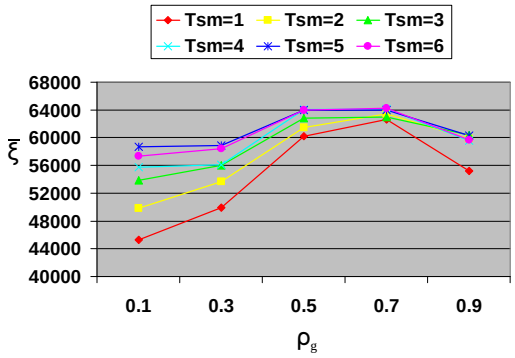

(c) EEMMASMP

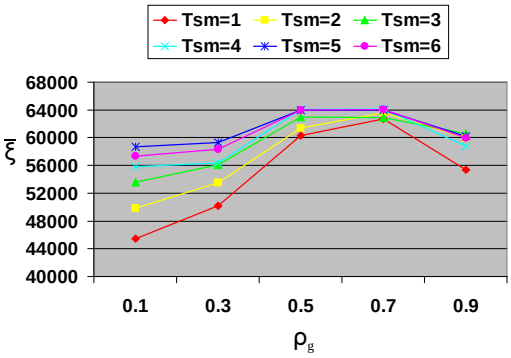

(d) EEMMASMH

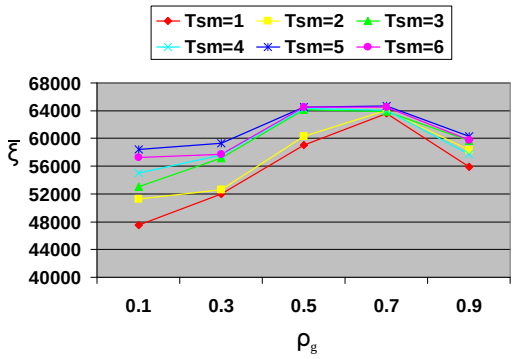

(e) EEMACOMC

Figure 7.21: Influence of ρ_g on $\bar{\xi}$ metric, for different change frequencies, T_{sm}

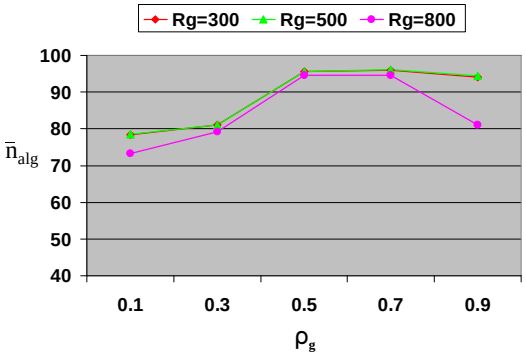

(a) EEMACOMP

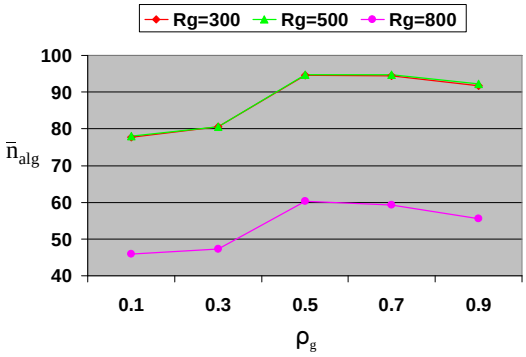

(b) EEMACOMH

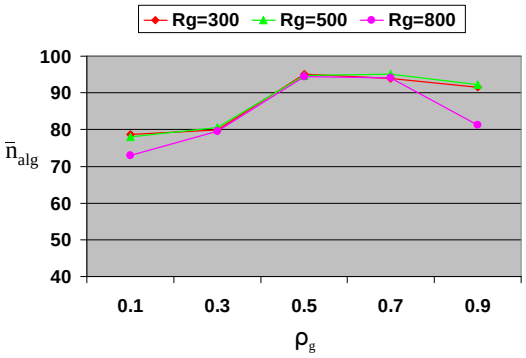

(c) EEMMASMP

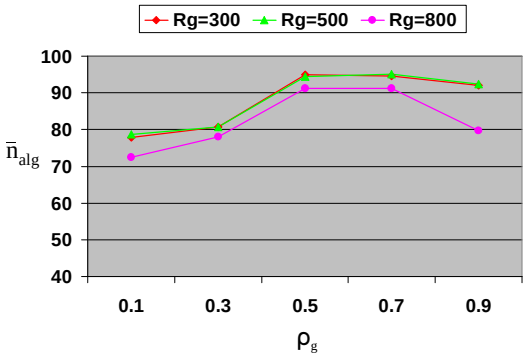

(d) EEMMASMH

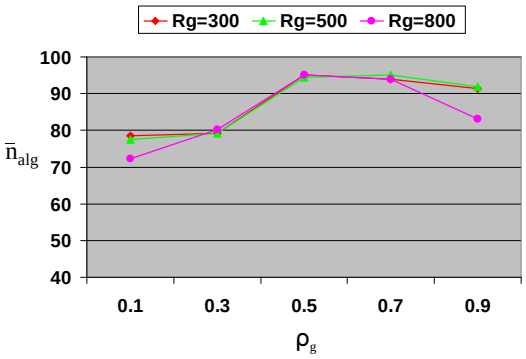

(e) EEMACOMC

Figure 7.22: Influence of ρ_g on $\bar{n}_{alg}$ metric, for different change severities, R_g

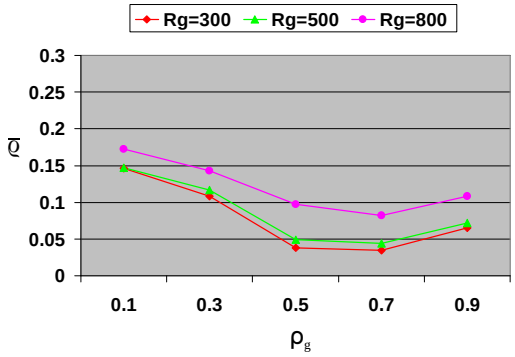

(a) EEMACOMP

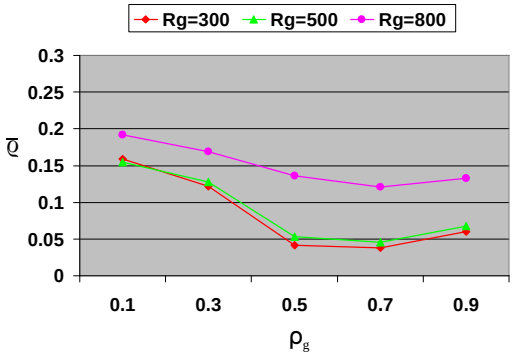

(b) EEMACOMH

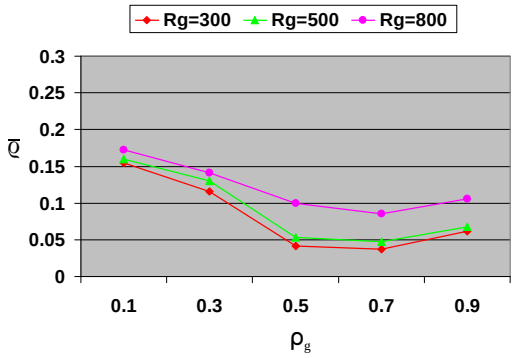

(c) EEMMASMP

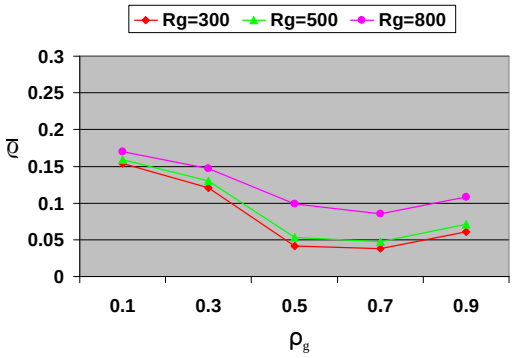

(d) EEMMASMH

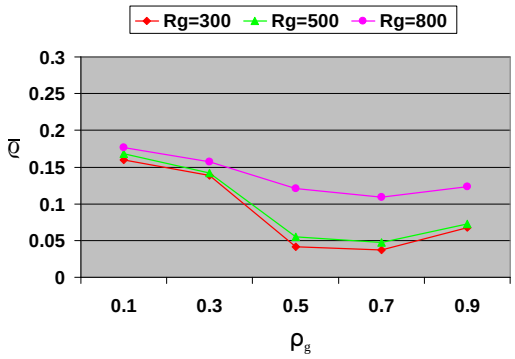

(e) EEMACOMC

Figure 7.23: Influence of ρ_g on $\bar{\varrho}$ metric, for different change severities, R_g

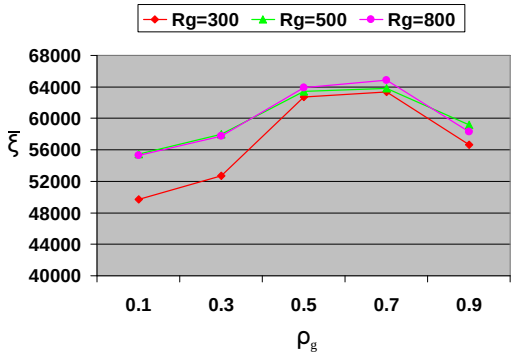

(a) EEMACOMP

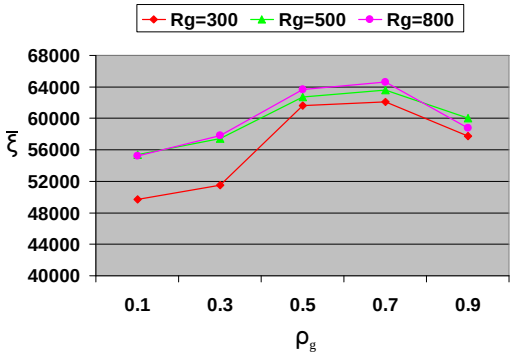

(b) EEMACOMH

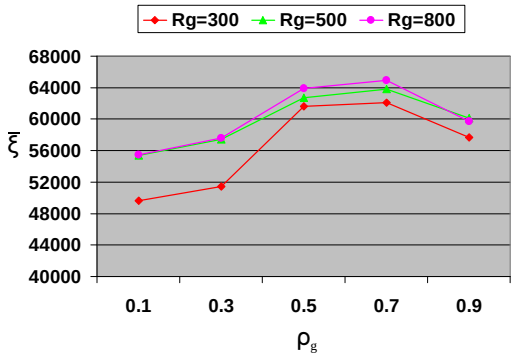

(c) EEMMASMP

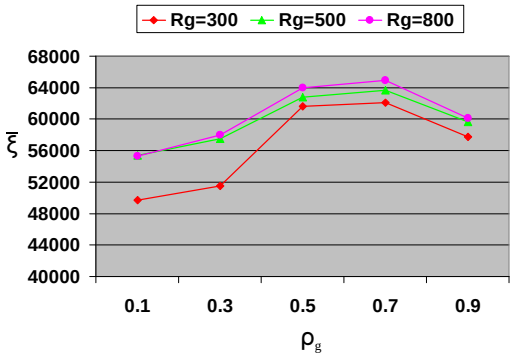

(d) EEMMASMH

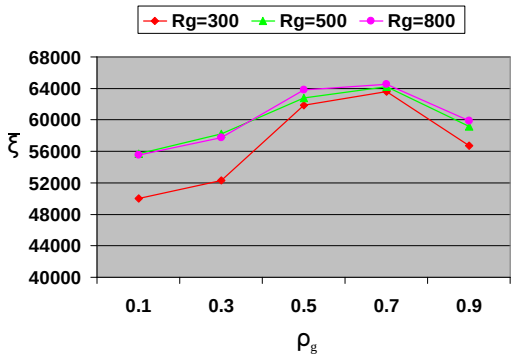

(e) EEMACOMC

Figure 7.24: Influence of ρ_g on $\bar{\xi}$ metric, for different change severities, R_g

7.2.5 Importance of the Pheromone Trail Concentrations Parameter, α

As illustrated in equations (6.42) and (6.48), α controls the balance between exploration and exploitation. Diversification of the solution searching process in the solution space can be emphasized by decreasing the value of α and exploitation can be increased by increasing the value of α. If $\alpha = 0$, no pheromone information is used, i.e. previous search experience is neglected. The search then degrades to a stochastic greedy search.

Because α is used only in equations (6.42) and (6.48), the influence of α was investigated only for EEMMASMP and EEMMASMH. For the other three algorithms, α was set to one.

In order to find the best value for α, six values were considered, namely $\alpha \in \{1,\ 1.5,\ 2,\ 2.5,\ 3,\ 3.5\}$.

The following parameter values were used based on the results of sections 7.2.1-7.2.4: $\beta_\nu = 3.5$, $\beta_\xi = 4.0$, $\beta_\pi = 4.5$, $\beta_\varrho = 4.5$, $\beta_\varsigma = 5.0$, $r_0 = 0.5$, $\rho_l = 0.5$, and $\rho_g = 0.7$. The rest of the parameter values were fixed as in Section 7.2.

Tables D.13-D.15 summarise the empirical results for α using the $\bar{n}_{alg}$, $\bar{\varrho}$ and $\bar{\xi}$ metrics. Results are visualised in Figures E.49-E.54 and 7.25-7.30. The rest of this section discusses the results obtained from the experiments with regards to the influence of α on the performance metrics.

1. **Influence of α on the number of non-dominated solutions, $\bar{n}_{alg}$.**

   For $\alpha = 3$ and $\alpha = 3.5$ all the algorithms produced a very low number of non-dominated solutions compared to lower values of α. The best values for α are for $\alpha \in \{1,\ 1.5,\ 2,\ 2.5\}$, for all change frequencies and all change severities (refer to Tables D.13-D.15 and Figures E.49, E.52, 7.25 and 7.28). For these values all algorithms produced a very large number of non-dominated solutions.

   The graphs indicate a small decrease in the number of non-dominated solutions with increase in change frequency which is expected (refer to Figures E.49, E.52 and 7.25). As pointed out in section 7.2.1 on page 159, as change frequency increases, the time available for adaptation becomes shorter and it becomes harder to find optimum solutions.

   Also, there is a small decrease in the number of non-dominated solutions with increase in change severity (refer to Figures E.49, E.52 and 7.28).

2. **Influence of α on the spread metric, $\bar{\varrho}$.**

   The graphs indicate a small deterioration of the solution spread with higher values of α (refer to Figures E.50 and E.53). The best values for the solution spread were produced with $\alpha \in \{1,\ 1.5,\ 2\}$, for all change frequencies and all change severities.

   Figure 7.26 indicates a deterioration of the solution spread (i.e. higher $\bar{\varrho}$) with increase in change frequency which is expected (refer to Section 7.2.1 on page 160). Also, there is a deterioration of the solution spread with increase in change severity (refer to Figure 7.29). This result is expected since, when R_g increases, more iterations are needed to track the optima after the change occurred and therefore less time is available to reach a good distribution of solutions.

3. **Influence of α on the hypervolume metric, $\bar{\xi}$.**

   Values of $\alpha \in \{1,\ 3,\ 3.5\}$ produced the worst results for the hypervolume metric (refer to Figures E.51 and E.54). This observation is true for all change frequencies (refer to Figure 7.27) and all change severities (refer to Figure 7.30). That is, high exploration and high exploitation negatively affected the $\bar{\xi}$ metric.

   The graphs indicate a small increase in $\bar{\xi}$, with decrease in change frequency (refer to Figure 7.27).

   There is no pattern between $\bar{\xi}$ and R_g, which indicates insensitivity of $\bar{\xi}$ to R_g (refer to Figure 7.30).

   The best values for the hypervolume were produced with $\alpha \in \{1.5,\ 2,\ 2.5\}$, for all change frequencies and all change severities (refer to Tables D.13-D.15 and Figures E.51, E.54, 7.27 and 7.30).

A value of $\alpha = 1.5$ offered the best trade-off between metrics $\bar{n}_{alg}$, $\bar{\varrho}$ and $\bar{\xi}$ for all change frequencies and all change severities. Accordingly, the value of $\alpha = 1.5$ was adopted for the remainder of the simulations.

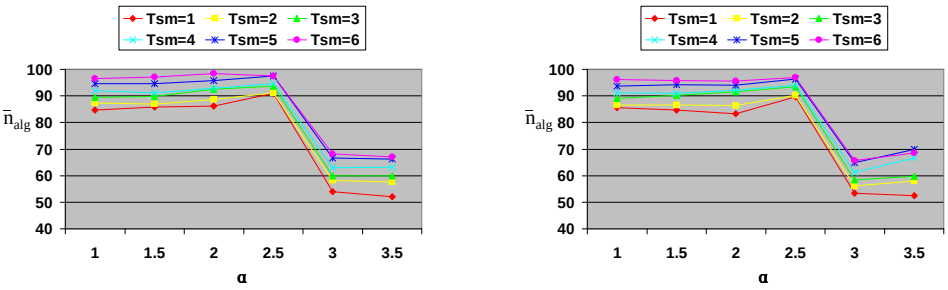

(a) EEMMASMP (b) EEMMASMH

Figure 7.25: Influence of α on $\bar{n}_{alg}$ metric, for different change frequencies, T_{sm}

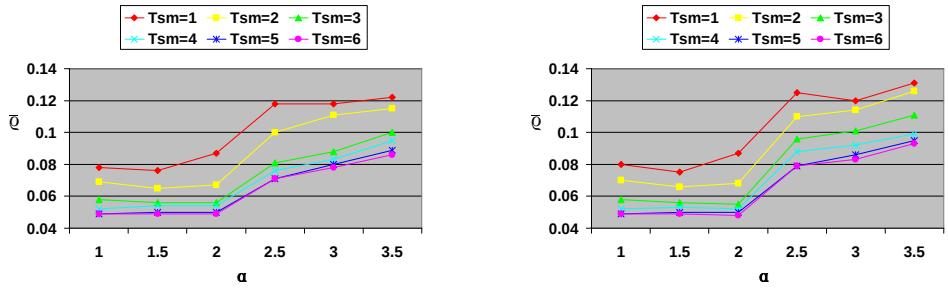

(a) EEMMASMP (b) EEMMASMH

Figure 7.26: Influence of α on $\bar{\varrho}$ metric, for different change frequencies, T_{sm}

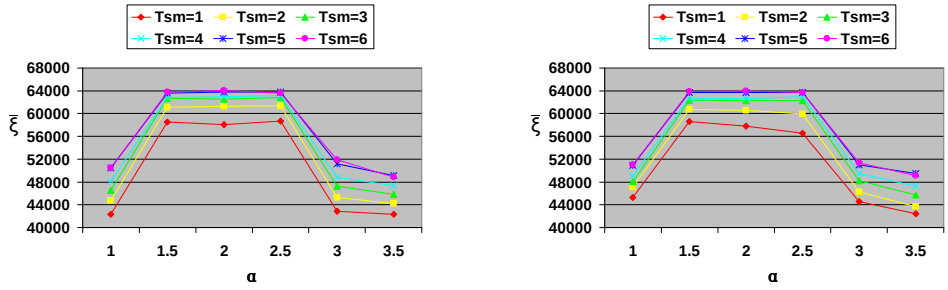

(a) EEMMASMP (b) EEMMASMH

Figure 7.27: Influence of α on $\bar{\xi}$ metric, for different change frequencies, T_{sm}

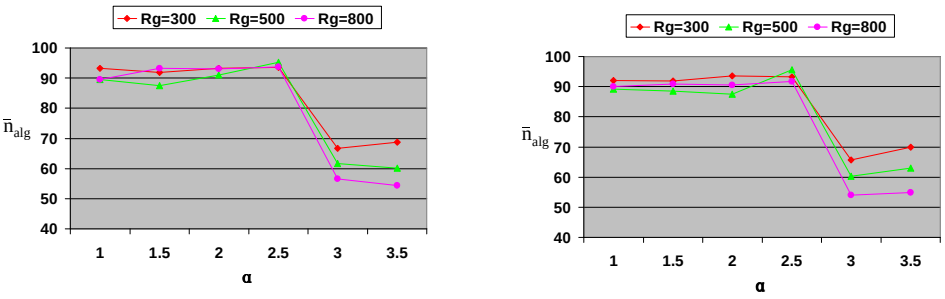

(a) EEMMASMP (b) EEMMASMH

Figure 7.28: Influence of α on $\bar{n}_{alg}$ metric, for different change severities, R_g

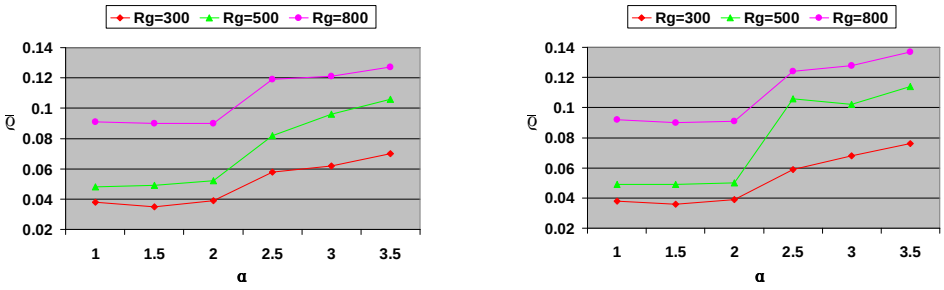

(a) EEMMASMP (b) EEMMASMH

Figure 7.29: Influence of α on $\bar{\varrho}$ metric, for different change severities, R_g

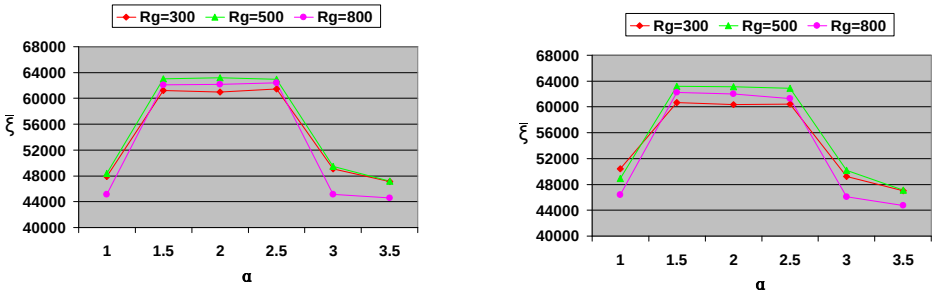

(a) EEMMASMP (b) EEMMASMH

Figure 7.30: Influence of α on $\bar{\xi}$ metric, for different change severities, R_g

7.2.6 η-Strategy Parameter

The η-strategy parameter, noted λ_E, is used to determine the reset value to reinitialise pheromone values on links. The η-strategy is applied after a change in the environment occurs in order to promote diversity. If $\lambda_E \rightarrow \infty$ there is no pheromone conservation and exploration is emphasized. For lower values of λ_E there is a higher pheromone conservation and exploitation is promoted.

All algorithms were run using the η-strategy. The influence of λ_E on the performance metrics $\bar{n}_{alg}$, $\bar{\varrho}$, and $\bar{\xi}$ was therefore evaluated. In order to find the best value for λ_E, four values for λ_E were considered, namely $\lambda_E \in \{2,\ 4,\ 6,\ 8\}$.

The following parameter values were used based on the result of sections 7.2.1-7.2.5: $\beta_\nu = 3.5$, $\beta_\xi = 4.0$, $\beta_\pi = 4.5$, $\beta_\varrho = 4.5$, $\beta_\varsigma = 5.0$, $r_0 = 0.5$, $\rho_l = 0.5$, $\rho_g = 0.7$, and $\alpha = 1.5$. The rest of the parameter values were fixed as in Section 7.2.

Tables D.16-D.18 summarise the empirical results for the control parameter λ_E using the $\bar{n}_{alg}$, $\bar{\varrho}$ and $\bar{\xi}$ metrics. Results are visualised in Figures E.55-E.69 and 7.31-7.36.

The rest of this subsection discusses the results obtained from the experiments with regards to the influence of λ_E on the performance metrics $\bar{n}_{alg}$, $\bar{\varrho}$, and $\bar{\xi}$.

1. **Influence of λ_E on the number of non-dominated solutions, $\bar{n}_{alg}$.**

   Results for $\lambda_E = 2$ and $\lambda_E = 8$ show that all the algorithms struggled to find many non-dominated solutions irrespective of change frequency (refer to Figure 7.31) and irrespective of change severity (refer to Figure 7.34). All the algorithms produced the largest number of non-dominated solutions for $\lambda_E = 4$ and $\lambda_E = 6$ (refer to Figures E.55, E.58, E.61, E.64, E.67).

   The graphs indicate a decrease in the number of non-dominated solutions with increase in change frequency (refer to Figure 7.31).

   Results for $R_g = 800$ show that the EEMACOMH algorithm produced the lowest number of non-dominated solutions irrespective of the λ_E value (refer to Figure 7.34(b)).

2. **Influence of λ_E on the spread metric, $\bar{\varrho}$.**

Irrespective of the change frequency and change severity, for $\lambda_E = 2$ and $\lambda_E = 8$ all the algorithms displayed a higher value for $\bar{\varrho}$ which means less uniformly distributed solutions (refer to Figures E.56, E.59, E.62, E.65, and E.68). For $\lambda_E = 4$ and $\lambda_E = 6$ lower values of $\bar{\varrho}$ (more uniformly distributed solutions) were obtained.

A decrease in change frequency lead to more uniformly distributed solutions (refer to Figure 7.32). As pointed out in section 7.2.1 on page 160, as frequency of change decreases, the time available for adaptation becomes larger and the crowding distance operator is applied more times on the archive. At the end the archive will contain more non-dominated solutions which are in the least crowded area in the objective space, therefore, maintaining a good spread of non-dominated solutions.

The graphs indicate a deterioration of the solution spread with increase in change severity (refer to Figure 7.35). That is, high change severity negatively affected the solution spread. When the change severity increases there is not much information gained from the past to reuse, and it takes more time to optimise the problem and less time to explore, which explains the poor distribution of solutions as R_g increases.

The best solution distribution is produced with $\lambda_E = 4$ and $\lambda_E = 6$, for all change frequencies and all change severities (refer to Tables D.16-D.18 and Figures E.56, E.59, E.62, E.65, E.68, 7.32, 7.35).

3. **Influence of λ_E on the hypervolume metric, $\bar{\xi}$.**

   A general trend that is observed over all values of T_{sm} and R_g is that performance with reference to the hypervolume metric peaks at $\lambda_E = 4$ and $\lambda_E = 6$ (refer to Figures E.57, E.60, E.63, E.66, E.69, 7.33, and 7.36). Again, this indicates that a balance between exploration and exploitation is best for this dynamic environment. With $\lambda_E = 4$ and $\lambda_E = 6$, the relative difference of the pheromone trails is small enough to increase exploration of new paths and large enough to increase exploitation of existing paths.

   The graphs indicate an increase in $\bar{\xi}$ with decrease in change frequency (refer to Figure 7.33).

   There is no pattern between $\bar{\xi}$ and R_g, which indicates insensitivity of $\bar{\xi}$ to R_g (refer to Figure 7.36), excluding the EEMACOMH which showed a decrease in $\bar{\xi}$

with $R_g = 800$ (refer to Figure 7.36(b)).

A value of $\lambda_E = 4$ and $\lambda_E = 6$ offered the best trade-off between metrics $\bar{n}_{alg}$, $\bar{\varrho}$ and $\bar{\xi}$ for all change frequencies and all change severities. Accordingly, the value off $\lambda_E = 6$ was adopted for the remainder of the simulations.

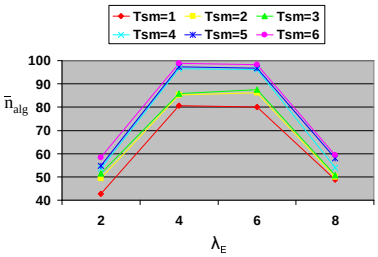

(a) EEMACOMP

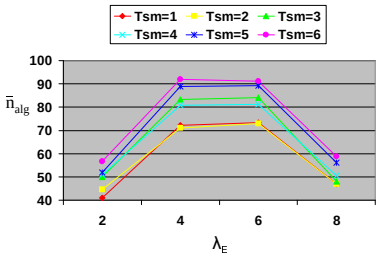

(b) EEMACOMH

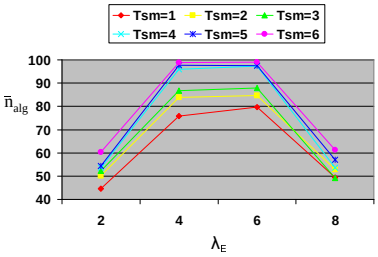

(c) EEMMASMP

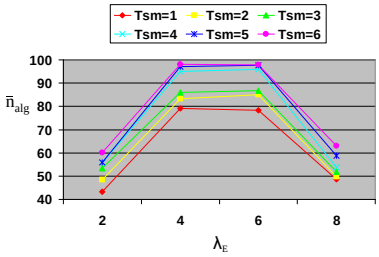

(d) EEMMASMH

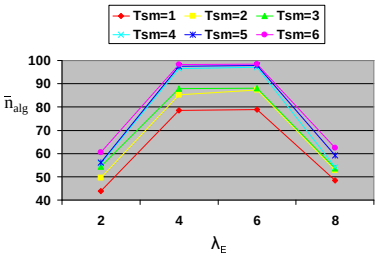

(e) EEMACOMC

Figure 7.31: Influence of λ_E on $\bar{n}_{alg}$ metric, for different change frequencies, T_{sm}

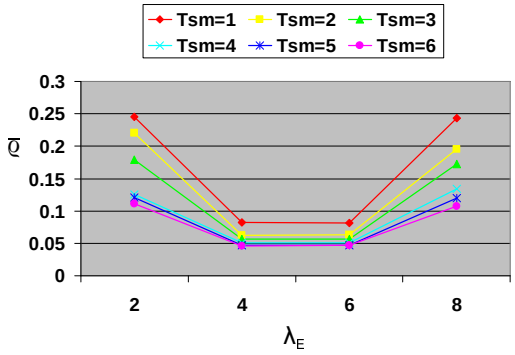

(a) EEMACOMP

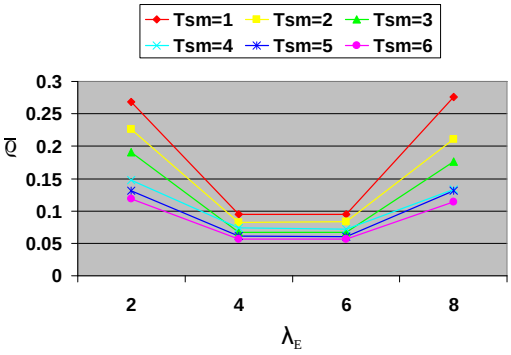

(b) EEMACOMH

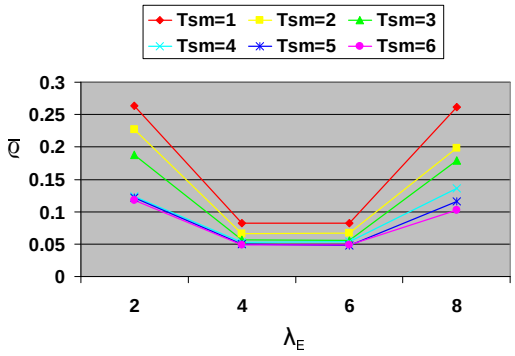

(c) EEMMASMP

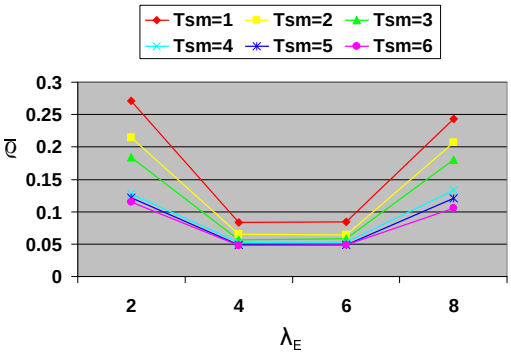

(d) EEMMASMH

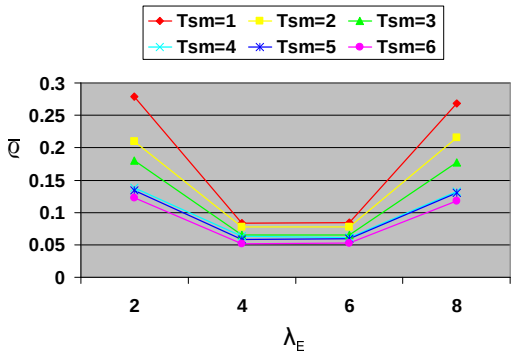

(e) EEMACOMC

Figure 7.32: Influence of λ_E on $\bar{\varrho}$ metric, for different change frequencies, T_{sm}

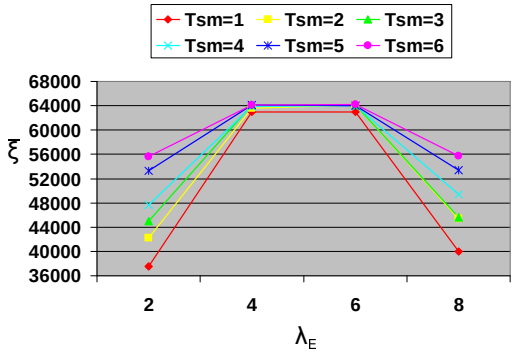

(a) EEMACOMP

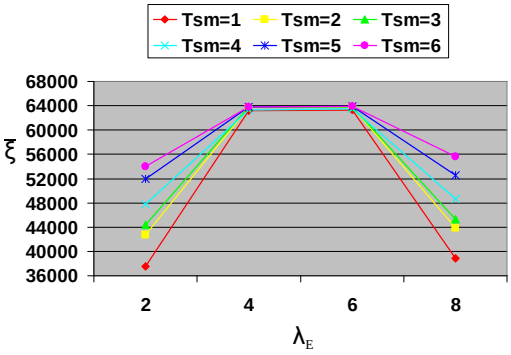

(b) EEMACOMH

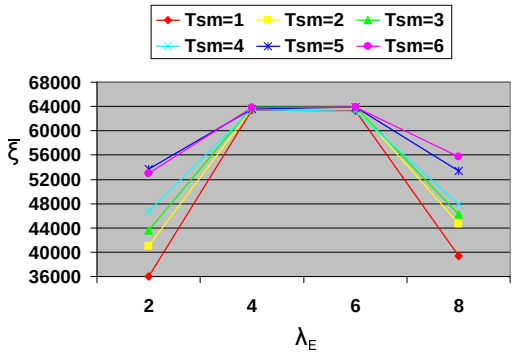

(c) EEMMASMP

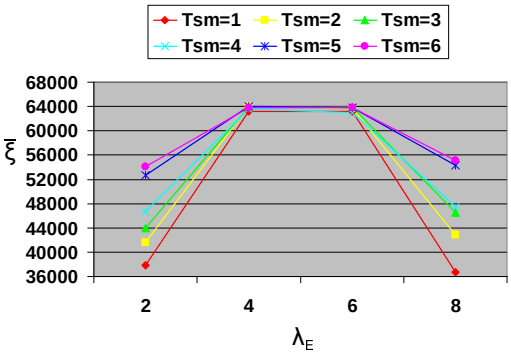

(d) EEMMASMH

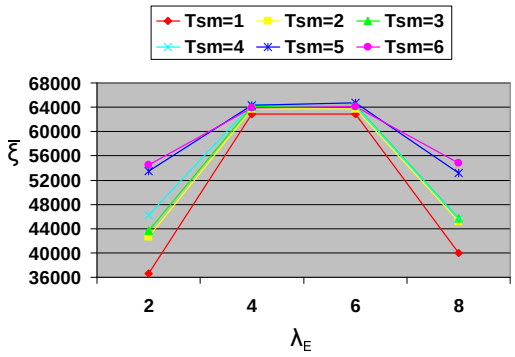

(e) EEMACOMC

Figure 7.33: Influence of λ_E on $\bar{\xi}$ metric, for different change frequencies, T_{sm}

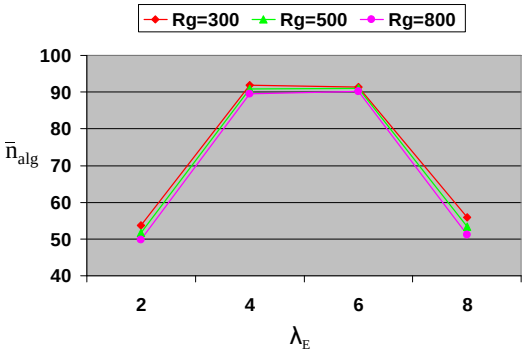

(a) EEMACOMP

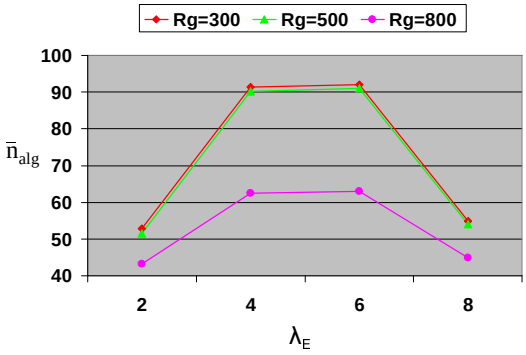

(b) EEMACOMH

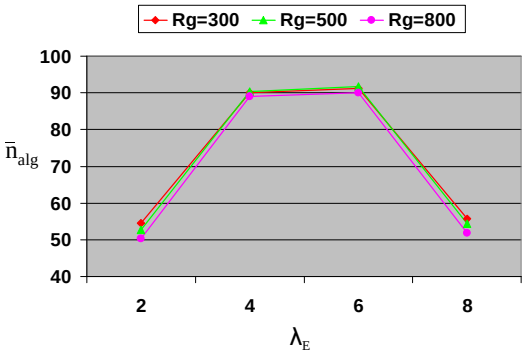

(c) EEMMASMP

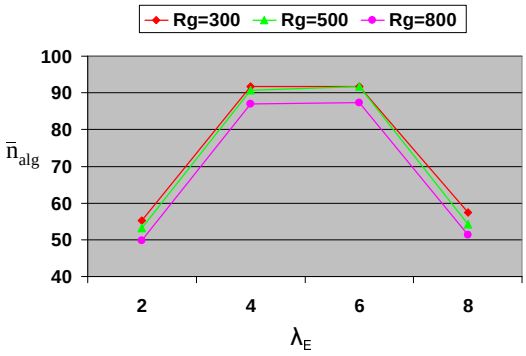

(d) EEMMASMH

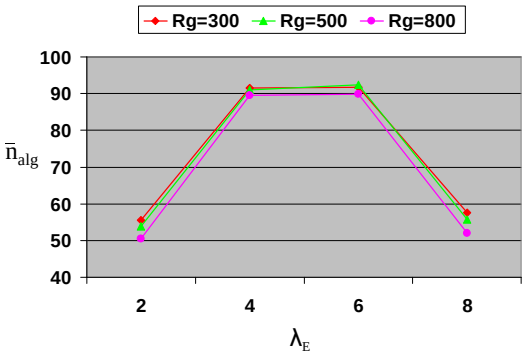

(e) EEMACOMC

Figure 7.34: Influence of λ_E on $\bar{n}_{alg}$ metric, for different change severities, R_g

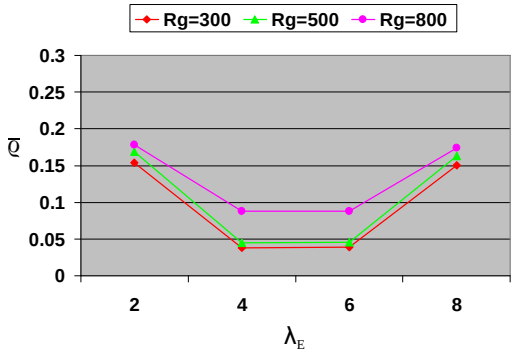

(a) EEMACOMP

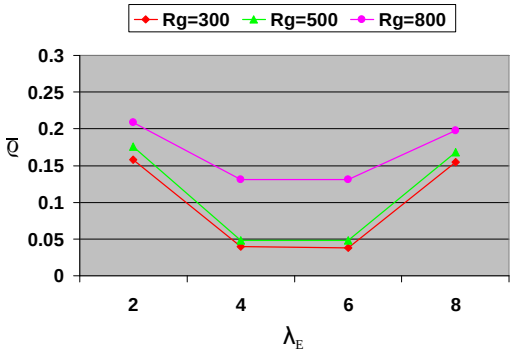

(b) EEMACOMH

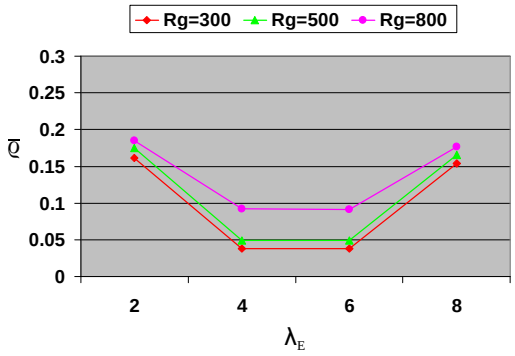

(c) EEMMASMP

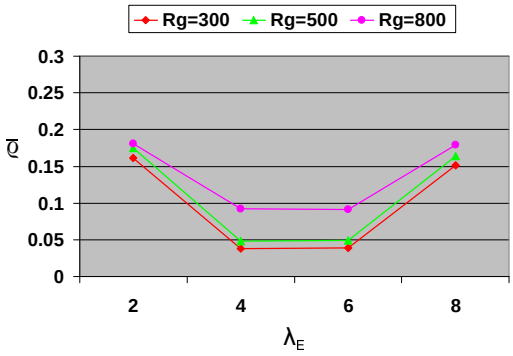

(d) EEMMASMH

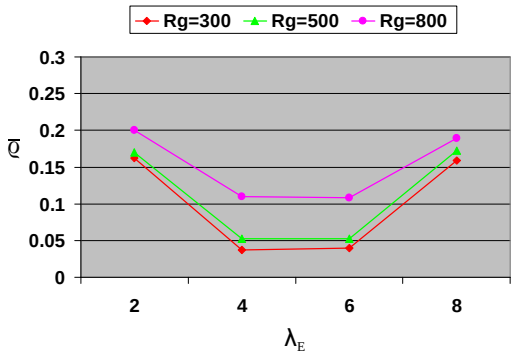

(e) EEMACOMC

Figure 7.35: Influence of λ_E on $\bar{\varrho}$ metric, for different change severities, R_g

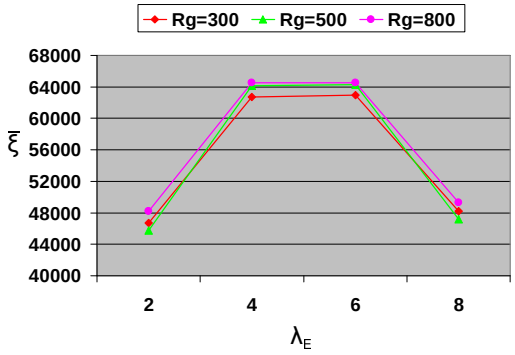

(a) EEMACOMP

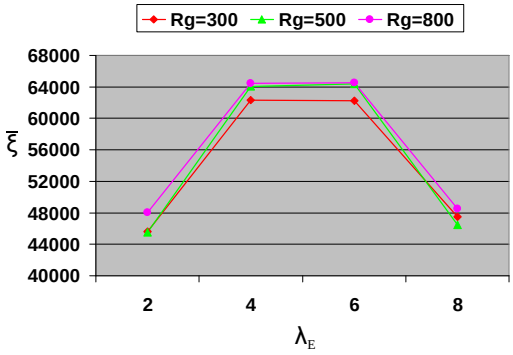

(b) EEMACOMH

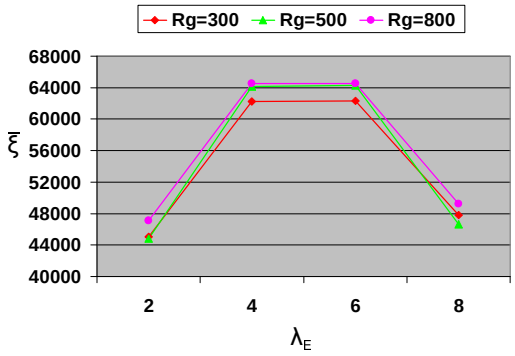

(c) EEMMASMP

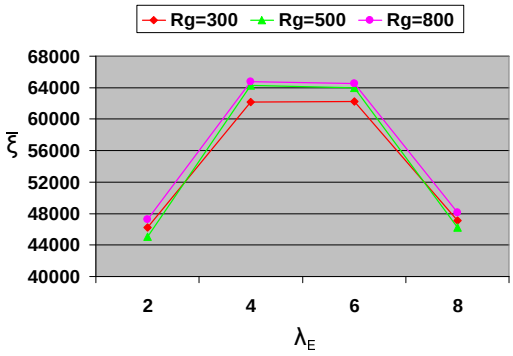

(d) EEMMASMH

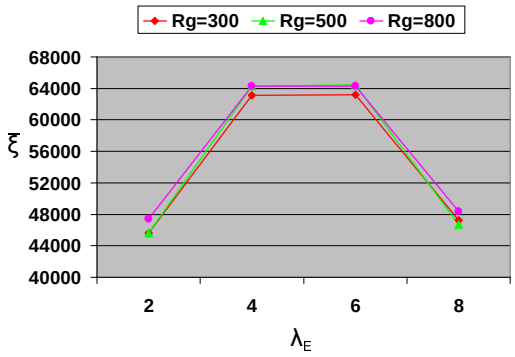

(e) EEMACOMC

Figure 7.36: Influence of λ_E on $\bar{\xi}$ metric, for different change severities, R_g

7.2.7 Importance of the Objectives Parameters

The parameters λ_ν, λ_ξ, λ_π, λ_ϱ, $\lambda_\varsigma \in [0, 1]$ are user-defined parameters which set the importance of the objectives in the search. For this thesis the assumption was made that the objectives have the same importance in the search. Therefore, the value for all λ_ψ was set to 0.2. It is suggested that future research investigates the influence of different values for these parameters on performance.

7.2.8 Pareto Archive Size

The size of the archive is fixed. If the number of solutions is more than the archive size, solutions which have high density in the objective space, i.e. solutions with a lower value of the crowding distance (refer to Section 4.6.2), are removed. On the other hand if the archive is not full, the current non-dominated solutions are added until the archive becomes full. Keeping a bound on the archive size may be important because the Pareto-optimal set may be infinitely large, but also because updating and searching through the archive will become very time-consuming if the archive is allowed to grow without bound.

The size of the Pareto archive was limited to 100 since this value has been used by different researchers [120, 225].

7.2.9 Summary of Ant Based Control Parameters which Affect Exploration and Exploitation

In order for ACO algorithms to be applied to DOPs, mechanisms should be employed that maintain diversity. This section summarises the control parameters for ACO algorithms which influence the exploration and exploitation.

- **Heuristics vs Pheromone Parameters, β_ψ**

  Parameters β_ψ=β_ν, β_ξ, β_π, β_ϱ, and β_ς set the relative importance of heuristic versus pheromone information. The larger the value of β_ψ, the smaller the emphasis on heuristic information, and learned desirability discovered by pheromone trails is favored. On the other hand, a small value for β_ψ gives higher priority to heuristic information over pheromone and the algorithm becomes more greedy and leads to increased exploration.

Higher values of β_ψ, and therefore a strong focus on pheromone information, produce a better solution spread. The highest number of non-dominated solutions and the best value for the hypervolume metric are obtained with a balance between exploration and exploitation which is achieved for the values of $(\beta_\nu,\ \beta_\xi,\ \beta_\pi,\ \beta_\varrho,\ \beta_\varsigma) \in \{(3.5, 4, 4.5, 4, 5),\ (4.5, 5, 3.5, 4, 4), (5, 5, 5, 5, 5)\}$.

- **Exploration Vs Exploitation Parameter,** r_0

  The parameter, r_0, is used in the ACS transition rule (refer to equations (6.20), (6.31), (6.54)) to control the balance between exploration and exploitation of the search space. Parameter r_0 takes values within the interval $[0, 1]$. When r_0 approaches zero, exploration is favoured. More focus can be given on exploitation instead of exploration by increasing the value of r_0.

  Irrespective of change frequencies and change severities, high exploration negatively affected the number of non-dominated solutions while for high exploitation all the algorithms produced the largest number of non-dominated solutions.

  The best values for the hypervolume and the solution spread were produced with a balance between exploration and exploitation which is achieved for the value of $r_0 = 0.5$, for all change frequencies and all change severities.

- **Local Decay Parameter,** ρ_l

  The local decay parameter, ρ_l, determines the rate at which pheromone on all the paths are evaporated after each step. Parameter ρ_l has values within the interval $[0, 1]$. A high value of ρ_l leaves less pheromone at each step. Consequently, the ants have less information on other ants' paths, and the search is less focused, favouring exploration. More focus can be given on exploitation instead of exploration by decreasing the value of ρ_l.

  A balance of exploration and exploitation is needed, which is achieved with a $\rho_l \in \{0.5, 0.7\}$. These values offer the best trade-off between metrics $\bar{n}_{alg}$, $\bar{\varrho}$ and $\bar{\xi}$ for all change frequencies and all change severities.

- **Global Decay Parameter,** ρ_g

  The global decay or global evaporation parameter, ρ_g, sets the amount of pheromone that evaporate on the paths after each iteration, as for ρ_l. A high value of ρ_g will help to find more solutions instead of focusing on a specific solution.

Irrespective of change frequencies and change severities, a balance of exploration and exploitation is needed, which is achieved with a $\rho_g \in \{0.5, 0.7\}$. These values offer the best trade-off between metrics $\bar{n}_{alg}$, $\bar{\varrho}$ and $\bar{\xi}$.

- **Pheromone Trail Concentrations Parameter,** α

  Diversification of the solution searching process in the solution space (exploration) can be emphasized by decreasing the value of α and exploitation can be increased by increasing the value of α. If $\alpha = 0$, no pheromone information is used, i.e. previous search experience is neglected. The search then degrades to a stochastic greedy search.

  For high values of α (high exploitation) all the algorithms produced a very low number of non-dominated solutions compared to lower values of α. The best values for α for the $\bar{n}_{alg}$ metric are for $\alpha \in \{1,\ 1.5,\ 2,\ 2.5\}$, for all change frequencies and all change severities

  There is a small deterioration of the solution spread with higher values of α. The best values for the solution spread were produced with $\alpha \in \{1,\ 1.5,\ 2\}$, for all change frequencies and all change severities.

  High exploration and high exploitation negatively affected the $\bar{\xi}$ metric. The best values for the hypervolume were produced with $\alpha \in \{1.5,\ 2,\ 2.5\}$, for all change frequencies and all change severities.

- **η-Strategy Parameter**

  The η-strategy parameter, noted λ_E, is used to determine the reset value to reinitialise pheromone values on links. The η-strategy is applied after a change in the environment occurs in order to promote diversity. If $\lambda_E \rightarrow \infty$ there is no pheromone conservation and exploration is emphasized. For lower values of λ_E there is a higher pheromone conservation and exploitation is promoted.

  A general trend that is observed over all values of change frequency and change severity is that performance with reference to all the three metrics peaks at $\lambda_E = 4$ and $\lambda_E = 6$. Again, this indicates that a balance between exploration and exploitation is best for this dynamic environment. With $\lambda_E = 4$ and $\lambda_E = 6$, the relative difference of the pheromone trails is small enough to increase exploration of new paths and large enough to increase exploitation of existing paths.

7.2.10 Summary of Ant Based Control Parameters

The performed empirical analysis of the ant based algorithms control parameters (refer to Sections 7.2.1-7.2.8) showed that the performance and quality of the ACO algorithms is sensitive to control parameters. The empirical analysis showed that a balance between exploration and exploitation is good for the dynamic power aware optimization problem. Also, high exploration negatively affected the number of non-dominated solutions and the solution spread for high change frequencies.

Table 7.3 summarises the simulation control parameters and their values as resulted from this empirical study for the proposed multi-objective power-aware routing ACO algorithms.

7.3 NSGA-II-MPA Parameters

The control parameters of NSGA-II-MPA have been optimised using the same process as described and conducted in section 7.2 for the ant-based algorithms. Table 7.4 lists the values for the NSGA-II-MPA parameters that produced the best results for these experiments.

7.4 Algorithm Comparison

This section has as its main objective to compare the EEMACOMP, EEMACOMH, EEMMASMP, EEMMASMH, and EEMACOMC algorithms to each other and also to the NSGA-II-MPA.

The remainder of this section is organised as follows: Subsection 7.4.1 describes the followed experimental procedure. Section 7.4.2 discusses performance with reference to the number of non-dominated solutions. Performance with reference to the spacing metric is covered in Section 7.4.3. Section 7.4.4 discusses the results with reference to the hypervolume metric. Section 7.4.5 analyses the performance of the algorithms over time with reference to the performance metrics. Section 7.4.6 discusses the performance of the optimisation criteria (power-aware routing objectives). Section 7.4.7 gives an overview of the ranking of the algorithms. Section 7.4.8 discusses the computational complexity of the algorithms, while Section 7.4.9 gives a summary of the overall performance of the algorithms.

Table 7.3: Simulation parameters for the MOO ACO algorithms

Parameter	Value	Applicable Algorithms
Number of Nodes, N_G	30, 100, 300	ALL
Transmission Range, T_r	400m	ALL
R_g	300m, 500m, 800m	ALL
Simulation Time	120	ALL
Mobility Model	RPGM	ALL
Number of Ants	25	ALL
Source Node, S	4	ALL
Destination Node, D	28 if $N_G = 30$ 98 if $N_G = 100$ or $N_G = 300$	ALL
Network Timer, T_{sm}	1, 2, 3, 4, 5, 6 sec	ALL
Exploration Vs Exploitation Parameter, r_0	0.5	EEMACOMP, EEMACOMH, EEMACOMC
Local Evaporation Parameter, ρ_l	0.5	EEMACOMP, EEMACOMH, EEMACOMC
Global Evaporation Parameter, ρ_g	0.7	ALL
α	1.50	EEMMASMP, EEMMASMH
Initial Energy for Node i, E_i	400	ALL
η-Strategy Parameter, λ_E	6	ALL
λ_ν	0.2	EEMACOMP, EEMMASMP
λ_ξ	0.2	EEMACOMP, EEMMASMP
λ_π	0.2	EEMACOMP, EEMMASMP
λ_ϱ	0.2	EEMACOMP, EEMMASMP
λ_ς	0.2	EEMACOMP, EEMMASMP
β_ν	3.5	ALL
β_ξ	4.0	ALL
β_π	4.5	ALL
β_ϱ	4.5	ALL
β_ς	5.0	ALL
Pareto Archive Size	100	ALL

Table 7.4: Simulation parameters for the NSGA-II algorithm

Parameter	value
Population size	100
Crossover probability	0.9
Mutation probability	0.125
R	256
N_e	30

7.4.1 Experimental Procedure

Each estimated pareto front, $\mathcal{PF}$, produced by the EEMACOMP, EEMACOMH, EEMMASMP, EEMMASMH, EEMACOMC, and NSGA-II-MPA algorithms is evaluated using three performance metrics, namely the $\bar{n}_{alg}$, $\bar{\varrho}$, and $\bar{\xi}$ (refer to Section 7.1.3). The performance of each algorithm was tested under different scenarios for different change frequencies, change severities and number of nodes as outlined in section 7.1.1. The influence of the change frequency, the change severity and the number of nodes on the performance of each algorithm was evaluated. For each of the scenarios 30 simulations were executed and results are reported as averages over these simulations together with the standard deviations.

Results obtained from the EEMACOMP, EEMACOMH, EEMMASMP, EEMMASMH, EEMACOMC, and NSGA-II-MPA algorithms are summarised in Tables F.1 to F.54 in the appendix F. Each table represents the results of the execution for each algorithm, for a specific scenario. A total of 54 scenarios, generated as listed in Table 7.2 for different values combinations of $N_G \in \{30, 100, 300\}$, $T_{sm} \in \{1, 2, 3, 4, 5, 6\}$, and $R_g \in \{300, 500, 800\}$, were tested.

In each table, the following information is provided for each algorithm:

- $\bar{n}_{alg}$: average number of non-dominated solutions found by each algorithm.
- $\bar{\varrho}$: average value of the spacing metric.
- $\bar{\xi}$: average value of the hypervolume metric.
- n^w_{alg} : number of times that the algorithm has a better $\bar{n}_{alg}$ than the others, for each environment change.

- ϱ^w : number of times that the algorithm has a better $\bar{\varrho}$ than the others, for each environment change.
- ξ^w : number of times that the algorithm has a better $\bar{\xi}$ than the others, for each environment change.
- *Rank* : overall rank of the algorithm. For each of the performance metrics the algorithm is ranked according to the number of times that the algorithm has a better performance than all the other algorithms with reference to this performance metric, for each environment change. The algorithm's average rank is calculated and then the algorithm is ranked accordingly.
- CI : the 95% confidence intervals using the t-test for each algorithm and each performance metric.

For all of the experiments, the algorithms used the best found values for the control parameters as listed in tables 7.3 and 7.4.

Appendix G presents three dimensional graphs to illustrate the influence of change frequency, T_{sm}, and change severity, R_g, on the performance metrics, $\bar{n}_{alg}$, $\bar{\varrho}$, and $\bar{\xi}$ for different number of nodes, based on Tables F.1 to F.54.

For each algorithm the following hypotheses or questions were investigated :

1. Is there a statistical significant difference in the performance of the algorithms?
2. Does performance deteriorate with increase in change frequency?
3. Does performance deteriorate with increase in change severity?
4. Are the algorithms scalable?
5. Is there an algorithm that is less affected by change frequency / change severity?

To test whether there is a statistical significant difference in the performance of any two algorithms, algorithm1 and algorithm2, with reference to the performance metric, p_{metric}, the following two hypotheses were considered:

$$H_0 : \quad \mu^{p_{metric}}_{algorithm1} = \mu^{p_{metric}}_{algorithm2}$$
$$H_1 : \quad \mu^{p_{metric}}_{algorithm1} > \mu^{p_{metric}}_{algorithm2}$$

where H_0 is the null hypothesis and H_1 is the alternative hypothesis.

In order to test these hypotheses the Mann-Whitney U test [129] was applied over the 30 p_{metric} values (one for each simulation) for each algorithm and for each T_{sm}, R_g and N_G combination. A 95% confidence level was used together with a 1-tail test. The critical value for U is 317, where U is the test statistic for the Mann-Whitney test. Results are illustrated in appendix H using Fluxviz [1] graphs. Each graph contains 4 axes. The first axis represents the change frequency, T_{sm}, the second axis represents the change severity, R_g, and the third axis represents the number of nodes, N_G. The last axis represents the results of the Mann-Whitney U test one for each of the T_{sm}, R_g and N_G combinations. Each combination corresponds to a specific scenario. If the null hypothesis, H_0, is accepted for a specific scenario, the value of 0 and the symbol "$\approx$" are displayed next to the scenario (last axis), showing that there is no statistical significant difference between the performance of the two compared algorithms. If H_0 is rejected the value of one and the symbol ">" are displayed next to the scenario, showing that the first algorithm is better than the second one for the respective scenario.

7.4.2 Number of Non-Dominated Solutions Metric

This subsection analyses the empirical results of each algorithm in terms of the average number of non-dominated solutions metric, $\bar{n}_{alg}$. The $\bar{n}_{alg}$ metric measures how well the algorithms performed in identifying solutions along the Pareto front. Larger values for $\bar{n}_{alg}$ are preferred as it indicates that many efficient solutions were found which is preferred by the decision maker.

Figures G.1-G.3 in Appendix G illustrate the influence of T_{sm} and R_g on the $\bar{n}_{alg}$ metric under different N_G values, using the values of Tables F.1 to F.54. The following observations can be made from the figures and tables:

1. **Influence of T_{sm} on the $\bar{n}_{alg}$ metric.**

   Figures G.1-G.3 indicate that $\bar{n}_{alg}$ increased for all ACO algorithms as T_{sm} increases (change frequency decreases). Figures G.1(f), G.2(f) and G.3(f) indicate that $\bar{n}_{alg}$ increased for the NSGA-II-MPA algorithm as T_{sm} increases, for all scenarios, excluding those with $N_G \in \{100, 300\}$ and $R_g = 800$.

Table 7.5 displays the average values for $\bar{n}_{alg}$ over all the N_G and R_g values while Figure 7.37 illustrates the results of Table 7.5. Table 7.5 and Figure 7.37 indicate that $\bar{n}_{alg}$ increased for each algorithm as change frequency decreases. This result is expected as low change frequencies (high pause time, T_{sm}) provides more time to explore the search space, thereby finding more solutions.

Table 7.5: Average value for $\bar{n}_{alg}$ over all the N_G and R_g values

	T_{sm}					
$\mathcal{PF}$	1	2	3	4	5	6
$P_{EEMACOMP}$	78.56	82.48	85.68	86.87	88.26	91.26
$P_{EEMACOMH}$	52.70	54.57	57.99	57.29	61.50	63.85
$P_{EEMMASMP}$	75.60	77.79	80.01	80.72	83.18	85.78
$P_{EEMMASMH}$	72.52	75.47	77.88	79.15	81.41	83.82
$P_{EEMACOMC}$	72.69	76.18	76.70	78.56	81.02	83.23
$P_{NSGA-II-MPA}$	34.99	39.40	41.67	41.58	41.33	41.72

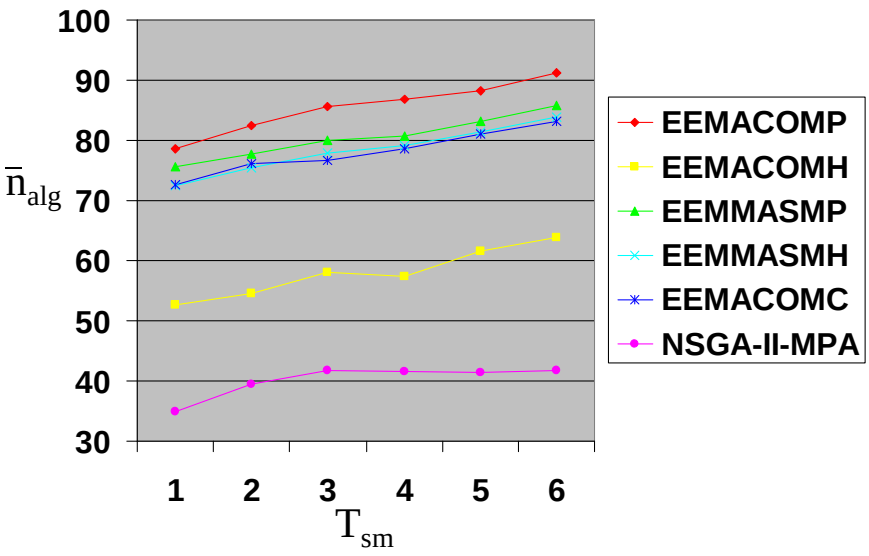

Figure 7.37: Average value for $\bar{n}_{alg}$ over all the N_G and R_g values

It is also to be noted from Table 7.5 and Figure 7.37 that EEMACOMH and NSGA-II-MPA are significantly worse than the other algorithms. In other words, EEMACOMH and NSGA-II-MPA do not scale well with reference to T_{sm}.

2. **Influence of R_g on the $\bar{n}_{alg}$ metric.**

Figures G.1-G.3 show that in most cases the number of non-dominated solutions decreased with increase in change severity, R_g. For the rest of the scenarios, $\bar{n}_{alg}$ increased when R_g increased to 500, and decreased again with $R_g = 800$. In order to better visualise the relation between R_g and $\bar{n}_{alg}$, Table 7.6 displays the average values for $\bar{n}_{alg}$ over all the N_G and T_{sm} values while Figure 7.38 illustrates the results of Table 7.6.

Table 7.6: Average value for $\bar{n}_{alg}$ over all the N_G and T_{sm} values

	R_g		
$\mathcal{PF}$	300	500	800
$P_{EEMACOMP}$	99.25	88.87	68.48
$P_{EEMACOMH}$	75.93	69.46	34.05
$P_{EEMMASMP}$	97.33	83.68	60.66
$P_{EEMMASMH}$	94.92	81.82	58.90
$P_{EEMACOMC}$	95.75	82.02	57.57
$P_{NSGA-II-MPA}$	53.15	41.62	25.92

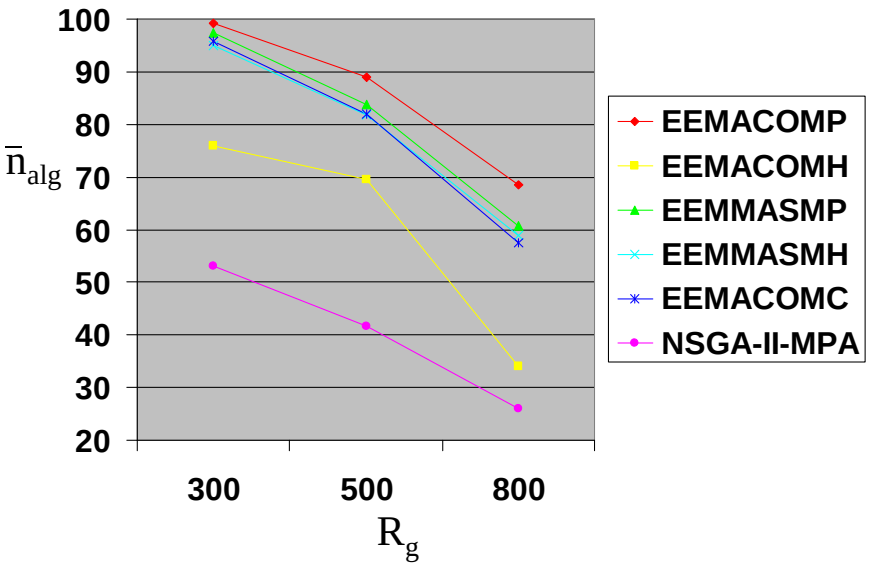

Figure 7.38: Average value for $\bar{n}_{alg}$ over all the N_G and T_{sm} values

Table 7.6 and Figure 7.38 show that when $\bar{n}_{alg}$ is taken as the average value over all the N_G and T_{sm} values, the number of non-dominated solutions decreased with increase in R_g. This trend is expected, because an increase in change severity, R_g, causes only some of the nodes to be within transmission range. The number of alternative paths by which to send a packet from source to destination and the number of non-dominated solutions therefore decreases.

It is also to be noted from Table 7.6 and Figure 7.38 that EEMACOMH and NSGA-II-MPA are affected the most by the change severity.

3. **Performance of multi-pheromone approaches vs single-pheromone approaches with reference to the $\bar{n}_{alg}$ metric.**

   Multi-pheromone approaches are EEMACOMP and EEMMASMP where a pheromone matrix is associated with each objective. Single-pheromone approaches are EEMACOMH and EEMMASMH where one pheromone matrix is associated with all the objectives.

   Figures G.1(a), G.2(a), G.3(a), G.1(c), G.2(c), and G.3(c) illustrate the influence of R_g and T_{sm} on the $\bar{n}_{alg}$ metric for the multi-pheromone approaches, while figures G.1(b), G.2(b), G.3(b), G.1(d), G.2(d), and G.3(d) illustrate the influence of R_g and T_{sm} on the $\bar{n}_{alg}$ metric for the single-pheromone approaches. The figures show that the multi-pheromone approaches produced a larger $\bar{n}_{alg}$ in most scenarios compared to single pheromone approaches.

   To test whether there is a statistical significant difference in the performance of the multi-pheromone approach, EEMACOMP, and the single pheromone approach, EEMACOMH, the following two hypotheses were considered:

$$H_0: \quad \mu^{\bar{n}_{alg}}_{EEMACOMP} = \mu^{\bar{n}_{alg}}_{EEMACOMH}$$
$$H_1: \quad \mu^{\bar{n}_{alg}}_{EEMACOMP} > \mu^{\bar{n}_{alg}}_{EEMACOMH}$$

   In order to test these hypotheses the Mann-Whitney U test was applied over all scenarios for the EEMACOMP and EEMACOMH.

Figure H.1 illustrates the results of the Mann-Whitney U test. Results show that the multi-pheromone approach, EEMACOMP, produced significantly more non-dominated solutions than the single pheromone approach, EEMACOMH, for 95% of the scenarios (all scenarios except scenarios with $\{N_G = 30,\ R_G = 300,\ T_{sm} \in \{3, 4, 5, 6\}\}$ and $\{N_G = 30,\ R_G = 500,\ T_{sm} \in \{3, 5, 6\}\}$). EEMACOMP increases the coverage of the solution space, therefore finding more non-dominated solutions than the EEMACOMH algorithm.

Following the same procedure as with EEMACOMP and EEMACOMH, to test whether there is a statistical significant difference in the performance of the multi-pheromone approach, EEMMASMP, and the single pheromone approach, EEMMASMH, the following two hypotheses were considered:

$$H_0: \ \mu^{\bar{n}_{alg}}_{EEMMASMP} = \mu^{\bar{n}_{alg}}_{EEMMASMH}$$
$$H_1: \ \mu^{\bar{n}_{alg}}_{EEMMASMP} > \mu^{\bar{n}_{alg}}_{EEMMASMH}$$

Results of the Mann-Whitney U test are illustrated in Figure H.2. The Mann-Whitney U test shows that EEMMASMP produced significantly more non-dominated solutions than EEMMASMH for all scenarios, excluding those with $\{N_G = 30,\ R_G \in \{300, 500\},\ \forall T_{sm}\}$ and $\{N_G = 300,\ R_G = 500,\ T_{sm} \in \{1, 2, 3\}\}$ (72% of the scenarios).

For the scenarios where the null hypothesis is rejected, EEMMASMP increases the coverage of the solution space, therefore finding more non-dominated solutions than the EEMMASMH algorithm.

4. **Performance of the multi-colony approach vs single-colony approaches with reference to the $\bar{n}_{alg}$ metric.**

   EEMACOMC is a multi-colony approach assigning a colony to each objective, while EEMACOMP, EEMACOMH, EEMMASMP, and EEMMASMH are single-colony approaches assigning the same colony for all objectives.

   Figures G.1(a), G.2(a), G.3(a), G.1(b), G.2(b), G.3(b), G.1(c), G.2(c), G.3(c), G.1(d), G.2(d), and G.3(d) illustrate the influence of R_g and T_{sm} on the $\bar{n}_{alg}$ metric

for the single-colony approaches, while figures G.1(e), G.2(e), and G.3(e) illustrate the influence of R_g and T_{sm} on the $\bar{n}_{alg}$ metric for the multi-colony approach.

Figures G.1(a), G.1(e), G.2(a), G.2(e), G.3(a), and G.3(e) show that the single-colony approach, EEMACOMP, produced in most scenarios more non-dominated solutions than the multi-colony approach, EEMACOMC.

To test whether there is a statistical significant difference in the performance of EEMACOMP and EEMACOMC the following two hypotheses were considered:

$$\begin{aligned} H_0: &\quad \mu^{\bar{n}_{alg}}_{EEMACOMP} = \mu^{\bar{n}_{alg}}_{EEMACOMC} \\ H_1: &\quad \mu^{\bar{n}_{alg}}_{EEMACOMP} > \mu^{\bar{n}_{alg}}_{EEMACOMC} \end{aligned}$$

Results of the Mann-Whitney U test are illustrated in Figure H.3. The Mann-Whitney U test shows that EEMACOMP is significantly better than EEMACOMC with reference to the $\bar{n}_{alg}$ metric for all scenarios with $N_G > 30$, excluding scenarios with $\{T_{sm} = 6,\ R_G = 300,\ N_G = 100\}$ and $\{T_{sm} = 1,\ R_G = 800,\ N_G = 100\}$ (better for 63% of the scenarios).

Figures G.1(b), G.1(e), G.2(b), G.2(e), G.3(b), and G.3(e) show that the multi-colony approach, EEMACOMC, produced in most scenarios more non-dominated solutions than the single-colony approach, EEMACOMH.

To test whether there is a statistical significant difference in the performance of EEMACOMC and EEMACOMH the following two hypotheses were considered:

$$\begin{aligned} H_0: &\quad \mu^{\bar{n}_{alg}}_{EEMACOMC} = \mu^{\bar{n}_{alg}}_{EEMACOMH} \\ H_1: &\quad \mu^{\bar{n}_{alg}}_{EEMACOMC} > \mu^{\bar{n}_{alg}}_{EEMACOMH} \end{aligned}$$

Results of the Mann-Whitney U test are illustrated in Figure H.4. The Mann-Whitney U test shows that EEMACOMC is significantly better than EEMACOMH with reference to the $\bar{n}_{alg}$ metric for all scenarios, excluding those with $\{N_G = 30,\ R_g = 300,\ T_{sm} \in \{3, 4, 5, 6\}\}$ and $\{N_G = 30,\ R_g = 500,\ T_{sm} \in \{5, 6\}\}$ (better for 88% of the scenarios).

5. **Performance of ACO approaches vs the NSGA-II-MPA approach with reference to the $\bar{n}_{alg}$ metric.**

   Figures G.1-G.3 show that all the ACO approaches displayed a higher value for $\bar{n}_{alg}$ when compared to the NSGA-II-MPA approach.

   To test whether there is a statistical significant difference in the performance of the ACO approaches and the NSGA-II-MPA approach the following two hypotheses were considered:

$$H_0: \quad \mu_{ACO}^{\bar{n}_{alg}} = \mu_{NSGA-II-MPA}^{\bar{n}_{alg}}$$
$$H_1: \quad \mu_{ACO}^{\bar{n}_{alg}} > \mu_{NSGA-II-MPA}^{\bar{n}_{alg}}$$

   where ACO takes the values EEMACOMP, EEMACOMH, EEMMASMP, EEMMASMH, and EEMACOMC.

   Results of the Mann-Whitney U tests are illustrated in Figures H.5-H.9. The Mann-Whitney U tests show that all the ACO approaches excluding EEMACOMH found significantly more non-dominated solutions than the NSGA-II-MPA approach, for all scenarios. EEMACOMH produced significantly more non-dominated solutions than NSGA-II-MPA for all scenarios, excluding those with $\{N_G \in \{100, 300\}$, $R_g = 800\ \}$ (better for 77% of the scenarios).

6. **Performance of ACS approaches vs MAX-MIN approaches with reference to the $\bar{n}_{alg}$ metric**.

   EEMACOMP and EEMACOMH are ACS approaches, while EEMMASMP and EEMMASMH are MAX-MIN approaches. Figures G.1(a), G.2(a), G.3(a), G.1(b), G.2(b), and G.3(b) illustrate the influence of R_g and T_{sm} on the $\bar{n}_{alg}$ metric for the ACS approaches, while Figures G.1(c), G.2(c), G.3(c), G.1(d), G.2(d), and G.3(d) illustrate the influence of R_g and T_{sm} on the $\bar{n}_{alg}$ metric for the MAX-MIN approaches.

   Figures G.1(a), G.1(c), G.1(d), G.2(a), G.2(c), G.2(d), G.3(a), G.3(c), and G.3(d) show that the ACS approach, EEMACOMP, produced a higher $\bar{n}_{alg}$ for higher number of nodes compared to the MAX-MIN approaches, EEMMASMP, and EEMMASMH.

To test whether there is a statistical significant difference in the performance of the EEMACOMP, and the EEMMASMP and EEMMASMH, approaches, the following two hypotheses were considered:

$$H_0: \ \mu^{\bar{n}_{alg}}_{EEMACOMP} = \mu^{\bar{n}_{alg}}_{EEMAXMIN}$$
$$H_1: \ \mu^{\bar{n}_{alg}}_{EEMACOMP} > \mu^{\bar{n}_{alg}}_{EEMAXMIN}$$

where EEMAXMIN takes the values EEMMASMP and EEMMASMH.

In order to test these hypotheses the Mann-Whitney U test was applied and the results are illustrated in Figures H.10 and H.11. Figure H.10 shows that EEMACOMP produced significantly more non-dominated solutions than EEMMASMP for all scenarios with $N_G = 100$ and $R_g = 800$, scenarios with $N_G = 300$, irrespective of T_{sm} and R_g, and scenarios with $\{R_g = 800,\ N_G = 30,\ T_{sm} \in \{1, 2, 3, 4\}\}$ (better for 63% of the scenarios). Figure H.11 shows that EEMACOMP produced significantly more non-dominated solutions than EEMMASMH for all scenarios, excluding those with $\{R_g = 300,\ N_G = 30,\ \forall T_{sm}\}$, $\{R_g = 500,\ N_G = 30,\ T_{sm} \in \{1, 3, 4, 5, 6\}\}$, $\{R_g = 800,\ N_G = 30,\ T_{sm} = 1\}$, and $\{R_g = 500,\ N_G = 100,\ T_{sm} = 6\}$ (better for 75% of the scenarios).

Figures G.1(b), G.1(c), G.1(d), G.2(b), G.2(c), G.2(d), G.3(b), G.3(c), and G.3(d) show that the MAX-MIN approaches, EEMMASMP and EEMMASMH, produced on average a higher $\bar{n}_{alg}$ compared to the ACS approach EEMACOMH.

To test whether there is a statistical significant difference in the performance of the EEMMASMP and EEMMASMH approaches, and the EEMACOMH approach, the following two hypotheses were considered:

$$H_0: \ \mu^{\bar{n}_{alg}}_{EEMAXMIN} = \mu^{\bar{n}_{alg}}_{EEMACOMH}$$
$$H_1: \ \mu^{\bar{n}_{alg}}_{EEMAXMIN} > \mu^{\bar{n}_{alg}}_{EEMACOMH}$$

In order to test these hypotheses the Mann-Whitney U test was applied and the results are illustrated in Figures H.12 and H.13. Figure H.12 shows that EEMMASMP produced significantly more non-dominated solutions than EEMACOMH

for all scenarios, except those with $\{R_g = 300,\ N_G = 30,\ T_{sm} \in \{3,4,5,6\}\}$ and $\{R_g = 500,\ N_G = 30,\ T_{sm} \in \{3,5,6\}\}$ (better for 87% of the scenarios). Figure H.13 shows the same results when comparing EEMMASMH and EEMACOMH.

7. **Influence of N_G on the $\bar{n}_{alg}$ metric.**

   Figures G.1-G.3 show that $\bar{n}_{alg}$ decreased for each algorithm as the number of nodes, N_G, increased. With increase in number of nodes the computational complexity is much higher and there is not enough time for the algorithms to explore the search space and to track the optima after the change occurred, thereby finding less solutions.

7.4.3 Spacing Metric

This subsection analyses the empirical results of each algorithm in terms of the average spacing metric, $\bar{\varrho}$. The spacing metric serves as an indicator of the distribution of solutions in the obtained Pareto front for each algorithm. The higher the value of $\bar{\varrho}$, the less uniformity in the distribution of solutions. The ideal value for the spacing metric is zero, in which case all solutions would be equidistantly spaced. Smaller values for $\bar{\varrho}$ are therefore preferred.

Figures G.4-G.6 in Appendix G illustrate the influence of T_{sm} and R_g on the $\bar{\varrho}$ metric under different N_G values, using the values of Tables F.1 to F.54. The following observations can be made from the figures and tables:

1. **Influence of T_{sm} on the $\bar{\varrho}$ metric.**

   Figures G.4-G.6 show that the solution spread improved ($\bar{\varrho}$ decreased) with decrease in change frequency. In order to derive different trends, Table 7.7 displays the average values for $\bar{\varrho}$ over all the N_G and R_g values while Figure 7.39 illustrates the results of Table 7.7.

   Table 7.7 and Figure 7.39 indicate that the solution spread improved with decrease in change frequency. Lower change frequencies provide more time to explore the search space. This helps to identify solutions along the full extent of the Pareto front and keeps the solutions more uniformly distributed in the whole Pareto-

Table 7.7: Average value for $\bar{\varrho}$ over all the N_G and R_g values

	T_{sm}					
$\mathcal{PF}$	1	2	3	4	5	6
$P_{EEMACOMP}$	0.084	0.070	0.062	0.057	0.056	0.050
$P_{EEMACOMH}$	0.129	0.114	0.101	0.102	0.097	0.087
$P_{EEMMASMP}$	0.093	0.082	0.072	0.068	0.065	0.059
$P_{EEMMASMH}$	0.098	0.085	0.077	0.073	0.070	0.066
$P_{EEMACOMC}$	0.110	0.095	0.084	0.080	0.077	0.070
$P_{NSGA-II-MPA}$	0.188	0.139	0.133	0.134	0.139	0.136

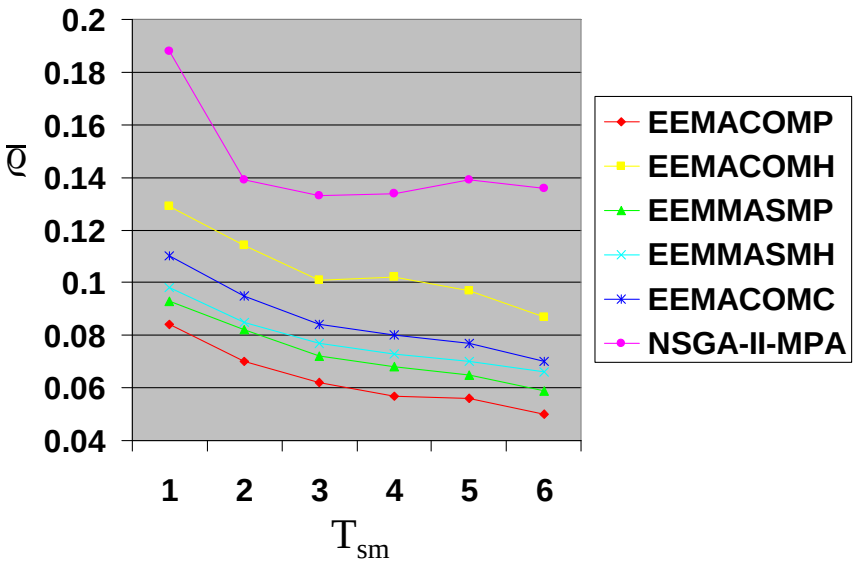

Figure 7.39: Average value for $\bar{\varrho}$ over all the N_G and R_g values

optimal set, instead of gathering in a small region. A decrease in change frequency leads to more uniformly distributed solutions, which justifies the obtained results.

It is also to be noted from Table 7.7 and Figure 7.39 that EEMACOMP is better than the other algorithms while NSGA-II-MPA is significantly worse than all the ACO algorithms.

2. **Influence of R_g on the $\bar{\varrho}$ metric.**

Figures G.4-G.6 show that, for all the ACO algorithms, the solution spread deteriorated with increase in change severity, R_g. The same applied to the NSGA-II-MPA algorithm for scenarios with $N_G = 30$. For scenarios with $N_G > 30$, NSGA-II-MPA had a strange behaviour: For scenarios with $N_G = 100$ (refer to Figure G.5(f)), NSGA-II-MPA had the worst solution spread for $R_g = 300$. With $R_g = 300$, the network has a small diameter and combined with a medium number of nodes ($N_G = 100$) may produce many redundant solutions. Redundancy may slow down the optimisation process and have a negative impact on the exploration ability of the algorithm. For scenarios with $N_G = 300$ (refer to Figure G.6(f)), NSGA-II-MPA had a parabolic behaviour with worst $\bar{\varrho}$ at $R_g = 500$ and best $\bar{\varrho}$ at $R_g = 300$. With $N_G = 300$ and $R_g = 300$, the redundancy of solutions is probably not uniform and may be beneficial for the optimisation process. From these solutions many new solution candidates may be reached, thus improving diversity.

In order to derive different trends, Table 7.8 displays the average values for $\bar{\varrho}$ over all the N_G and T_{sm} values while Figure 7.40 illustrates the results of Table 7.8. Table 7.8 and Figure 7.40 indicate that when $\bar{\varrho}$ is taken as the average value over all the N_G and T_{sm} values, $\bar{\varrho}$ increased (the solution spread deteriorated) with increase in R_G for all algorithms.

Table 7.8: Average value for $\bar{\varrho}$ over all the N_G and T_{sm} values

	R_g		
$\mathcal{PF}$	300	500	800
$P_{EEMACOMP}$	0.034	0.057	0.100
$P_{EEMACOMH}$	0.057	0.098	0.163
$P_{EEMMASMP}$	0.040	0.068	0.112
$P_{EEMMASMH}$	0.043	0.073	0.120
$P_{EEMACOMC}$	0.043	0.071	0.145
$P_{NSGA-II-MPA}$	0.106	0.125	0.200

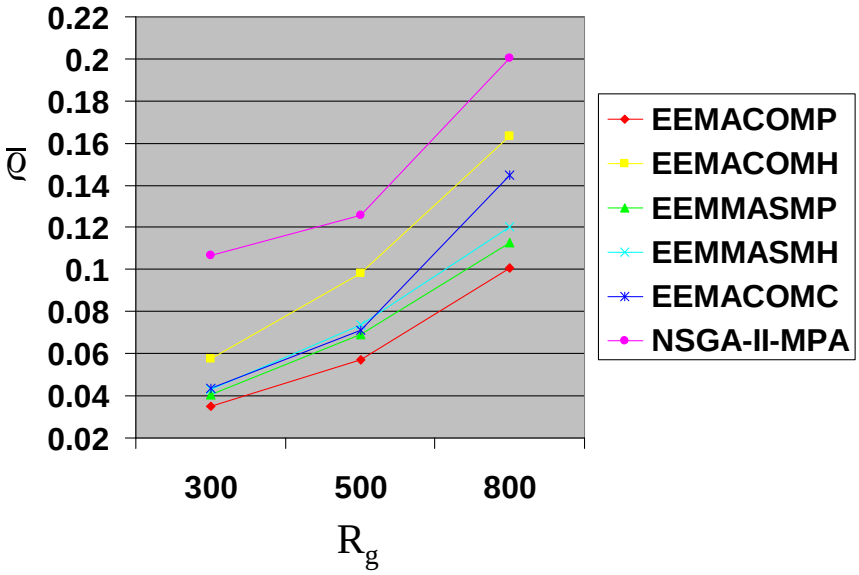

Figure 7.40: Average value for $\bar{\varrho}$ over all the N_G and T_{sm} values

The global range, R_g, relates to the connectivity of the network. When R_g is small the network is highly connected which means that it is easy to move from any one vertex to any other vertex in a few steps. Thus, the network has a small diameter and many alternate disjoint paths between vertices. With a high value of R_g, only part of the nodes are within transmission range from one another, and the number of alternative paths available to send a packet from source to destination decreases. Thus, it is logical that the diversity will deteriorate when the network range increases. On the other side, when the change severity, R_g, increases, it becomes more difficult for the optimiser to adapt current solutions to a changing environment. There is not much information gained from the past to reuse and it takes more time to optimise the problem and less time to explore, which explains the poor distribution of solutions as R_g increases.

It is also to be noted from Table 7.8 and Figure 7.40 that NSGA-II-MPA is significantly worse than all the ACO algorithms.

3. **Performance of multi-pheromone approaches vs single-pheromone ap-**

proaches with reference to $\bar{\varrho}$ metric.

Figures G.4(a), G.5(a), G.6(a), G.4(c), G.5(c), and G.6(c) illustrate the influence of R_g and T_{sm} on the $\bar{\varrho}$ metric for the multi-pheromone approaches, while Figures G.4(b), G.5(b), G.6(b), G.4(d), G.5(d), and G.6(d) illustrate the influence of R_g and T_{sm} on the $\bar{\varrho}$ metric for the single-pheromone approaches.

Figures G.4(a), G.4(b), G.5(a), G.5(b), G.6(a), and G.6(b) show that the multi-pheromone approach, EEMACOMP, outperformed the corresponding single pheromone approach, EEMACOMH, in terms of the solution spread. To test whether there is a statistical significant difference in the performance of the two approaches, the following two hypotheses were considered:

$$\begin{aligned} H_0: &\quad \mu^{\bar{\varrho}}_{EEMACOMP} = \mu^{\bar{\varrho}}_{EEMACOMH} \\ H_1: &\quad \mu^{\bar{\varrho}}_{EEMACOMP} > \mu^{\bar{\varrho}}_{EEMACOMH} \end{aligned}$$

In order to test these hypotheses the Mann-Whitney U test was applied over all scenarios for EEMACOMP and EEMACOMH.

Figure H.14 illustrates the results of the Mann-Whitney U test. Results show that the multi-pheromone approach, EEMACOMP, had a significantly better solution spread than the single pheromone approach, EEMACOMH, except for the scenario with $T_{sm} = 1$, $N_G = 30$, and $R_G = 500$ (better for 98% of the scenarios). EEMACOMP improves the coverage of the solution space, therefore, leading to more uniformly distributed solutions.

Figures G.4(c), G.4(d), G.5(c), G.5(d), G.6(c), and G.6(d) show that the multi-pheromone approach, EEMMASMP, produced results similar to the corresponding single pheromone approach, EEMMASMH, in terms of the solution spread. Following the same procedure as with EEMACOMP and EEMACOMH, the Mann-Whitney U test has been applied for EEMMASMP and EEMMASMH. The Mann-Whitney U test shows that there is no statistical significant difference in the average performance between EEMMASMP and EEMMASMH with reference to the $\bar{\varrho}$ metric except for 33% of the scenarios, i.e scenarios with ($R_g = 300$, $N_G = 100$, $T_{sm} \in \{3, 5, 6\}$), ($R_g = 800$, $N_G = 100$, $T_{sm} = 1$), ($R_g = 300$, $N_G = 300$,

$T_{sm} \in \{1, 3, 4, 5, 6\}$), ($R_g = 500$, $N_G = 300$, $T_{sm} \in \{2, 3, 4\}$), ($R_g = 500$, $N_G = 300$, $T_{sm} = 6$), and ($R_g = 800$, $N_G = 300$, $T_{sm} \in \{1, 3, 4, 5, 6\}$) (refer to Figure H.15).

4. **Performance of the multi-colony approach vs single-colony approaches with reference to $\bar{\varrho}$ metric**.

   Figures G.4(a), G.5(a), G.6(a), G.4(b), G.5(b), G.6(b), G.4(c), G.5(c), G.6(c), G.4(d), G.5(d), and G.6(d) illustrate the influence of R_g and T_{sm} on the $\bar{\varrho}$ metric for the single-colony approaches, while figures G.4(e), G.5(e), and G.6(e) illustrate the influence of R_g and T_{sm} on the $\bar{\varrho}$ metric for the multi-colony approach.

   Figures G.4(a), G.4(e), G.5(a), G.5(e), G.6(a), and G.6(e) show that the single-colony approach, EEMACOMP, produced in most scenarios a better solution spread than the multi-colony approach, EEMACOMC. To test whether there is a statistical significant difference in the performance of EEMACOMP and EEMACOMC the following two hypotheses were considered:

$$H_0: \quad \mu^{\bar{\varrho}}_{EEMACOMP} = \mu^{\bar{\varrho}}_{EEMACOMC}$$
$$H_1: \quad \mu^{\bar{\varrho}}_{EEMACOMP} > \mu^{\bar{\varrho}}_{EEMACOMC}$$

   Results of the Mann-Whitney U test are illustrated in Figure H.16. The Mann-Whitney U test shows that EEMACOMP is significantly better than EEMACOMC with reference to the $\bar{\varrho}$ metric for all scenarios, excluding scenarios with $\{N_G = 30, R_g = 300, T_{sm} \in \{3, 4, 6\}\}$, $\{N_G = 30, R_g = 500, T_{sm} = 5\}$, and $\{N_G = 100, R_g = 500, T_{sm} = 6\}$ (better for 90% of the scenarios).

   Figures G.4(b), G.4(e), G.5(b), G.5(e), G.6(b), and G.6(e) show that the multi-colony approach, EEMACOMC produced in most scenarios a better solution spread than the single-colony approach, EEMACOMH.

   To test whether there is a statistical significant difference in the performance of EEMACOMC and EEMACOMH the following two hypotheses were considered:

$$H_0: \quad \mu^{\bar{\varrho}}_{EEMACOMC} = \mu^{\bar{\varrho}}_{EEMACOMH}$$
$$H_1: \quad \mu^{\bar{\varrho}}_{EEMACOMC} > \mu^{\bar{\varrho}}_{EEMACOMH}$$

Results of the Mann-Whitney U test are illustrated in Figure H.17. The Mann-Whitney U test shows that EEMACOMC is significantly better than EEMACOMH with reference to the $\bar{\varrho}$ metric for all scenarios, excluding scenarios with $\{N_G = 30,\ R_g = 300,\ T_{sm} \in \{2,3\}\}$, $\{N_G = 30,\ R_g = 500,\ T_{sm} = 6\}$, $\{N_G = 30,\ R_g = 800,\ T_{sm} \in \{3,5\}\}$, and $\{N_G = 100,\ R_g = 800,\ T_{sm} = 1\}$ (better for 89% of the scenarios).

5. **Performance of ACO approaches vs NSGA-II-MPA approach with reference to $\bar{\varrho}$ metric**.

   Figures G.4-G.6 show that all the ACO approaches produced in most scenarios a better solution spread compared to the NSGA-II-MPA approach.

   To test whether there is a statistical significant difference in the performance of the ACO approaches and the NSGA-II-MPA approach the following two hypotheses were considered:

$$H_0: \ \mu^{\bar{\varrho}}_{ACO} = \mu^{\bar{\varrho}}_{NSGA-II-MPA}$$
$$H_1: \ \mu^{\bar{\varrho}}_{ACO} > \mu^{\bar{\varrho}}_{NSGA-II-MPA}$$

   Results of the Mann-Whitney U tests are illustrated in Figures H.18-H.22. The Mann-Whitney U tests show that all the ACO approaches produced significantly better solution spread than the NSGA-II-MPA approach for all scenarios, excluding the following scenarios: $\{N_G = 30,\ R_g = 500,\ T_{sm} \in \{1,2\}\}$, $\{N_G = 100,\ R_g = 500,\ T_{sm} \in \{3,4,5,6\}\}$, $\{N_G = 100,\ R_g = 800,\ T_{sm} \in \{4,5,6\}\}$, and $\{N_G = 300,\ R_g = 800,\ T_{sm} \in \{3,4\}\}$ for EEMACOMP (better for 80% of the scenarios), $\{N_G = 30,\ R_g = 500,\ T_{sm} \in \{1,2,3\}\}$, $\{N_G = 100,\ R_g = 500,\ T_{sm} \in \{1,2\}\}$, and $\{N_G = 300,\ R_g = 300,\ T_{sm} \in \{1,2,4,5,6\}\}$ for EEMACOMH (better for 83% of the scenarios), $\{N_G = 30,\ R_g = 500,\ T_{sm} \in \{1,2,3\}\}$, $\{N_G = 100,\ R_g = 500,\ T_{sm} \in \{1,2,6\}\}$, and $\{N_G = 300,\ R_g = 800,\ T_{sm} \in \{2,5\}\}$ for EEMMASMP (better for 85% of the scenarios), $\{N_G = 30,\ R_g = 500,\ T_{sm} \in \{1,2,3\}\}$, $\{N_G = 100,\ R_g = 500,\ T_{sm} \in \{2,6\}\}$, and $\{N_G = 300,\ R_g = 800,\ T_{sm} \in \{5,6\}\}$ for EEMMASMH (better for 87% of the scenarios), and $\{N_G = 30,\ R_g = 500,\ T_{sm} \in \{2,3\}\}$, $\{N_G = 100,$

$R_g = 500, \forall\ T_{sm}\ \}$, and $\{N_G = 300,\ R_g = 800,\ T_{sm} \in \{6\}\}$ for EEMACOMC (better for 83% of the scenarios).

6. **Performance of ACS approaches vs MAX-MIN approaches with reference to $\bar{\varrho}$ metric**.

   Figures G.4(a), G.5(a), G.6(a), G.4(b), G.5(b), and G.6(b) illustrate the influence of R_g and T_{sm} on the $\bar{\varrho}$ metric for the ACS approaches, while Figures G.4(c), G.5(c), G.6(c), G.4(d), G.5(d), and G.6(d) illustrate the influence of R_g and T_{sm} on the $\bar{\varrho}$ metric for the MAX-MIN approaches.

   Figures G.4(a), G.4(c), G.4(d), G.5(a), G.5(c), G.5(d), G.6(a), G.6(c), and G.6(d) show that the ACS approach, EEMACOMP, produced in most scenarios a better solution spread for $N_G > 30$ compared to the MAX-MIN approaches, EEMMASMP and EEMMASMH.

   To test whether there is a statistical significant difference in the performance of EEMACOMP and the EEMMASMP and EEMMASMH approaches, the following two hypotheses were considered:

$$H_0: \quad \mu^{\bar{\varrho}}_{EEMACOMP} = \mu^{\bar{\varrho}}_{EEMAXMIN}$$
$$H_1: \quad \mu^{\bar{\varrho}}_{EEMACOMP} > \mu^{\bar{\varrho}}_{EEMAXMIN}$$

   In order to test these hypotheses the Mann-Whitney U test was applied and the results are illustrated in Figures H.23 and H.24. Figure H.23 shows that EEMACOMP, produced a significantly better solution spread than EEMMASMP for $N_G > 30$ excluding scenario with $\{N_G = 100,\ R_g = 800,\ T_{sm} = 1\}$ (better for 65% of the scenarios), while Figure H.24 indicates that EEMACOMP, produced a significantly better solution spread than EEMMASMH for $N_G > 30$ (better for 66% of the scenarios).

   Figures G.4(b), G.4(c), G.4(d), G.5(b), G.5(c), G.5(d), G.6(b), G.6(c), and G.6(d) show that the MAX-MIN approaches, EEMMASMP and EEMMASMH, produced

in most scenarios a better solution spread compared to the ACS approach EEMACOMH.

To test whether there is a statistical significant difference in the performance of the EEMMASMP and EEMMASMH approaches, and the EEMACOMH approach, the following two hypotheses were considered:

$$H_0: \ \mu^{\bar{\varrho}}_{EEMAXMIN} = \mu^{\bar{\varrho}}_{EEMACOMH}$$
$$H_1: \ \mu^{\bar{\varrho}}_{EEMAXMIN} > \mu^{\bar{\varrho}}_{EEMACOMH}$$

In order to test these hypotheses the Mann-Whitney U test was applied and the results are illustrated in Figures H.25 and H.26. Figure H.25 shows that EEMMASMP had a significantly better solution spread than EEMACOMH, except for scenarios with $\{N_G = 30,\ R_g = 300,\ T_{sm} \in \{1, 2\}\}$, and $\{N_G = 30,\ R_g = 500,\ T_{sm} \in \{1, 2, 3, 4, 6\}\}$ (better for 87% of the scenarios). Figure H.26 indicates that EEMMASMH had a significantly better solution spread than EEMACOMH for all scenarios, except those with $\{N_G = 30,\ R_g = 300,\ T_{sm} = 1\}$, and $\{N_G = 30,\ R_g = 500,\ T_{sm} \in \{1, 2, 3, 4, 5, 6\}\}$ (better for 87% of the scenarios).

7. **Influence of N_G on the $\bar{\varrho}$ metric.**

   Figures G.4-G.6 show that when the number of nodes increased from 100 to 300 the distribution of solutions for all algorithms deteriorated. This is both an interesting and an unexpected result, which is possibly related to the computational complexity of the algorithms and scalability. The problem with scalability is that, as the number of nodes increases, it becomes necessary for the routing protocol to search more nodes in order to reach the destination, thus affecting diversity. When the number of nodes increased from 30 to 100 the distribution of solutions for all algorithms improved.

7.4.4 Hypervolume Metric

This subsection analyses the empirical results of each algorithm in terms of the hypervolume metric, $\bar{\xi}$. The hypervolume metric measures how well the algorithms performed

in identifying solutions along the full extent of the Pareto front. High values of the hypervolume metric indicate the closeness of the solutions to the optimal Pareto set.

Figures G.7-G.9 in Appendix G illustrate the influence of T_{sm} and R_g on the $\bar{\xi}$ metric under different N_G values, using the values of Tables F.1 to F.54. The following observations can be made from the figures and tables:

1. **Influence of T_{sm} on the hypervolume metric, $\bar{\xi}$.**

   Figures G.7-G.9 show a small increase of $\bar{\xi}$ as change frequency decreases, for all the ACO algorithms. This observation is confirmed when looking at Table 7.9 and Figure 7.41. Table 7.9 displays the average values for $\bar{\xi}$ over all the N_G and R_g values while Figure 7.41 illustrates the results of Table 7.9. This observation is expected as change frequency determines how often the problem changes and it seems intuitive to assume that a high change frequency makes a problem more difficult for an algorithm to solve as less time is available at each T_{sm} to reach the new global optima and optimise the multi-objective problem. Low change frequency gives more iterations, and theoretically is supposed to produce a uniform distribution of the solutions and closeness of the solutions to the optimal Pareto set.

Table 7.9: Average value for $\bar{\xi}$ over all the N_G and R_g values

	T_{sm}					
$\mathcal{PF}$	1	2	3	4	5	6
$P_{EEMACOMP}$	60831.05	61552.60	61894.07	62010.58	62179.96	62485.17
$P_{EEMACOMH}$	59205.85	59677.70	59843.11	59936.95	60076.63	60365.10
$P_{EEMMASMP}$	60410.77	60999.21	61421.41	61440.03	61678.51	61995.58
$P_{EEMMASMH}$	60264.39	60804.01	61252.15	61290.71	61489.01	61811.21
$P_{EEMACOMC}$	61033.57	61753.97	62181.59	62308.67	62439.49	62701.89
$P_{NSGA-II-MPA}$	61514.60	60201.54	60078.20	60028.05	60041.14	60048.25

2. **Influence of R_g on the hypervolume metric, $\bar{\xi}$.**

   For the ACO algorithms there are different observations according to the number of nodes. Figure G.7 shows an increase in $\bar{\xi}$ when R_g increases to 500 and a decrease in $\bar{\xi}$ when R_g increases to 800, for scenarios with $N_G = 30$. For most scenarios with $N_G = 100$, there is an increase in $\bar{\xi}$ with increase in change severity (refer to Figure G.8). For scenarios with $N_G = 300$, Figure G.9 shows an increase in $\bar{\xi}$ with decrease in change severity.

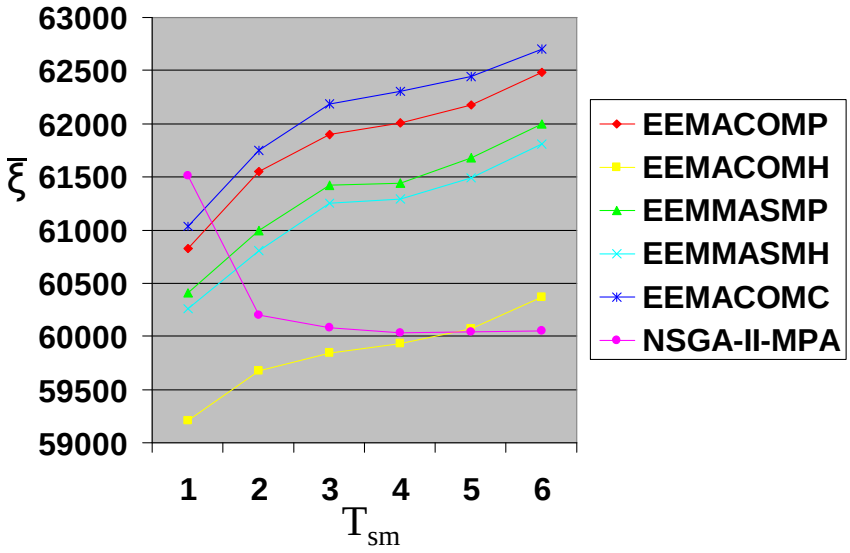

Figure 7.41: Average value for $\bar{\xi}$ over all the N_G and R_g values

For the NSGA-II-MPA algorithm, Figure G.7(f) shows an increase in $\bar{\xi}$ with increase in change severity, for scenarios with $N_G = 30$. For scenarios with $N_G = 100$, there is a decrease in $\bar{\xi}$ when R_g increases to 500 and an increase in $\bar{\xi}$ when R_g increases to 800 (refer to Figure G.8(f)). For scenarios with $N_G = 300$, Figure G.9(f) shows an increase in $\bar{\xi}$ when R_g increases to 500, and a decrease in $\bar{\xi}$ when R_g increases to 800.

Table 7.10: Average value for $\bar{\xi}$ over all the N_G and T_{sm} values

	R_g		
$\mathcal{PF}$	300	500	800
$P_{EEMACOMP}$	62046.719	62895.465	60677.192
$P_{EEMACOMH}$	60746.295	61105.342	57976.182
$P_{EEMMASMP}$	61491.817	62542.096	60083.312
$P_{EEMMASMH}$	61459.620	62419.858	59746.060
$P_{EEMACOMC}$	62708.710	62870.936	60783.509
$P_{NSGA-II-MPA}$	57908.890	59735.745	63251.480

Table 7.10 displays the average values for $\bar{\xi}$ over all the N_G and T_{sm} values while Figure 7.42 illustrates the results of Table 7.10. Table 7.10 and Figure 7.42 show

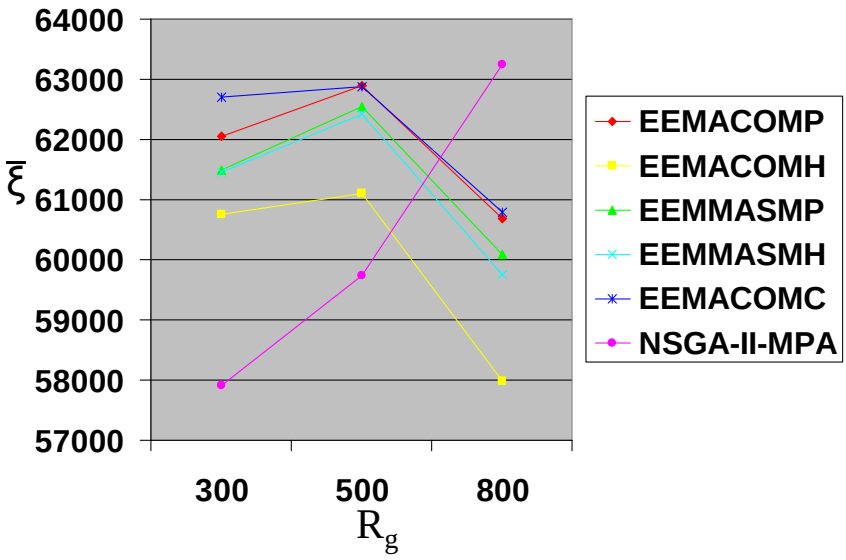

Figure 7.42: Average value for $\bar{\xi}$ over all the N_G and T_{sm} values

that when $\bar{\xi}$ is taken as the average value over all the N_G and T_{sm} values, $\bar{\xi}$ sharply decreases for $R_g = 800$ for the ACO algorithms and $\bar{\xi}$ sharply increases for $R_g = 800$ for the NSGA-II-MPA, outperforming the ACO algorithms. The expected result is a decrease in $\bar{\xi}$ with increase in change severity: It is a common assumption that smaller change severities are easier to adapt to, primarily by transferring solutions from the past optimisation problem which may help to accelerate the rate of convergence to the optima, after a change has occurred. Since R_g determines the change severity, the convergence to the optima, and therefore the closeness of the solutions to the optimal Pareto set, should be getting worse as the change severity increases.

3. **Performance of multi-pheromone approaches vs single-pheromone approaches with reference to the hypervolume metric.**

   Figures G.7(a), G.8(a), G.9(a), G.7(c), G.8(c), and G.9(c) illustrate the influence of R_g and T_{sm} on the $\bar{\xi}$ metric for the multi-pheromone approaches, while figures G.7(b), G.8(b), G.9(b), G.7(d), G.8(d), and G.9(d) illustrate the influence of

R_g and T_{sm} on the $\bar{\xi}$ metric for the single-pheromone approaches.

Figures G.7(a), G.7(b), G.8(a), G.8(b), G.9(a), and G.9(b) show that the multi-pheromone approach, EEMACOMP, displayed a higher value for the $\bar{\xi}$ metric compared to the single pheromone approach, EEMACOMH.

To test whether there is a statistical significant difference in the performance of EEMACOMP and EEMACOMH the following two hypotheses were considered:

$$H_0: \ \mu^{\bar{\xi}}_{EEMACOMP} = \mu^{\bar{\xi}}_{EEMACOMH}$$
$$H_1: \ \mu^{\bar{\xi}}_{EEMACOMP} > \mu^{\bar{\xi}}_{EEMACOMH}$$

In order to test these hypotheses the Mann-Whitney U test was applied over all scenarios for the EEMACOMP and EEMACOMH.

Figure H.27 illustrates the results of the Mann-Whitney U test. Results show that EEMACOMP produced a significantly higher value for the $\bar{\xi}$ metric than EEMACOMH for all scenarios, excluding those with $\{N_G = 30,\ R_g = 500,\ T_{sm} = 1\}$ and $\{N_G = 30,\ R_g = 800,\ T_{sm} = 1\}$ (better for 96% of the scenarios).

4. **Performance of the multi-colony approach vs single-colony approaches with reference to the hypervolume metric.**

   Figures G.7(a), G.8(a), G.9(a), G.7(b), G.8(b), G.9(b), G.7(c), G.8(c), G.9(c), G.7(d), G.8(d), and G.9(d) illustrate the influence of R_g and T_{sm} on the $\bar{\xi}$ metric for the single-colony approaches, while figures G.7(e), G.8(e), and G.9(e) illustrate the influence of R_g and T_{sm} on the $\bar{\xi}$ metric for the multi-colony approach.

   Figures G.7(b), G.7(e), G.8(b), G.8(e), G.9(b), and G.9(e) show that the multi-colony approach, EEMACOMC, produced in most scenarios a higher value for the hypervolume metric than the single-colony approach, EEMACOMH.

   To test whether there is a statistical significant difference in the performance of EEMACOMC and EEMACOMH the following two hypotheses were considered:

$$H_0: \ \mu^{\bar{\xi}}_{EEMACOMC} = \mu^{\bar{\xi}}_{EEMACOMH}$$
$$H_1: \ \mu^{\bar{\xi}}_{EEMACOMC} > \mu^{\bar{\xi}}_{EEMACOMH}$$

Results of the Mann-Whitney U test are illustrated in Figure H.28. The Mann-Whitney U test shows that EEMACOMC is significantly better than EEMACOMH with reference to the $\bar{\xi}$ metric for all scenarios, excluding scenarios with $\{N_G = 30,\ R_g = 500,\ T_{sm} = 1\}$ and $\{N_G = 30,\ R_g = 800,\ T_{sm} \in \{2, 6\}\}$ (better for 94% of the scenarios).

5. **Performance of ACO approaches vs the NSGA-II-MPA approach with reference to the hypervolume metric.**

   Figures G.7-G.9 and Tables F.1 to F.54 show that all the ACO approaches displayed a higher value for the hypervolume metric when compared to the NSGA-II-MPA approach, except for scenarios with $N_G = 300$ and $R_g \in \{500, 800\}$ and for scenarios with $N_G = 30$ and $R_g = 800$.

   To test whether there is a statistical significant difference in the performance of the ACO approaches and the NSGA-II-MPA approach the following two hypotheses were considered:

$$H_0: \ \mu^{\bar{\xi}}_{ACO} = \mu^{\bar{\xi}}_{NSGA-II-MPA}$$
$$H_1: \ \mu^{\bar{\xi}}_{ACO} > \mu^{\bar{\xi}}_{NSGA-II-MPA}$$

   Results of the Mann-Whitney U tests are illustrated in Figures H.29-H.33. The Mann-Whitney U tests show that all the ACO approaches displayed a significantly higher value for the hypervolume than the NSGA-II-MPA approach for all scenarios, excluding the following scenarios: $\{N_G = 30,\ R_g = 800,\ T_{sm} = 1\}$, $\{N_G = 100,\ R_g = 300,\ T_{sm} = 2\}$, $\{N_G = 100,\ R_g = 500,\ T_{sm} = 1\}$, and $\{N_G = 100,\ R_g = 800,\ T_{sm} = 1\}$ for EEMACOMP, EEMMASMP and EEMMASMH (better for 92% of the scenarios), $\{N_G = 30,\ R_g = 800,\ T_{sm} = 1\}$, $\{N_G = 100,\ R_g = 300,\ T_{sm} = 4\}$,

and $\{N_G = 100,\ R_g = 800,\ T_{sm} \in \{2, 3, 4\}$ for EEMACOMH (better for 90% of the scenarios), $\{N_G = 30,\ R_g = 800,\ T_{sm} \in \{1, 2\}\}$, $\{N_G = 100,\ R_g = 300,\ T_{sm} = 2\}$, and $\{N_G = 100,\ R_g = 500,\ T_{sm} = 1\}$ for EEMACOMC (better for 92% of the scenarios).

6. **Performance of ACS approaches vs MAX-MIN approaches with reference to the hypervolume metric**.

   Tables F.1 to F.54 and Figures G.7-G.9 show no trend between the performance of the ACS approaches and the MAX-MIN approaches with reference to the hypervolume metric.

7. **Influence of N_G on the hypervolume metric.**

   Figures G.7-G.9 show that, for scenarios with $N_G = 300$ and $R_g = 800$, all algorithms displayed a lower value for the hypervolume metric.

   There are two possible explanations for this result:

   (a) Computational complexity of the algorithms: As the number of nodes increases it becomes necessary for the routing protocol to search more nodes in order to reach the destination, which, in turn, increases the convergence time and affects closeness towards the true Pareto front.

   (b) Premature convergence towards local optima: With a high number of nodes the population tends to contain similar individuals and the diversity decreases rapidly. The suboptimal solutions which may have helped in finding the global optima are deleted too rapidly and the closeness towards the true Pareto front gets worst.

7.4.5 Performance of the Algorithms Over the Environmental Changes

This subsection compares the performance of the algorithms for each environment change. For each environmental change the average values for all the solutions of the iteration before a change to the environment occurs were calculated for each metric. These values were then averaged over all R_g and N_G and further averaged over the 30 simulations. The obtained values are referred to as $\bar{n}_{alg}$, $\bar{\varrho}$, and $\bar{\xi}$.

Figure 7.43 visualises the performance of the algorithms over time with reference to $\bar{n}_{alg}$. The graphs show that, for all change frequencies, there is little variance in $\bar{n}_{alg}$ over time. This shows the ability of all the algorithms, excluding the EEMACOMH and the NSGA-II-MPA, to react to change and find an adequate number of non-dominated solutions. Also, results show that transferring of solutions from the environment before the change occurs helps to accelerate search after the environment has changed and find a satisfactory number of non-dominated solutions. Therefore, in each environment, good solutions were likely to be found where good solutions have been in the previous environment. The EEMACOMP algorithm found more non-dominated solutions than all the other algorithms and the NSGA-II-MPA found the least number of non-dominated solutions. For low change frequencies all algorithms displayed the largest values for $\bar{n}_{alg}$.

Figure 7.43(a) shows a linear decrease over time for the NSGA-II-MPA algorithm for $T_{sm} = 1$ (high change frequency). NSGA-II-MPA had less time to react to changes and the time to find solutions was increased at each environment change.

Figure 7.43(f) shows an increase of $\bar{n}_{alg}$ over time for the EEMACOMH algorithm for $T_{sm} = 6$ (low change frequency). The optimiser had enough time to exploit the solutions transferred from the previous environment and improve the tracking performance of the optima and reduce the time to find solutions.

Figure 7.44 visualises the performance of the algorithms over time with reference to $\bar{\varrho}$. The graphs show that, for all change frequencies, $\bar{\varrho}$ had a very small value, showing a very good distribution of the solutions. For NSGA-II-MPA, $\bar{\varrho}$, remained constant over time for $T_{sm} \in \{3, 4, 5, 6\}$ and displayed an increase over time for $T_{sm} = 1$. For all ACO algorithms, $\bar{\varrho}$ remained at relatively the same level, for all environment changes, which again shows the robustness of the ACO algorithms. The assumption can be made here that a diverse spread of non-dominated solutions can adapt more easily to changes when the environment change is not too severe. For severe environment changes, the performance of the algorithms are similar to restarting the optimisation from scratch, and the optimum tracking becomes difficult. That is the case for NSGA-II-MPA, for $T_{sm} = 1$.

The EEMACOMP algorithm had the best solution spread and the NSGA-II-MPA had the worst solution spread compared to the rest of the algorithms.

Figure 7.45 visualises the performance of the algorithms over time with reference to the $\bar{\xi}$ metric. The graphs show high values of $\bar{\xi}$ for all change frequencies. The value

of $\bar{\xi}$ is similar for all environment changes, showing that there is a good adaptability to environment changes by all the algorithms. The size of the objective space which is dominated by the non-dominated solutions is over 80% of the total hypervolume of 75000, where 75000 is the maximum hypervolume calculated using the values of 100.0, 0.1, 500.0, 0.5, and 30.0, corresponding to a maximum value for each of the objectives. This indicates the closeness of the solutions to the optimal set and the good spread of solutions across the objective space. All algorithms displayed a similar value of $\bar{\xi}$.

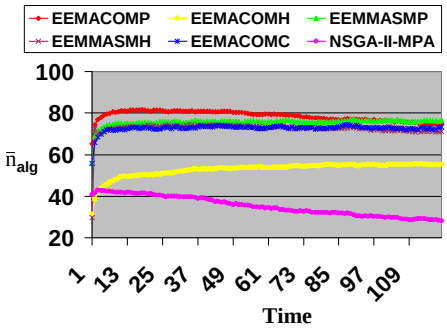

(a) $T_{sm} = 1$

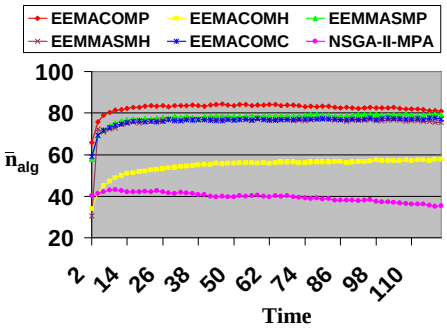

(b) $T_{sm} = 2$

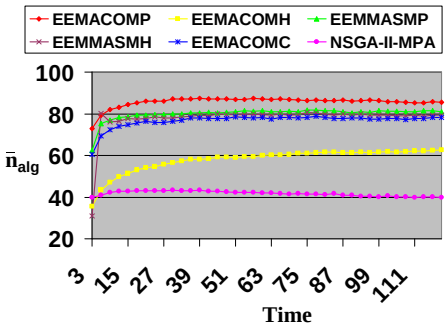

(c) $T_{sm} = 3$

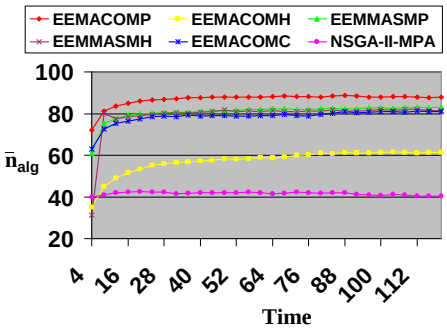

(d) $T_{sm} = 4$

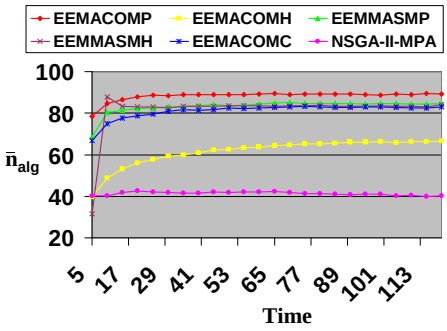

(e) $T_{sm} = 5$

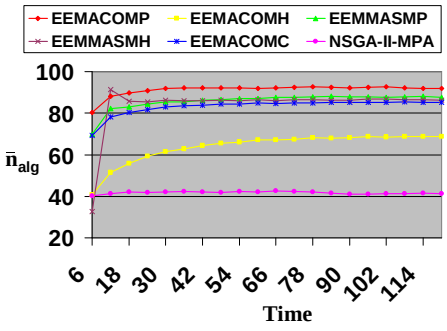

(f) $T_{sm} = 6$

Figure 7.43: Performance of the algorithms over time with regard to the number of non-dominated solutions metric, $\bar{n}_{alg}$

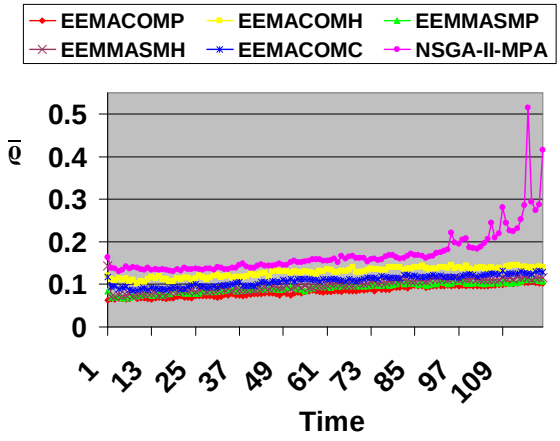

(a) $T_{sm} = 1$

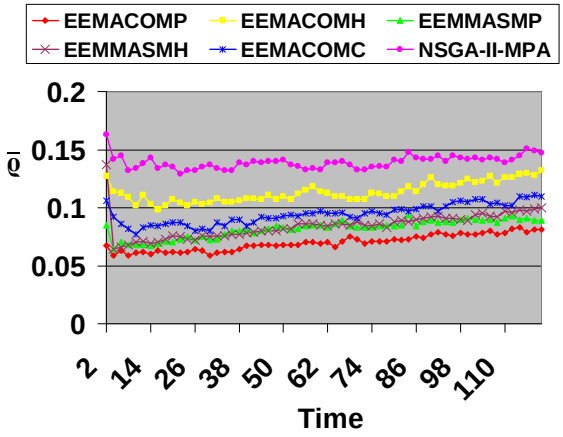

(b) $T_{sm} = 2$

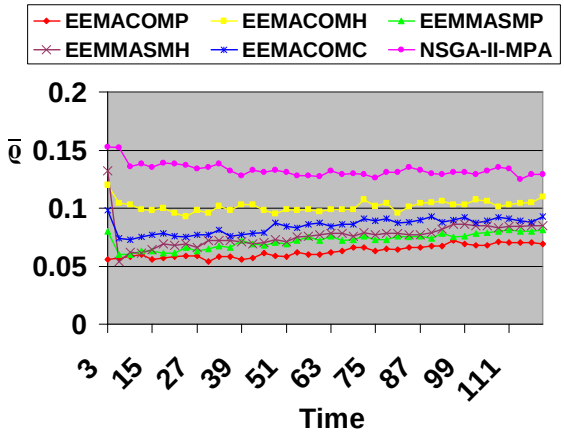

(c) $T_{sm} = 3$

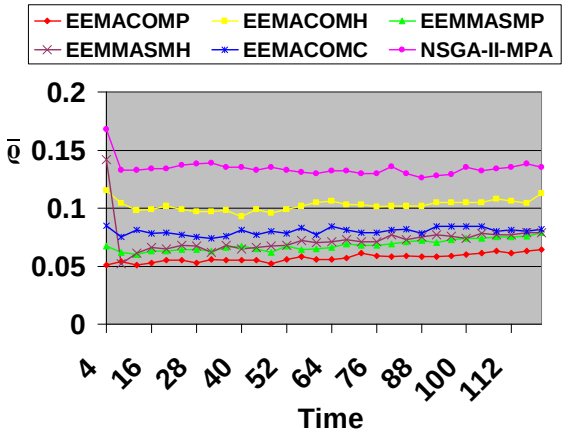

(d) $T_{sm} = 4$

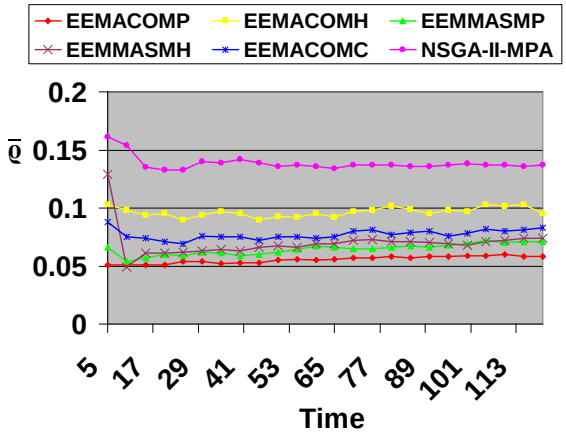

(e) $T_{sm} = 5$

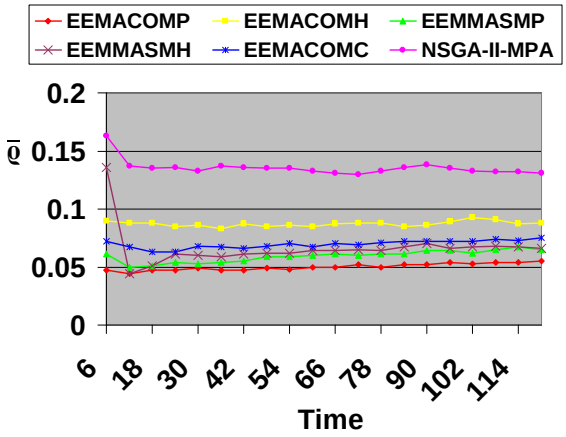

(f) $T_{sm} = 6$

Figure 7.44: Performance of the algorithms over time with regard to the spacing metric, $\bar{\varrho}$

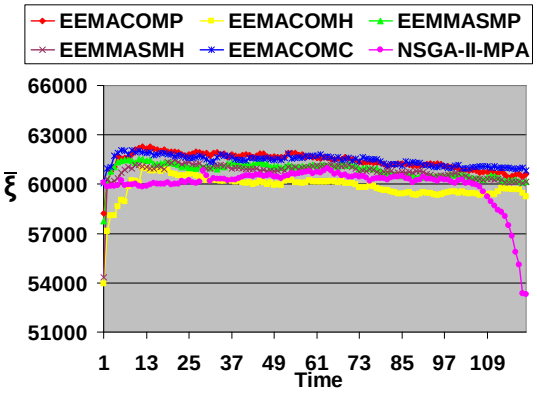

(a) $T_{sm} = 1$

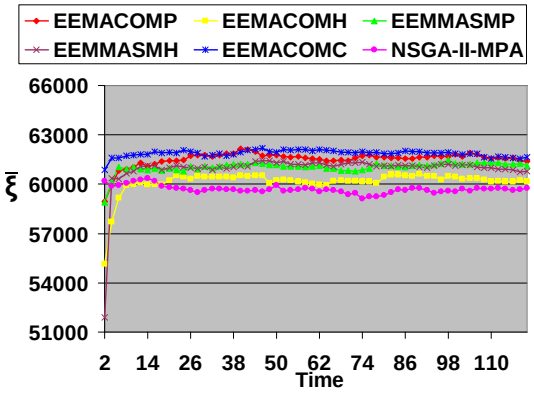

(b) $T_{sm} = 2$

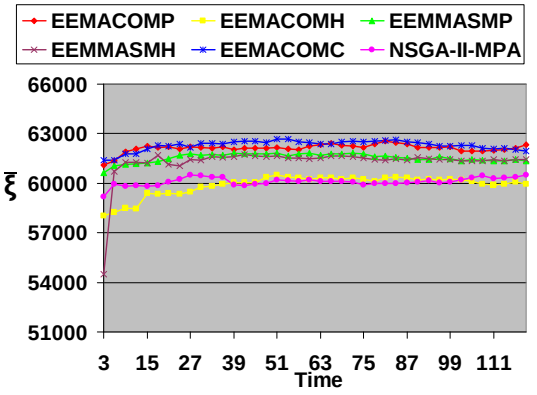

(c) $T_{sm} = 3$

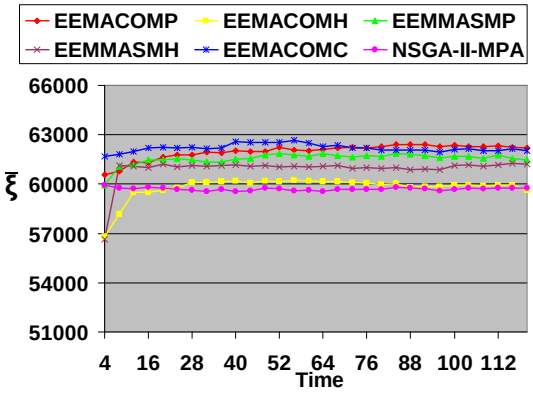

(d) $T_{sm} = 4$

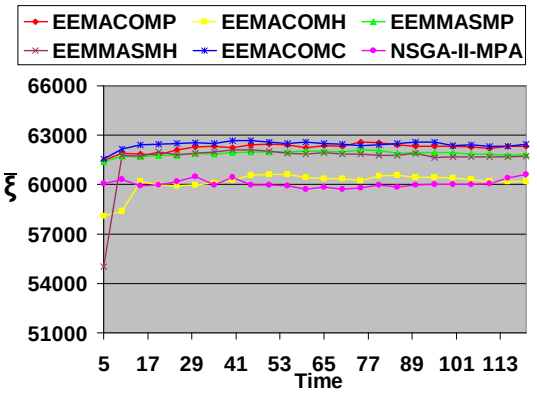

(e) $T_{sm} = 5$

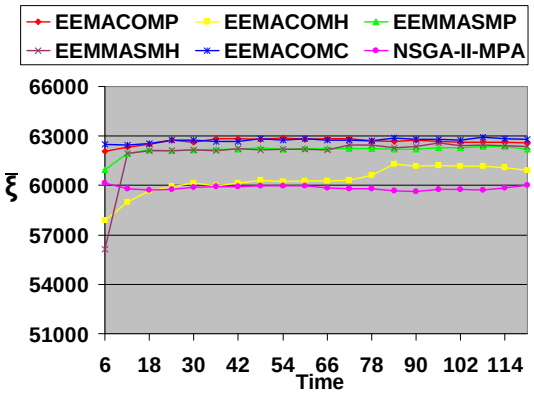

(f) $T_{sm} = 6$

Figure 7.45: Performance of the algorithms over time with regard to the hypervolume metric, $\bar{\xi}$

7.4.6 Optimization Criteria

This section analyses the performance of each algorithm in terms of the optimisation criteria (objective functions). The performance of each algorithm was tested under different scenarios for different change frequencies, change severities, and number of nodes as outlined in section 7.1.1. For each scenario the Pareto front, $\mathcal{PF}$, produced by the EEMACOMP, EEMACOMH, EEMMASMP, EEMMASMH, EEMACOMC, and NSGA-II-MPA algorithms is estimated. The influence of the change frequency, the change severity, and the number of nodes on the value of each objective function is evaluated.

For each of the scenarios 30 simulations have been executed and results were reported as averages over these simulations over all environment changes together with the standard deviations.

Results obtained from the EEMACOMP, EEMACOMH, EEMMASMP, EEMMASMH, EEMACOMC, and NSGA-II-MPA algorithms are summarised in Tables I.1 to I.45 in appendix I for the different scenarios. Based on these tables, appendix J illustrates the influence of change frequency, T_{sm}, and change severity, R_g, on the EP, TNP, VNP, CP, and MNC optimisation criteria (refer to Section 6.3 for a discussion of these criteria) for different number of nodes, N_G, using Fluxviz graphs.

Figures J.1-J.3 visualise the influence of T_{sm} and R_g on the EP criterion based on the results of Tables I.1-I.9. Figures J.4-J.6 visualise the influence of T_{sm} and R_g on the TNP criterion based on the results of Tables I.10-I.18. Figures J.7-J.9 visualise the influence of T_{sm} and R_g on the VNP criterion based on the results of Tables I.19-I.27. Figures J.10-J.12 graphically illustrate the influence of T_{sm} and R_g on the CP criterion based on the results of Tables I.28-I.36, while Figures J.13-J.15 visualise the influence of T_{sm} and R_g on the MNC criterion based on the results of Tables I.37-I.45.

The algorithms were compared in terms of the value of the objective functions. To test whether there is a statistical significant difference in the performance of any two algorithms with reference to the optimisation criteria, the Mann-Whitney U test as outlined in section 7.4.1 was applied.

- **Energy consumed per packet, EP, objective**

  Tables I.1-I.9 and Figures J.1-J.3 show no variation in EP with increase in change frequency for $N_G = 30$ and no pattern between EP and change frequency for

$N_G \in \{100, 300\}$.

Table 7.11 displays the average values of EP over all the N_G and R_g values using the results of Tables I.1-I.9. Figure 7.46 illustrates the results of Table 7.11. Table 7.11 and Figure 7.46 indicate no significant difference in EP value as change frequency increases. It is also to be noted from Table 7.11 and Figure 7.46 that when EP is taken as the average value over all the N_G and R_g values, NSGA-II-MPA is significantly better than the other algorithms, showing a very low EP.

Table 7.11: Average value of the EP objective over all the N_G and R_g values

	T_{sm}					
$\mathcal{PF}$	1	2	3	4	5	6
$P_{EEMACOMP}$	8.60	8.77	8.58	8.43	8.54	8.28
$P_{EEMACOMH}$	9.90	10.47	10.39	10.32	10.62	10.22
$P_{EEMMASMP}$	8.86	9.07	8.86	8.82	8.89	8.52
$P_{EEMMASMH}$	9.10	9.29	9.08	9.05	9.09	8.75
$P_{EEMULTCOL}$	8.72	8.90	8.66	8.60	8.68	8.34
$P_{NSGA-II-MPA}$	2.58	2.55	2.53	2.51	2.52	2.52

Tables I.1-I.9 and Figures J.1-J.3 indicate an increase in EP with increase in R_g for $N_G = 30$. For $N_G = 100$, EEMACOMC and NSGA-II-MPA produced the highest EP for $R_g = 800$, while the rest of the algorithms produced the highest EP for $R_g = 300$. For $N_G = 300$, EEMACOMH, EEMACOMC and NSGA-II-MPA produced the highest EP for $R_g = 800$ and no real trend between EP and change severity for $R_g \in \{300, 500\}$, while the rest of the algorithms presented no pattern between EP and change severity.

In order to better visualise the relation between R_g and EP, Table 7.12 displays the average values of EP over all the N_G and T_{sm} values while Figure 7.47 illustrates the results of Table 7.12. Table 7.12 and Figure 7.47 indicate that EP increased for each algorithm as R_g increased to the value of 800. This trend is expected, because an increase in change severity, R_g, causes only some of the nodes to be within transmission range and paths with minimum energy consumed per packet may not be possible. It is also to be noted from Table 7.12 and Figure 7.47 that when EP is taken as the average value over all the N_G and T_{sm} values, NSGA-II-MPA is significantly better than the other algorithms, showing a very low EP.

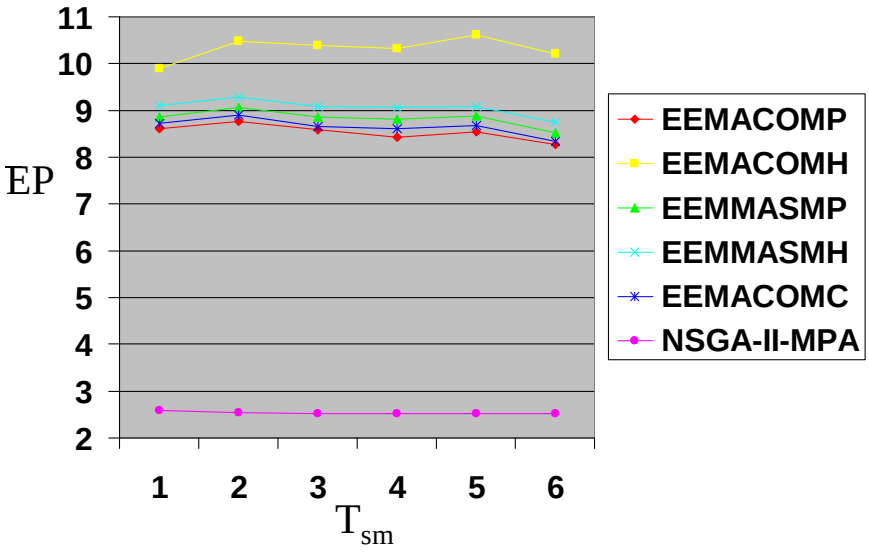

Figure 7.46: Average value of the EP objective over all the N_G and R_g values

Table 7.12: Average value of the EP objective over all the N_G and T_{sm} values

	R_g		
$\mathcal{PF}$	300	500	800
$P_{EEMACOMP}$	8.87	7.56	9.17
$P_{EEMACOMH}$	9.67	9.51	11.78
$P_{EEMMASMP}$	8.88	7.96	9.67
$P_{EEMMASMH}$	8.89	8.15	10.14
$P_{EEMULTCOL}$	7.75	7.59	10.61
$P_{NSGA-II-MPA}$	2.26	2.21	3.14

Tables I.1-I.9 and Figures J.1-J.3 show that the EP value increased significantly when the number of nodes increased to $N_G = 300$. This is an unexpected result which is possibly related to the computational complexity of the algorithms. As the number of nodes increases, it becomes necessary for the routing protocol to search more nodes in order to reach the destination, thus affecting diversity and the finding of the paths with the least energy consumed per packet.

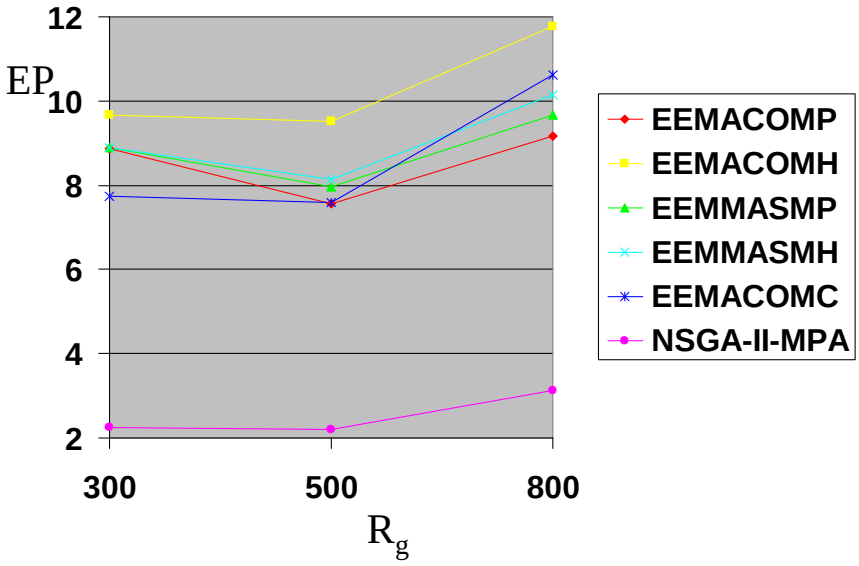

Figure 7.47: Average value of the EP objective over all the N_G and T_{sm} values

Tables I.1-I.9 show that all the ACO approaches displayed a higher value for EP and therefore worst performance when compared to the NSGA-II-MPA approach. To test whether there is a statistical significant difference in the performance of the NSGA-II-MPA approach and the ACO approaches, the following two hypotheses were considered:

$$H_0: \quad \mu^{EP}_{NSGA-II-MPA} = \mu^{EP}_{ACO}$$
$$H_1: \quad \mu^{EP}_{NSGA-II-MPA} > \mu^{EP}_{ACO}$$

where ACO takes the values EEMACOMP, EEMACOMH, EEMMASMP, EEMMASMH, and EEMACOMC.

Results of the Mann-Whitney U tests were the same for all the compared algorithms, as illustrated in Figure 7.48. The Mann-Whitney U tests show that the NSGA-II-MPA had a significantly lower energy consumed per packet than all the ACO algorithms for all the scenarios. This is possibly related to the effects of the

k shortest path algorithm used for NSGA-II-MPA, which selects the first R paths with minimum energy consumed per packet and with minimum cost per packet (refer to Section 6.7).

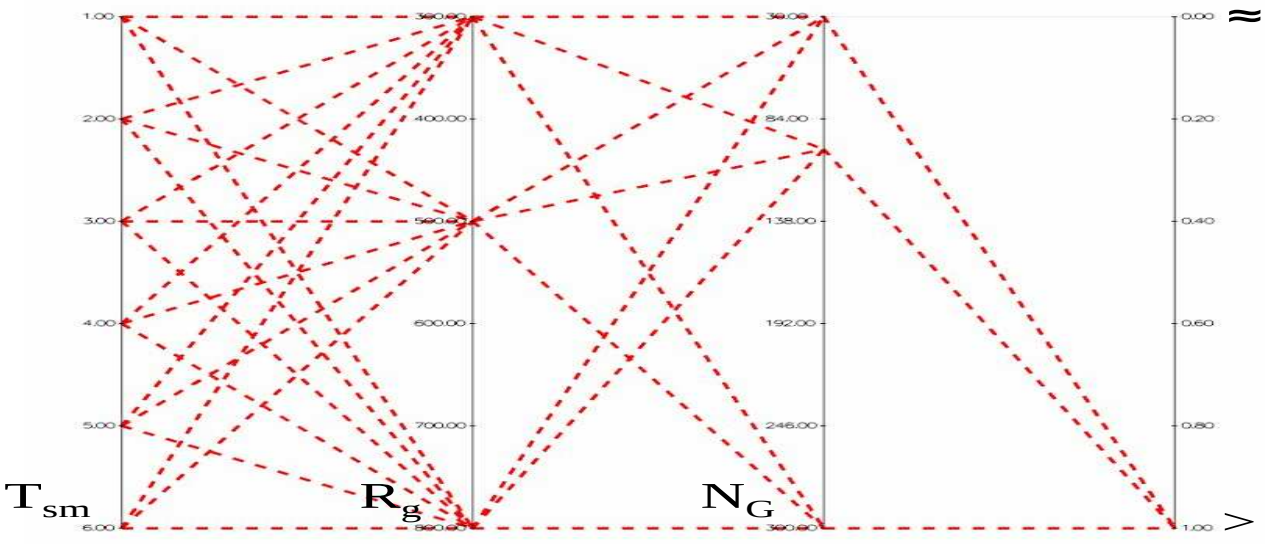

Figure 7.48: Comparing the NSGA-II-MPA algorithm against the ACO algorithms with regard to EP using the Mann-Whitney U test

- **Utilisation of the most heavily used link, TNP, objective**

  Tables I.10-I.18 and Figures J.4-J.6 indicate a small decrease in TNP with decrease in change frequency for all algorithms. In addition, the NSGA-II-MPA displayed a high value of TNP for $T_{sm} = 1$, showing a bad performance for high change frequency.

  Table 7.13 displays the average values of TNP over all the N_G and R_g values using the results of Tables I.10-I.18. Figure 7.49 illustrates the results of Table 7.13. Table 7.13 and Figure 7.49 indicate a very small decrease or no difference for TNP as T_{sm} increased (change frequency decreased), except for the NSGA-II-MPA algorithm which displayed a high value of TNP for $T_{sm} = 1$. Low change frequencies provide more time to better optimise the TNP objective.

Table 7.13: Average value of the TNP objective over all the N_G and R_g values

	T_{sm}					
$\mathcal{PF}$	1	2	3	4	5	6
$P_{EEMACOMP}$	0.0024	0.0022	0.0021	0.0021	0.0020	0.0020
$P_{EEMACOMH}$	0.0026	0.0024	0.0023	0.0022	0.0022	0.0022
$P_{EEMMASMP}$	0.0024	0.0022	0.0021	0.0021	0.0020	0.0020
$P_{EEMMASMH}$	0.0024	0.0022	0.0021	0.0021	0.0021	0.0021
$P_{EEMULTCOL}$	0.0023	0.0022	0.0022	0.0022	0.0021	0.0021
$P_{NSGA-II-MPA}$	0.0130	0.0026	0.0024	0.0023	0.0023	0.0022

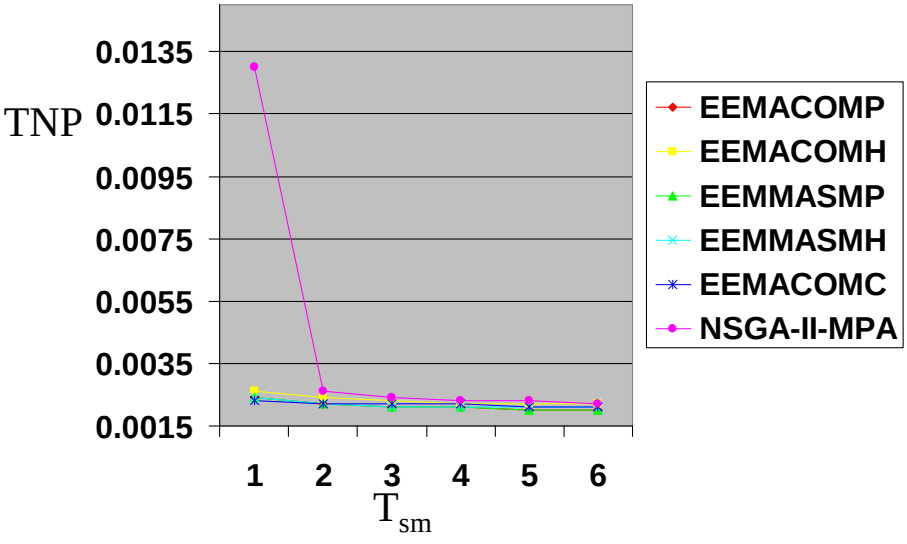

Figure 7.49: Average value of the TNP objective over all the N_G and R_g values

Tables I.10-I.18 and Figures J.4-J.6 indicate an increase in TNP with increase in change severity for all algorithms. In addition, the NSGA-II-MPA displayed a high value of TNP for $N_G = 100$, $R_g = 300$ and $T_{sm} = 1$.

In order to better visualise the relation between R_g and TNP, Table 7.14 displays the average values for TNP over all the N_G and T_{sm} values, while Figure 7.50 illustrates the results of Table 7.14. Table 7.14 and Figure 7.50 indicate that TNP increased for each algorithm as R_g increased. This trend is expected, because an increase in change severity, R_g, causes only some of the links to be valid, and it may not be possible to minimise or avoid the utilisation of the link with the least capacity.

Table 7.14: Average value of the TNP objective over all the N_G and T_{sm} values

	R_g		
$\mathcal{PF}$	300	500	800
$P_{EEMACOMP}$	0.0014	0.0018	0.0033
$P_{EEMACOMH}$	0.0014	0.0019	0.0036
$P_{EEMMASMP}$	0.0014	0.0018	0.0033
$P_{EEMMASMH}$	0.0014	0.0018	0.0033
$P_{EEMULTCOL}$	0.0014	0.0019	0.0033
$P_{NSGA-II-MPA}$	0.0021	0.0020	0.0083

Tables I.10-I.18 and Figures J.4-J.6 show that the TNP value decreased when the number of nodes increased. This is an expected result because as the number of nodes increases, more links are available and therefore it becomes more easy to minimise the utilisation of the link with the least capacity.

Tables I.10-I.18 show that all the ACO approaches displayed a lower value for the TNP for scenarios with $N_G = 300$ when compared to the NSGA-II-MPA approach. To test whether there is a statistical significant difference in the performance of the ACO approaches and the NSGA-II-MPA approach for $N_G = 300$, the following two hypotheses were considered:

$$H_0 : \quad \mu_{ACO}^{TNP} = \mu_{NSGA-II-MPA}^{TNP}$$
$$H_1 : \quad \mu_{ACO}^{TNP} > \mu_{NSGA-II-MPA}^{TNP}$$

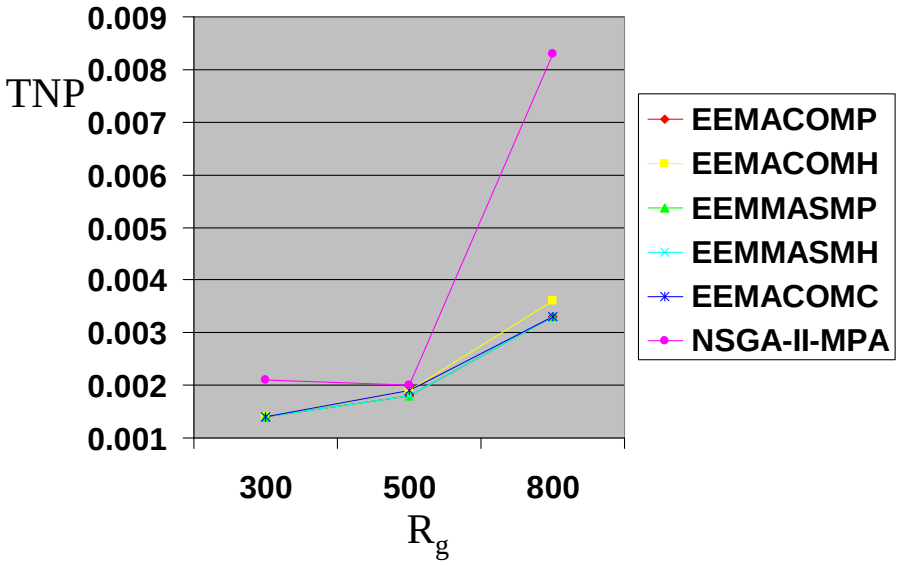

Figure 7.50: Average value of the TNP objective over all the N_G and T_{sm} values

Results of the Mann-Whitney U tests were the same for all the compared algorithms as illustrated in Figure 7.51. The Mann-Whitney U tests show that all ACO approaches are significantly better than the NSGA-II-MPA approach with reference to the TNP objective for $N_G = 300$. There is no significant difference between ACO approaches and the NSGA-II-MPA approach with reference to the TNP objective for $N_G \in \{30, 100\}$.

- **Variance in node power levels, VNP, objective**

  Tables I.19-I.27 and Figures J.7-J.9 show no pattern between VNP and change frequency.

  Table 7.15 displays the average values of VNP over all the N_G and R_g values using the results of Tables I.19-I.27. Figure 7.52 illustrates the results of Table 7.15. Table 7.15 and Figure 7.52 indicate a small decrease in VNP with a decrease in change frequency for the ACO algorithms and a small increase in VNP with

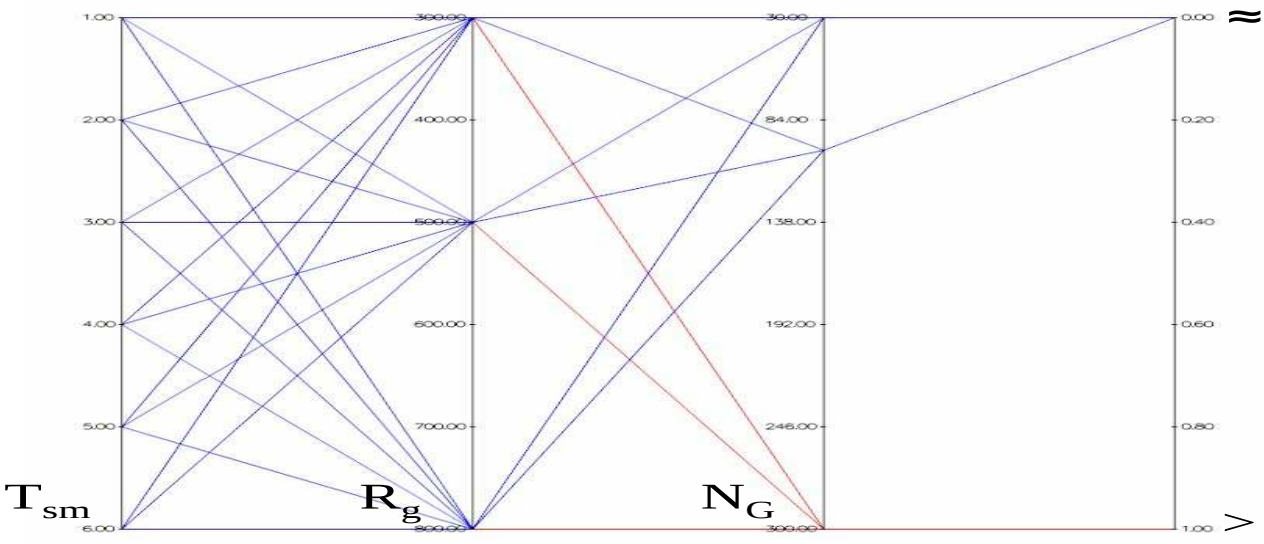

Figure 7.51: Comparing the ACO algorithms against the NSGA-II-MPA algorithm with regard to the TNP objective using the Mann-Whitney U test

a decrease in change frequency for the NSGA-II-MPA. Low change frequencies deteriorate the optimisation of the VNP for the NSGA-II-MPA.

Table 7.15: Average value of the VNP objective over all the N_G and R_g values

	T_{sm}					
$\mathcal{PF}$	1	2	3	4	5	6
$P_{EEMACOMP}$	81.53	80.63	80.55	80.07	79.29	78.78
$P_{EEMACOMH}$	90.00	89.60	87.98	88.16	86.32	85.55
$P_{EEMMASMP}$	82.95	82.46	82.75	82.18	81.17	80.82
$P_{EEMMASMH}$	83.33	82.70	83.08	82.54	81.95	81.03
$P_{EEMULTCOL}$	76.27	76.17	76.94	76.27	76.48	76.07
$P_{NSGA-II-MPA}$	114.67	117.40	119.43	121.03	120.62	121.65

Tables I.19-I.27 and Figures J.7-J.9 indicate a decrease in VNP with increase in R_g for $N_G = 30$. For $N_G = 100$ all the single-colony ACO algorithms produced the highest VNP for $R_g = 500$ and the lowest VNP for $R_g = 300$, while the EEMACOMC and the NSGA-II-MPA algorithms produced the lowest VNP for

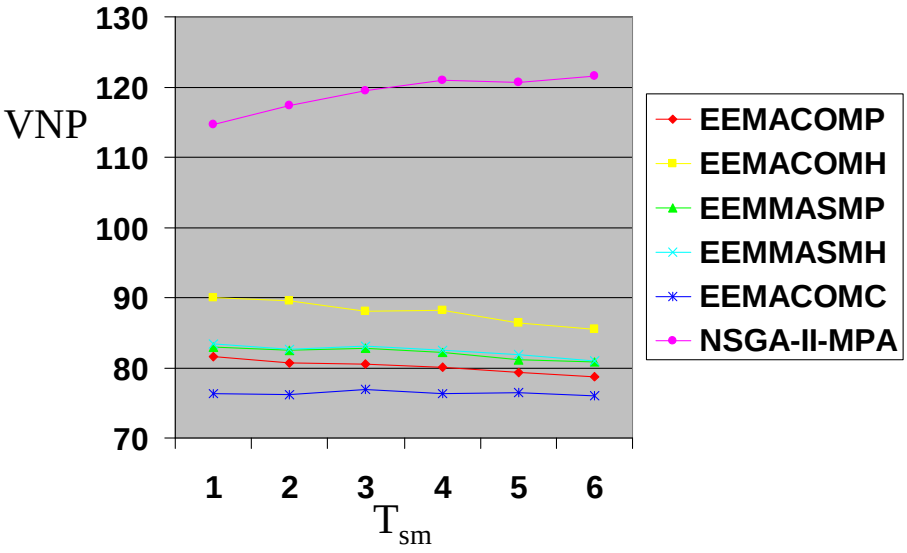

Figure 7.52: Average value of the VNP objective over all the N_G and R_g values

$R_g = 800$.

Table 7.16 displays the average values of VNP over all the N_G and T_{sm} values while Figure 7.53 illustrates the results of Table 7.16. Table 7.16 and Figure 7.53 indicate an increase in VNP with increase in change severity from 300 to 500 and then a decrease in VNP with increase in change severity from 500 to 800 for the ACO algorithms. The NSGA-II-MPA produced a decrease in VNP with increase in change severity. High change severities improve the optimisation of the VNP.

Table 7.16: Average value of the VNP objective over all the N_G and T_{sm} values

	R_g		
$\mathcal{PF}$	300	500	800
$P_{EEMACOMP}$	76.67	82.16	81.59
$P_{EEMACOMH}$	80.11	90.63	93.06
$P_{EEMMASMP}$	78.13	84.41	83.63
$P_{EEMMASMH}$	78.41	84.78	84.13
$P_{EEMULTCOL}$	75.57	81.00	72.53
$P_{NSGA-II-MPA}$	128.68	123.23	105.48

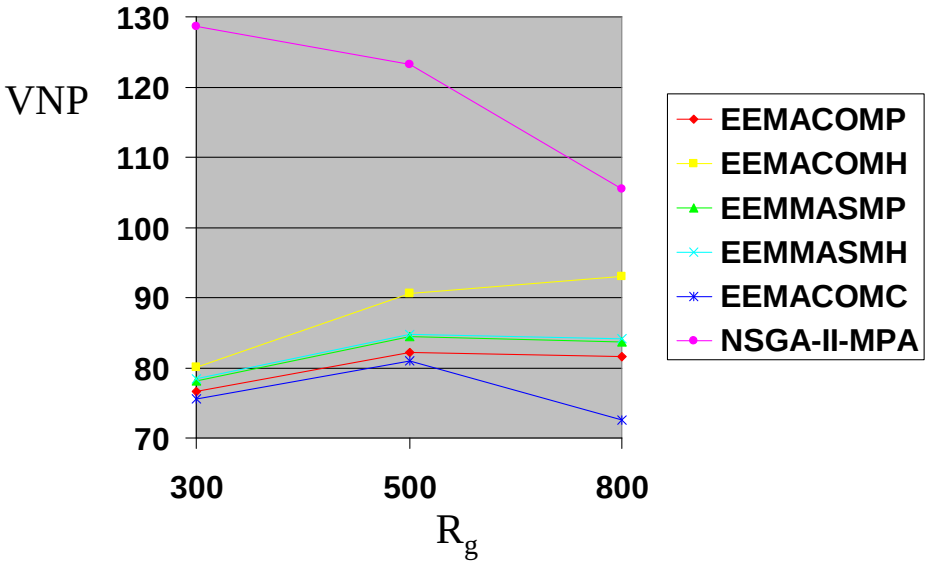

Figure 7.53: Average value of the VNP objective over all the N_G and T_{sm} values

Tables I.19-I.27 and Figures J.7-J.9 show no trend between the VNP value and the number of nodes.

Tables I.19-I.27 show that all the ACO approaches except the EEMACOMH approach, displayed a lower value for the VNP for all scenarios when compared to the NSGA-II-MPA approach. The EEMACOMH approach displayed a lower value for VNP for all scenarios except for scenarios with $R_g = 800$ and $N_G \in \{100, 300\}$ when compared to the NSGA-II-MPA approach. To test whether there is a statistical significant difference in the performance of EEMACOMP, EEMMASMP, EEMMASMH, and EEMACOMC and the NSGA-II-MPA approach, the following two hypotheses were considered:

$$H_0: \quad \mu_{ACO}^{VNP} = \mu_{NSGA-II-MPA}^{VNP}$$
$$H_1: \quad \mu_{ACO}^{VNP} > \mu_{NSGA-II-MPA}^{VNP}$$

where ACO takes the values EEMACOMP, EEMMASMP, EEMMASMH, and EEMACOMC.

Results of the Mann-Whitney U tests were the same for all the compared algorithms as illustrated in Figure 7.54. The Mann-Whitney U tests show that the EEMACOMP, EEMMASMP, EEMMASMH, and EEMACOMC approaches are significantly better than the NSGA-II-MPA approach with reference to the VNP objective for all scenarios.

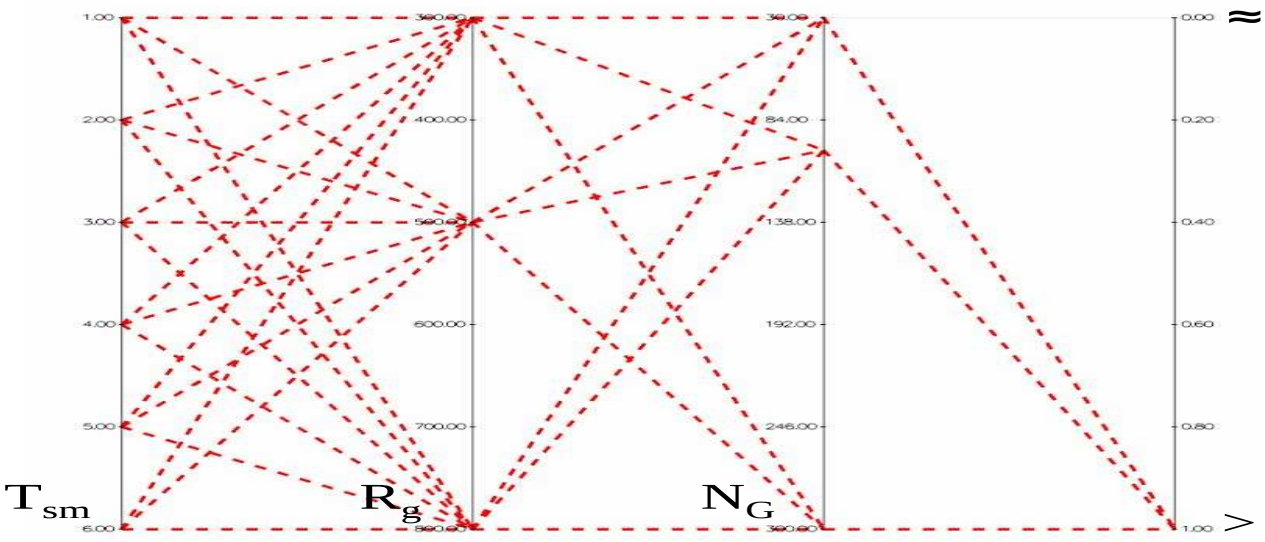

Figure 7.54: Comparing EEMACOMP, EEMMASMP, EEMMASMH, and EEMACOMC against the NSGA-II-MPA algorithm with regard to the VNP objective using the Mann-Whitney U test

To test whether there is a statistical significant difference in the performance of EEMACOMH and the NSGA-II-MPA approach for all scenarios except for scenarios with $R_g = 800$ and $N_G \in \{100, 300\}$, the following two hypotheses were considered:

$$H_0 : \ \mu^{VNP}_{EEMACOMH} = \mu^{VNP}_{NSGA-II-MPA}$$
$$H_1 : \ \mu^{VNP}_{EEMACOMH} > \mu^{VNP}_{NSGA-II-MPA}$$

Results of the Mann-Whitney U tests are illustrated in Figure 7.55. The Mann-Whitney U tests show that the EEMACOMH approach is significantly better than the NSGA-II-MPA approach with reference to the VNP objective for all scenarios except for scenarios with $R_g = 800$ and $N_G \in \{100, 300\}$.

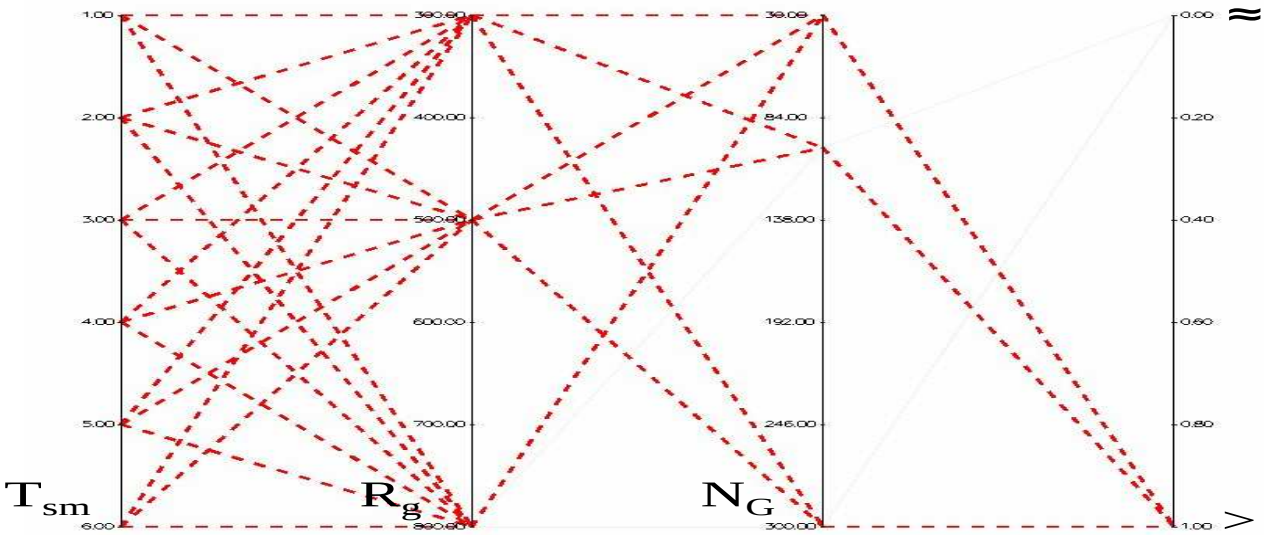

Figure 7.55: Comparing the EEMACOMH against the NSGA-II-MPA algorithm with regard to the VNP objective using the Mann-Whitney U test

- **Cost per packet, CP, objective**

  Tables I.28-I.36 and Figures J.10-J.12 show no trend between the CP value and the change frequency for $N_G = 300$, while for $N_G \in \{30, 100\}$ there is no difference in CP value as change frequency increases.

  Table 7.17 displays the average values of CP over all the N_G and R_g values using the results of Tables I.28-I.36. Figure 7.56 illustrates the results of Table 7.17. Table 7.17 and Figure 7.56 indicate no difference in CP value with change frequency variation except for NSGA-II-MPA which produced a higher value of CP for $T_{sm} = 1$. It is also to be noted from Table 7.17 and Figure 7.56 that when CP is taken

as the average value over all the N_G and R_g values, NSGA-II-MPA is significantly better than the other algorithms, showing a very low CP.

Tables I.28-I.36 and Figures J.10-J.12 show no trend between the CP value and the change severity for $N_G \in \{30, 300\}$. For $N_G = 100$, the CP value increased with increase in R_g for all ACO algorithms, while the NSGA-II-MPA algorithm produced the lowest CP for $R_g = 800$.

Table 7.17: Average value of the CP objective over all the N_G and R_g values

	T_{sm}					
$\mathcal{PF}$	1	2	3	4	5	6
$P_{EEMACOMP}$	0.043	0.044	0.043	0.043	0.043	0.042
$P_{EEMACOMH}$	0.050	0.054	0.053	0.054	0.055	0.053
$P_{EEMMASMP}$	0.045	0.047	0.045	0.045	0.046	0.044
$P_{EEMMASMH}$	0.047	0.048	0.047	0.047	0.047	0.045
$P_{EEMULTCOL}$	0.040	0.041	0.039	0.039	0.040	0.038
$P_{NSGA-II-MPA}$	0.017	0.010	0.010	0.010	0.010	0.010

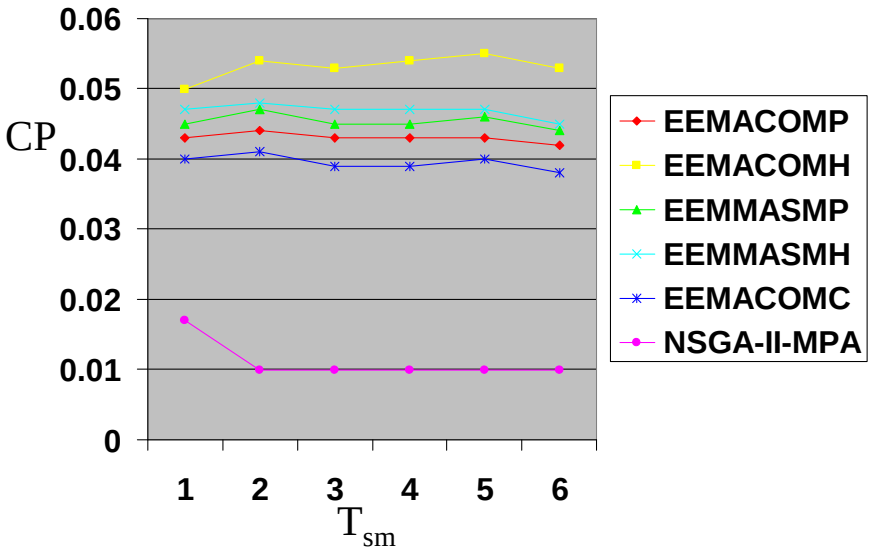

Figure 7.56: Average value of the CP objective over all the N_G and R_g values

Table 7.18 displays the average values of CP over all the N_G and T_{sm} values, while Figure 7.57 illustrates the results of Table 7.18. Table 7.18 and Figure 7.57 indicate that CP was higher for $R_g = 300$ which is not expected, because low change severity is supposed to delay the energy depletion of a node and therefore to maintain a low cost of using that node and lower value of CP.

Table 7.18: Average value of the CP objective over all the N_G and T_{sm} values

	R_g		
$\mathcal{PF}$	300	500	800
$P_{EEMACOMP}$	0.051	0.039	0.038
$P_{EEMACOMH}$	0.056	0.050	0.053
$P_{EEMMASMP}$	0.052	0.042	0.042
$P_{EEMMASMH}$	0.052	0.043	0.044
$P_{EEMULTCOL}$	0.043	0.037	0.038
$P_{NSGA-II-MPA}$	0.012	0.010	0.012

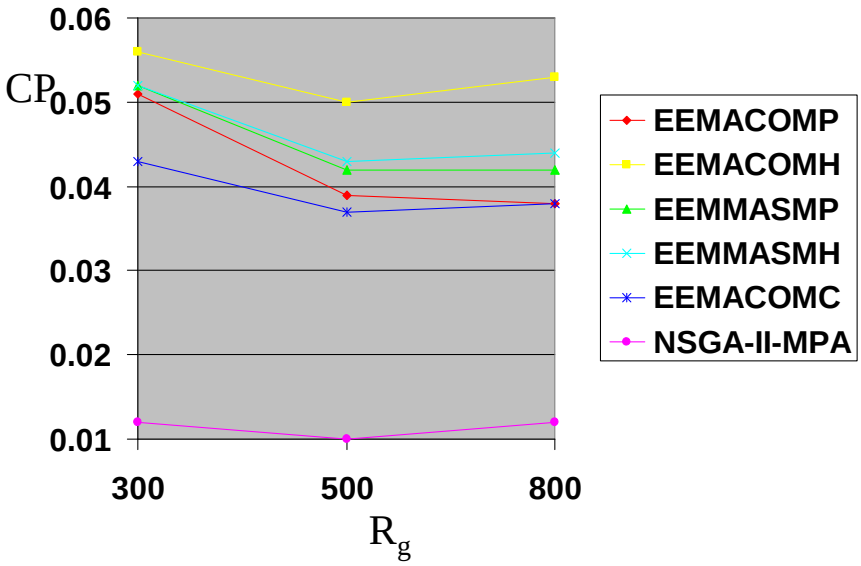

Figure 7.57: Average value of the CP objective over all the N_G and T_{sm} values

Tables I.28-I.36 show that the CP value increased when the number of nodes increased. This is an expected result because as the number of nodes increases, paths

consist on average of more nodes, and therefore the value of the CP objective which is a function of the residual energy of each node of the path increases.

Tables I.28-I.36 show that all the ACO approaches displayed a higher value for CP and therefore worst performance for all scenarios when compared to the NSGA-II-MPA approach. To test whether there is a statistical significant difference in the performance of the NSGA-II-MPA approach and the ACO approaches, the following two hypotheses were considered:

$$H_0: \quad \mu^{CP}_{NSGA-II-MPA} = \mu^{CP}_{ACO}$$
$$H_1: \quad \mu^{CP}_{NSGA-II-MPA} > \mu^{CP}_{ACO}$$

Results of the Mann-Whitney U tests were the same for all the compared algorithms as illustrated in Figure 7.58. The Mann-Whitney U tests show that the NSGA-II-MPA approach is significantly better than all the ACO approaches with reference to the CP objective for all scenarios. Again, this is possibly related to the effects of the k shortest path algorithm used in NSGA-II-MPA, which selects the first R paths with minimum energy consumed per packet and with minimum cost per packet (refer to Section 6.7).

- **Maximum node cost, MNC, objective**

  Tables I.37-I.45 and Figures J.13-J.15 indicate a decrease in MNC with decrease in change frequency for all algorithms.

  Table 7.19 displays the average values of MNC over all the N_G and R_g values using the results of Tables I.37-I.45. Figure 7.59 illustrates the results of Table 7.19. Table 7.19 and Figure 7.59 indicate an exponential decrease for MNC as change frequency decreased for all ACO algorithms and a small decrease for MNC as change frequency decreased for NSGA-II-MPA. That is an expected result, because low change frequencies give more time for the algorithms to find paths with low energy cost links.

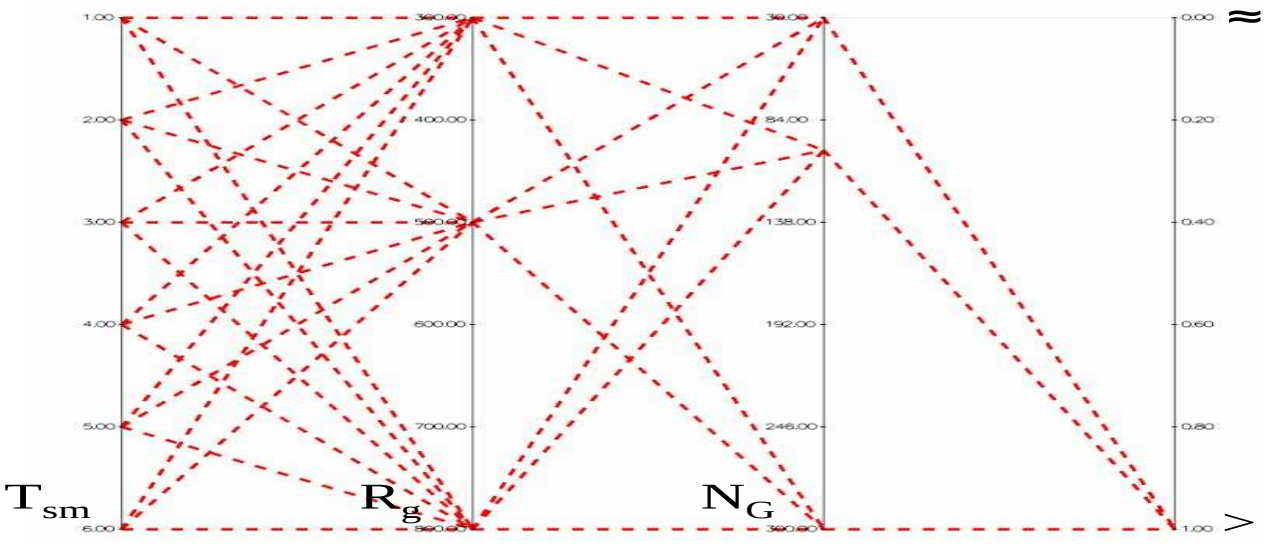

Figure 7.58: Comparing the NSGA-II-MPA algorithm against the ACO algorithms with regard to the CP objective using the Mann-Whitney U test

Tables I.37-I.45 and Figures J.13-J.15 indicate an increase in MNC with increase in change severity for most scenarios and for all algorithms.

Table 7.20 displays the average values for MNC over all the N_G and T_{sm} values while Figure 7.60 illustrates the results of Table 7.20. Table 7.20 and Figure 7.60 indicate that MNC increased for each ACO algorithm as R_g increased. This trend is expected, because an increase in change severity, R_g, causes only some of the links to be valid and it may not be possible to always find paths with low energy cost links. The value of MNC for NSGA-II-MPA increased when R_g increased from 500 to 800.

Tables I.37-I.45 and Figures J.13-J.15 show that the MNC value had a small increase when the number of nodes increased.

Tables I.37-I.45 and Figures J.13-J.15 show that all the ACO approaches displayed a higher value for MNC for all scenarios except for scenarios with $N_G = 300$ and $R_g = 800$ when compared to the NSGA-II-MPA approach. To test whether there is a statistical significant difference in the performance of the NSGA-II-MPA

Table 7.19: Average value of the MNC objective over all the N_G and R_g values

	T_{sm}					
$\mathcal{PF}$	1	2	3	4	5	6
$P_{EEMACOMP}$	2.830	2.023	1.727	1.569	1.485	1.410
$P_{EEMACOMH}$	2.794	1.999	1.778	1.602	1.518	1.456
$P_{EEMMASMP}$	3.091	2.219	1.830	1.678	1.580	1.475
$P_{EEMMASMH}$	3.067	2.220	1.828	1.665	1.579	1.516
$P_{EEMULTCOL}$	3.736	2.577	2.057	1.751	1.610	1.556

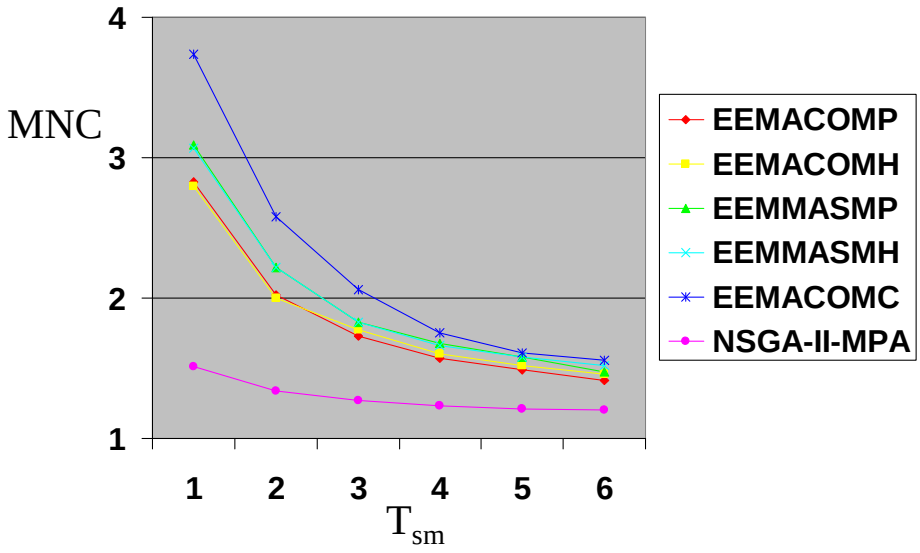

Figure 7.59: Average value of the MNC objective over all the N_G and R_g values

Table 7.20: Average value of the MNC objective over all the N_G and T_{sm} values

	R_g		
$\mathcal{PF}$	300	500	800
$P_{EEMACOMP}$	1.612	1.749	2.160
$P_{EEMACOMH}$	1.666	1.760	2.148
$P_{EEMMASMP}$	1.772	1.870	2.294
$P_{EEMMASMH}$	1.766	1.870	2.302
$P_{EEMULTCOL}$	1.802	2.011	2.830
$P_{NSGA-II-MPA}$	1.240	1.143	1.500

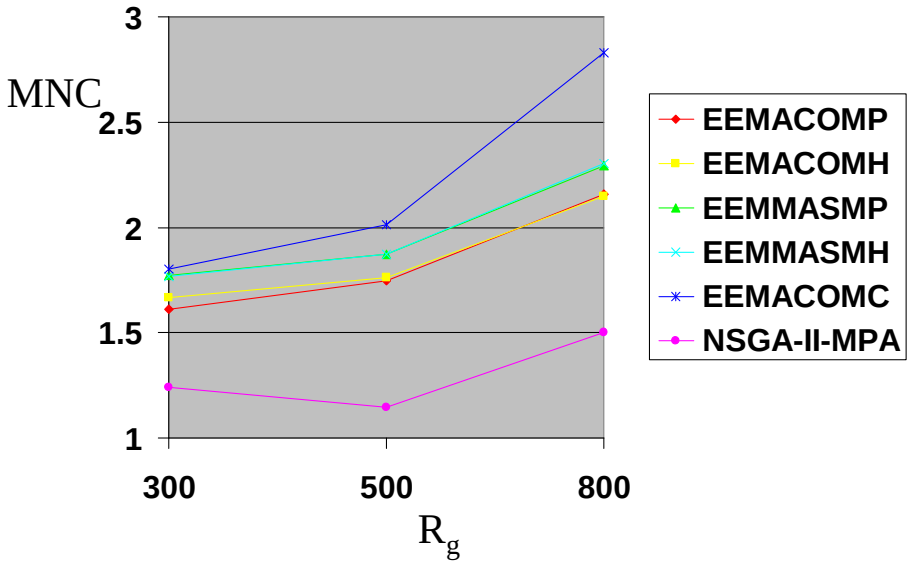

Figure 7.60: Average value of the MNC objective over all the N_G and T_{sm} values

approach and the ACO approaches the following two hypotheses were considered:

$$H_0: \quad \mu^{MNC}_{NSGA-II-MPA} = \mu^{MNC}_{ACO}$$
$$H_1: \quad \mu^{MNC}_{NSGA-II-MPA} > \mu^{MNC}_{ACO}$$

Results of the Mann-Whitney U tests were the same for all the compared algorithms as illustrated in Figure 7.61. The Mann-Whitney U tests show that the NSGA-II-MPA approach is significantly better than all the ACO approaches with reference to the MNC objective for all scenarios except for scenarios with $N_G = 300$ and $R_g = 800$ where the NSGA-II-MPA approach is equal to the ACO approaches.

The remainder of this section analyses the value of each optimisation criterion for each environment change.

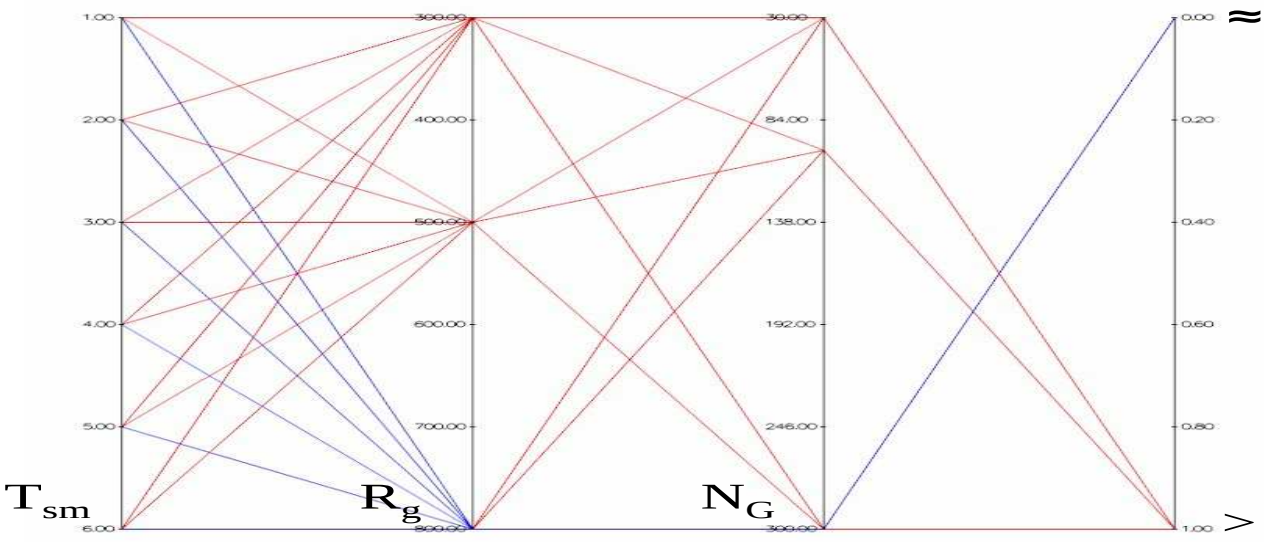

Figure 7.61: Comparing the NSGA-II-MPA algorithm against the ACO algorithms with regard to the MNC objective using the Mann-Whitney U test

Optimization criteria over time

For each optimisation criterion and for each iteration before a change to the environment occurs, the average value of that criterion is computed over all the number of solutions for this iteration, further averaged over all 30 simulations for all R_g and N_G values per T_{sm} value.

Figure 7.62 visualises the energy consumed per packet, EP, over time. For all change frequencies, a slight decrease in EP is observed over time. This decrease over time in EP shows that transferring solutions from the environment before the change occurs helps to accelerate the rate of convergence to the optima after the change occurred. Therefore more time is available to find solutions with equal or lower energy consumed per packet after the environment has changed. For all environment changes the NSGA-II-MPA produced a very low EP compared to the ACO algorithms.

Figure 7.63 visualises the utilisation of the most heavily used link, TNP, over time. All algorithms minimise the TNP criterion to a very low value. Because of this low value of TNP, the load among mobile nodes is divided so that the network will partition in such a way that nodes drain their energy at equal rates. This will help to maximise the

time to network partition. In addition, for NSGA-II-MPA, Figures 7.63(a) and 7.63(b) indicate an exponential increase for TNP over time for $T_{sm} = 1$ and $T_{sm} = 2$.

Figure 7.64 visualises the variance in node power levels, VNP, over time. NSGA-II-MPA displayed the highest value for VNP over all change frequencies, indicating a bad load distribution. It is also to be noted from Figures 7.64(b)-7.64(d) that for the NSGA-II-MPA, VNP decreased over time for $T_{sm} \in \{2, 3, 4\}$ which is good. Otherwise, for all algorithms, the value of VNP had a very small variation for all environment changes. This small variation of VNP, together with the relatively low value for VNP, will ensure that all the nodes in the network remain up and running for as long as possible.

Figure 7.65 visualises the cost per packet, CP, criterion over time. NSGA-II-MPA produced the best CP value, having a small value for all environment changes. Even-though NSGA-II-MPA produced the best cost results, all the ant algorithms achieved very low cost solutions. Minimising CP achieves the objective of avoiding those nodes with depleted energy reserves since these nodes have high node cost. In this way, network partition is delayed.

Figure 7.66 visualises the maximum node cost, MNC, over time. EEMACOMC produced the worst MNC values (highest MNC values), while NSGA-II-MPA produced the best MNC values. All algorithms produced low MNC values for all change frequencies, and environment changes. This will help delay node failure and reduce variance in remaining battery lives.

For all algorithms, there is a very small variation at each environment change in the values of the EP, TNP, CP, and VNP objectives. This shows the robustness and adaptability of all the algorithms to the environment changes.

7.4.7 Ranking Of The Algorithms Based On Performance Criteria

Tables 7.21-7.29 give the average rank of the algorithms for each scenario based on the results of Tables F.1-F.54. Symbols n_{alg}^{w}, ϱ^{w}, and ξ^{w} are defined in Section 7.4.1. For each of the performance metrics, each algorithm is ranked according to the number of times that the algorithm had a better performance than all the other algorithms with reference to this performance metric, for each environment change. The algorithm's average rank over all the performance criteria is calculated and then the algorithm is

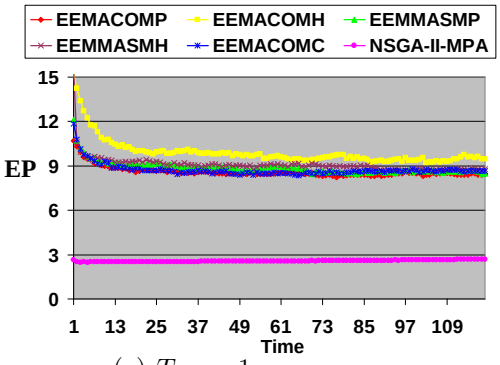

(a) $T_{sm} = 1$

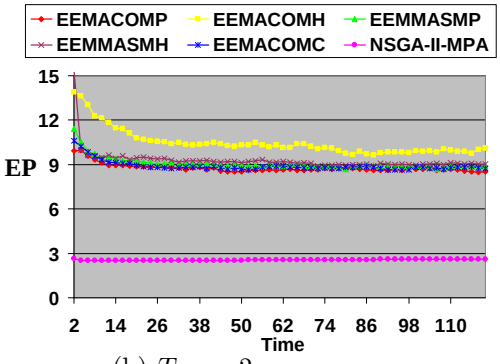

(b) $T_{sm} = 2$

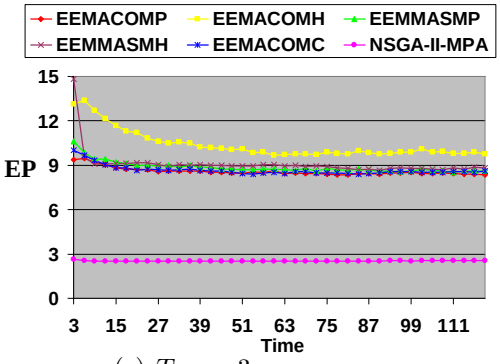

(c) $T_{sm} = 3$

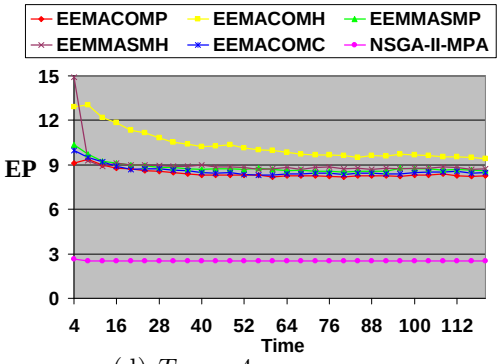

(d) $T_{sm} = 4$

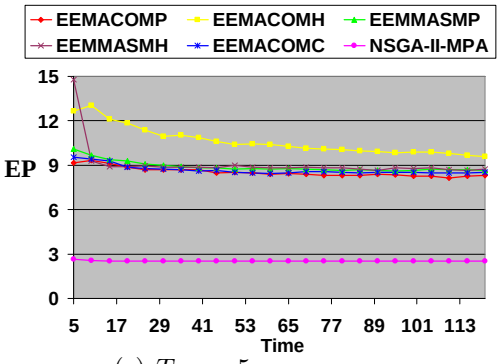

(e) $T_{sm} = 5$

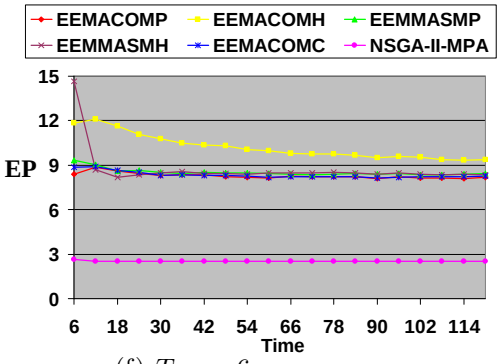

(f) $T_{sm} = 6$

Figure 7.62: Energy consumed per packet, EP, criterion over time

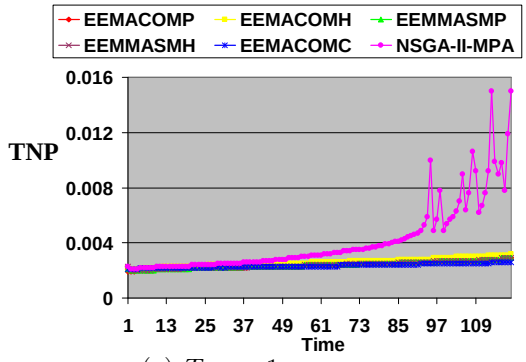

(a) $T_{sm} = 1$

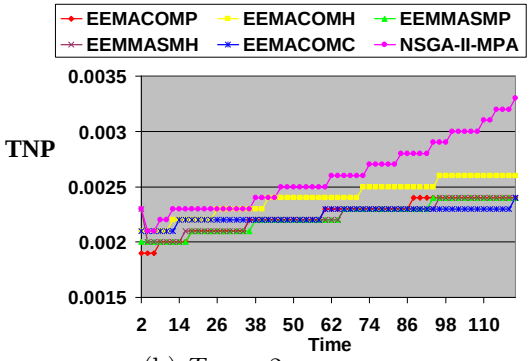

(b) $T_{sm} = 2$

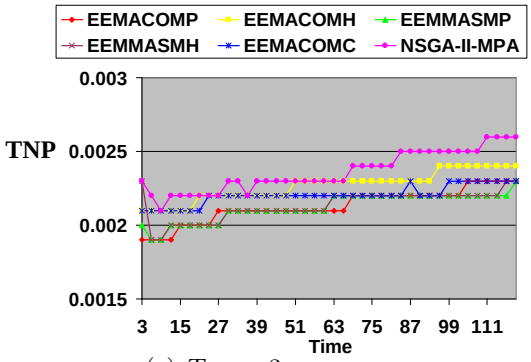

(c) $T_{sm} = 3$

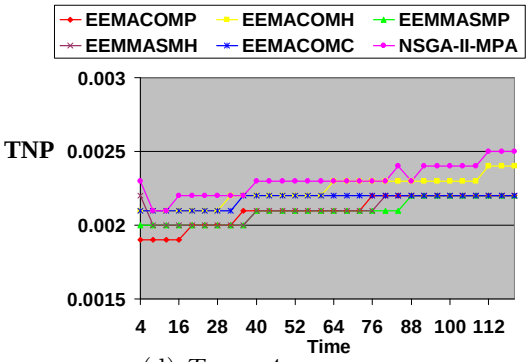

(d) $T_{sm} = 4$

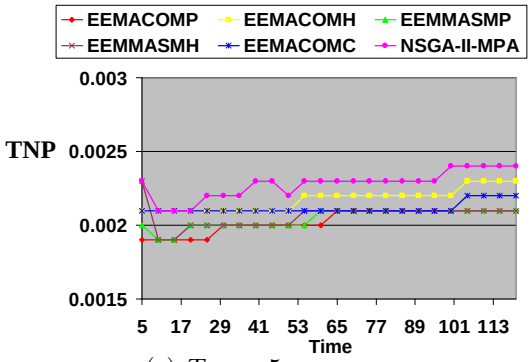

(e) $T_{sm} = 5$

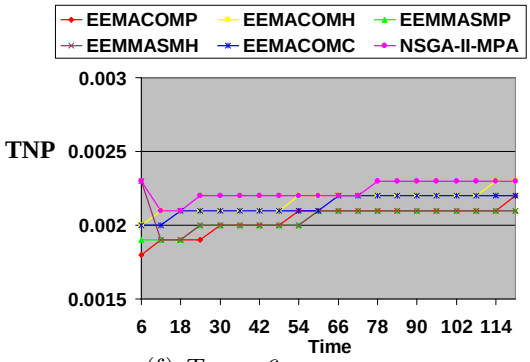

(f) $T_{sm} = 6$

Figure 7.63: Utilisation of the most heavily used link, TNP, criterion over time

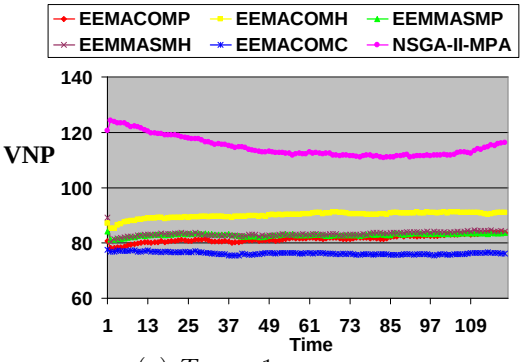

(a) $T_{sm} = 1$

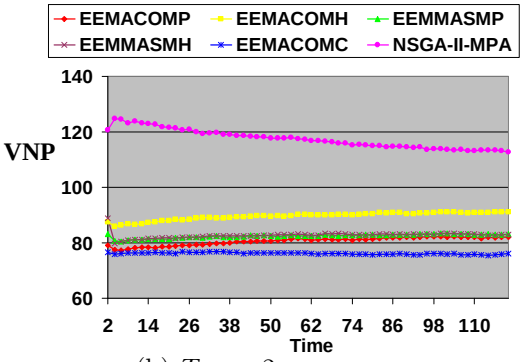

(b) $T_{sm} = 2$

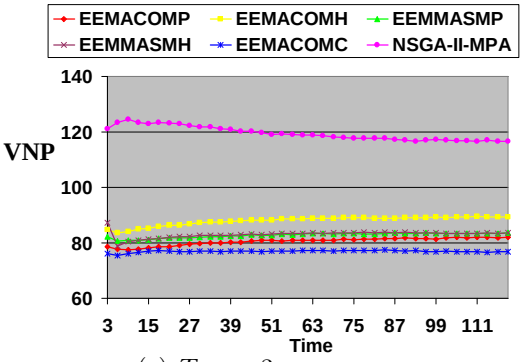

(c) $T_{sm} = 3$

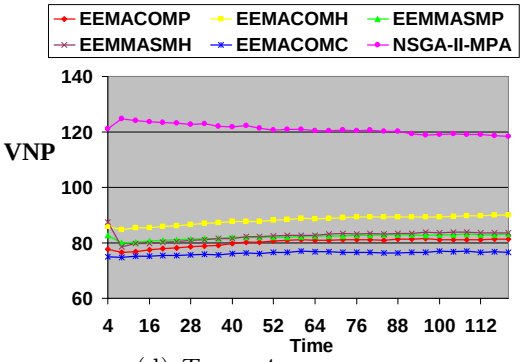

(d) $T_{sm} = 4$

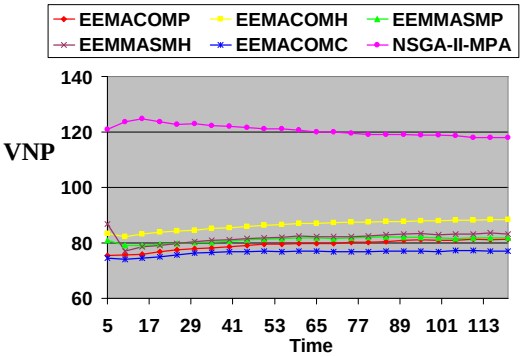

(e) $T_{sm} = 5$

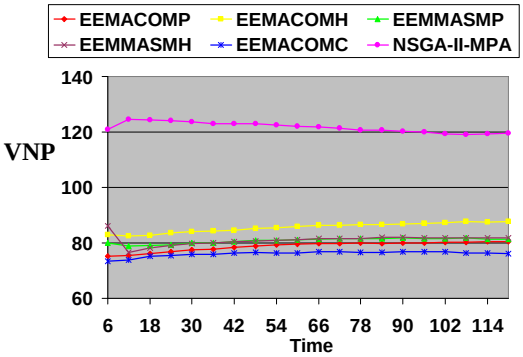

(f) $T_{sm} = 6$

Figure 7.64: Variance in node power levels, VNP, criterion over time

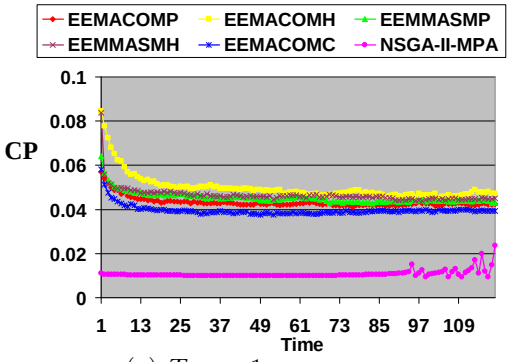

(a) $T_{sm} = 1$

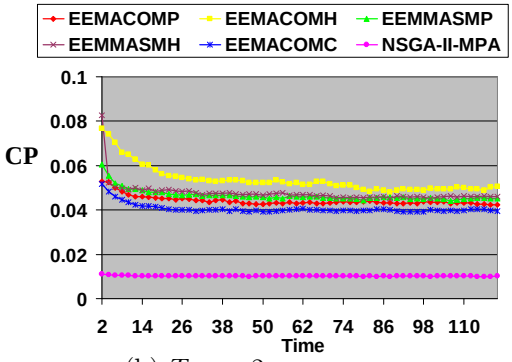

(b) $T_{sm} = 2$

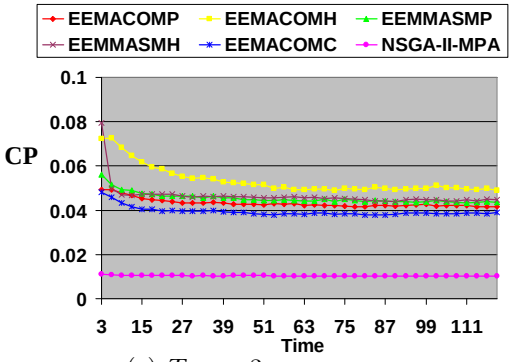

(c) $T_{sm} = 3$

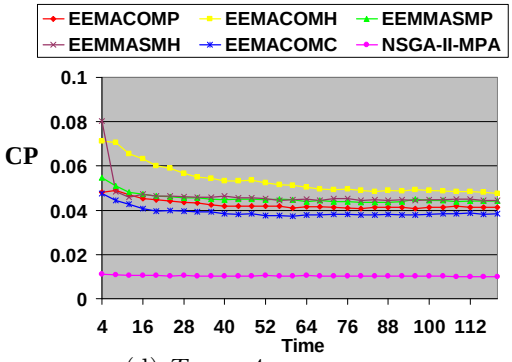

(d) $T_{sm} = 4$

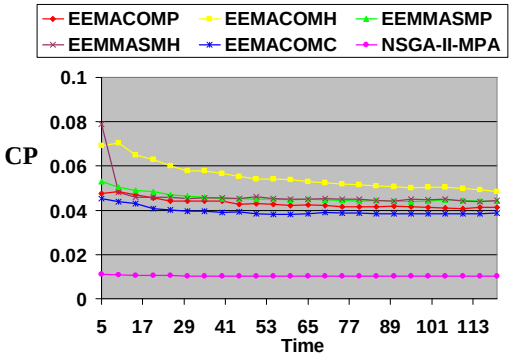

(e) $T_{sm} = 5$

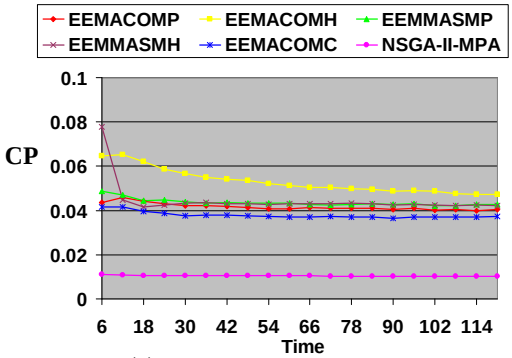

(f) $T_{sm} = 6$

Figure 7.65: Cost per packet, CP, criterion over time

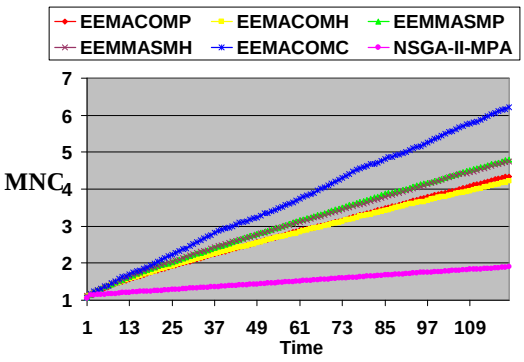

(a) $T_{sm} = 1$

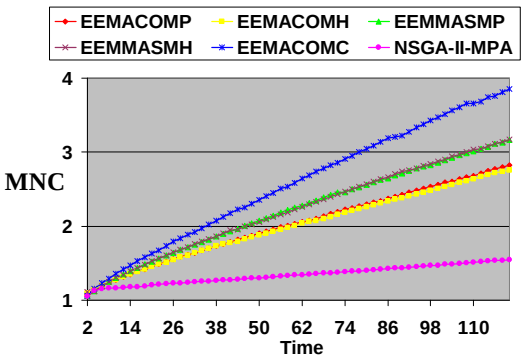

(b) $T_{sm} = 2$

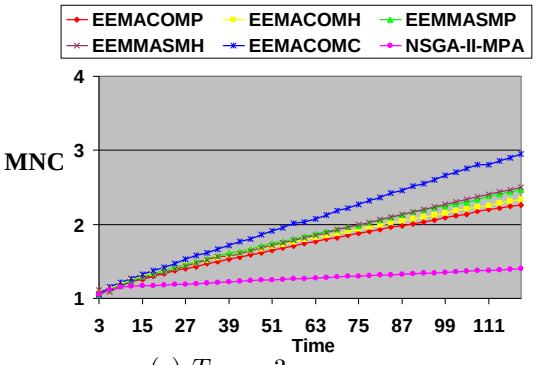

(c) $T_{sm} = 3$

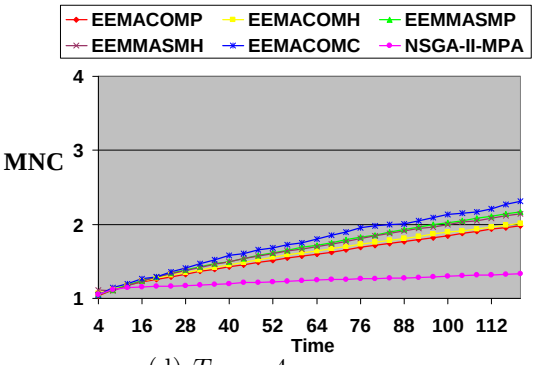

(d) $T_{sm} = 4$

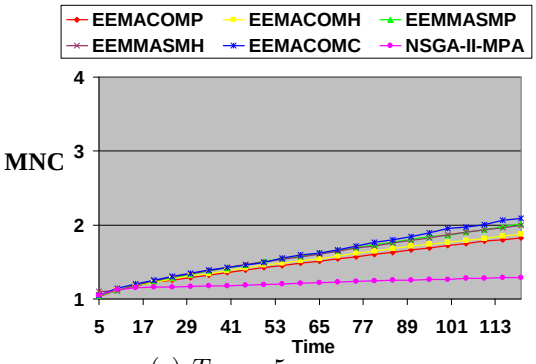

(e) $T_{sm} = 5$

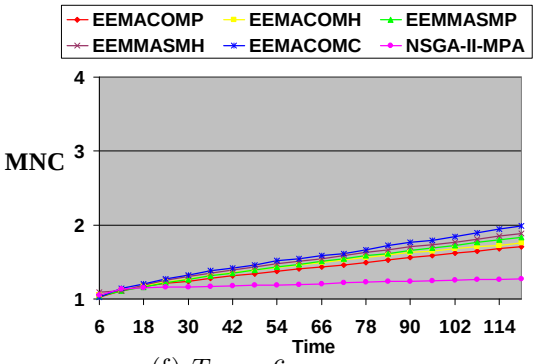

(f) $T_{sm} = 6$

Figure 7.66: Maximum node cost, MNC, criterion over time

ranked accordingly. Table 7.30 gives the average rank of the algorithms over all the scenarios, together with the standard deviation.

Tables 7.24-7.29 indicate that EEMACOMP ranked overall in first place for 88% of the scenarios with $N_G > 30$. For scenarios with $N_G = 30$, EEMACOMP ranked overall in first place for 44% of the scenarios (refer to Tables 7.21-7.23). EEMACOMH is ranked overall last for 87% of the scenarios. The NSGA-II-MPA algorithm had a better $\bar{\xi}$ than the other algorithms for almost all environment changes for scenarios with $N_G = 300$ and $R_g \in \{500, 800\}$ (refer to Tables 7.28-7.29).

Table 7.30 indicates that the EEMACOMP algorithm had on average the best rank over all the scenarios, while the EEMACOMH algorithm had on average the worst rank over all the scenarios.

Table 7.21: Ranks for scenarios with $N_G = 30$, $R_g = 300$

	T_{sm}																							
	1				2				3				4				5				6			
$\mathcal{PF}$	n^w_{alg}	ϱ^w	ξ^w	rank	n^w_{alg}	ϱ^w	ξ^w	rank	n^w_{alg}	ϱ^w	ξ^w	rank	n^w_{alg}	ϱ^w	ξ^w	rank	n^w_{alg}	ϱ^w	ξ^w	rank	n^w_{alg}	ϱ^w	ξ^w	rank
$\mathcal{P}_{EEMACOMP}$	0	3	0	4	0	0	0	5	0	0	0	4	0	0	0	4	0	0	0	4	0	0	0	4
$\mathcal{P}_{EEMACOMH}$	0	0	0	5	0	0	0	5	0	0	0	4	0	0	0	4	0	0	0	4	0	0	0	4
$\mathcal{P}_{EEMMASMP}$	5	0	0	3	1	0	0	3	0	0	0	4	0	1	0	3	0	0	0	4	0	0	0	4
$\mathcal{P}_{EEMMASMH}$	0	0	0	5	0	1	0	3	0	1	0	3	0	0	0	4	0	1	0	3	0	1	0	3
$\mathcal{P}_{EEMACOMC}$	10	0	120	1	0	0	60	1	0	0	40	1	0	0	30	1	0	0	24	1	0	1	20	1
$\mathcal{P}_{NSGA-II-MPA}$	0	117	0	2	0	59	0	2	0	39	0	2	0	29	0	2	0	23	0	2	0	18	0	2

Table 7.22: Ranks for scenarios with $N_G = 30$, $R_g = 500$

	T_{sm}																							
	1				2				3				4				5				6			
$\mathcal{PF}$	n^w_{alg}	ϱ^w	ξ^w	rank	n^w_{alg}	ϱ^w	ξ^w	rank	n^w_{alg}	ϱ^w	ξ^w	rank	n^w_{alg}	ϱ^w	ξ^w	rank	n^w_{alg}	ϱ^w	ξ^w	rank	n^w_{alg}	ϱ^w	ξ^w	rank
$\mathcal{P}_{EEMACOMP}$	5	54	9	1	0	31	13	1	0	29	6	1	0	28	0	2	0	18	0	2	0	14	0	2
$\mathcal{P}_{EEMACOMH}$	0	6	4	5	1	7	0	5	0	1	0	5	0	1	0	3	0	0	0	5	0	0	0	3
$\mathcal{P}_{EEMMASMP}$	4	43	20	2	0	9	4	4	0	6	0	3	0	3	0	3	0	3	0	3	0	0	0	3
$\mathcal{P}_{EEMMASMH}$	2	16	35	4	1	13	10	3	0	4	0	4	0	0	0	5	0	1	0	4	0	0	0	3
$\mathcal{P}_{EEMACOMC}$	1	1	52	3	0	0	33	2	0	0	34	2	0	0	30	1	0	2	24	1	0	6	20	1
$\mathcal{P}_{NSGA-II-MPA}$	0	0	0	6	0	0	0	6	0	0	0	6	0	0	0	5	0	0	0	5	0	0	0	3

Table 7.23: Ranks for scenarios with $N_G = 30$, $R_g = 800$

	T_{sm}																							
	1				2				3				4				5				6			
$\mathcal{PF}$	n^w_{alg}	ϱ^w	ξ^w	rank	n^w_{alg}	ϱ^w	ξ^w	rank	n^w_{alg}	ϱ^w	ξ^w	rank	n^w_{alg}	ϱ^w	ξ^w	rank	n^w_{alg}	ϱ^w	ξ^w	rank	n^w_{alg}	ϱ^w	ξ^w	rank
$\mathcal{P}_{EEMACOMP}$	6	28	23	4	11	43	31	1	4	13	39	1	6	20	29	1	4	14	17	1	3	11	20	1
$\mathcal{P}_{EEMACOMH}$	0	0	0	6	0	0	0	6	0	0	0	5	0	0	0	5	0	0	0	5	0	0	0	5
$\mathcal{P}_{EEMMASMP}$	21	50	19	2	0	9	1	4	5	8	1	3	4	6	1	3	3	2	2	4	2	3	0	3
$\mathcal{P}_{EEMMASMH}$	9	42	56	1	0	8	24	3	5	19	0	2	4	4	0	4	1	8	3	2	5	6	0	2
$\mathcal{P}_{EEMACOMC}$	73	0	0	3	49	0	0	2	14	0	0	3	13	0	0	2	8	0	2	3	5	0	0	3
$\mathcal{P}_{NSGA-II-MPA}$	0	0	22	5	0	0	4	5	0	0	0	5	0	0	0	5	0	0	0	5	0	0	0	5

Table 7.24: Ranks for scenarios with $N_G = 100$, $R_g = 300$

	T_{sm}																							
	1				2				3				4				5				6			
$\mathcal{PF}$	n^w_{alg}	ϱ^w	ξ^w	rank	n^w_{alg}	ϱ^w	ξ^w	rank	n^w_{alg}	ϱ^w	ξ^w	rank	n^w_{alg}	ϱ^w	ξ^w	rank	n^w_{alg}	ϱ^w	ξ^w	rank	n^w_{alg}	ϱ^w	ξ^w	rank
$\mathcal{P}_{\mathcal{EEMACOMP}}$	118	114	32	1	47	59	39	1	8	39	40	1	12	27	29	1	2	24	23	1	3	20	20	1
$\mathcal{P}_{\mathcal{EEMACOMH}}$	0	0	0	6	0	0	0	6	0	0	0	5	0	0	0	5	0	0	0	4	0	0	0	3
$\mathcal{P}_{\mathcal{EEMMASMP}}$	0	1	0	5	2	0	0	3	2	0	0	4	3	0	0	3	0	0	0	4	0	0	0	3
$\mathcal{P}_{\mathcal{EEMMASMH}}$	2	1	1	4	1	0	1	3	5	0	0	2	2	0	1	2	1	0	0	3	0	0	0	3
$\mathcal{P}_{\mathcal{EEMACOMC}}$	0	4	1	3	0	1	0	5	2	1	0	3	0	3	0	3	0	0	1	2	0	0	0	3
$\mathcal{P}_{\mathcal{NSGA-II-MPA}}$	0	0	86	2	0	0	20	2	0	0	0	5	0	0	0	5	0	0	0	4	0	0	0	2

Table 7.25: Ranks for scenarios with $N_G = 100$, $R_g = 500$

	T_{sm}																							
	1				2				3				4				5				6			
$\mathcal{PF}$	n^w_{alg}	ϱ^w	ξ^w	rank	n^w_{alg}	ϱ^w	ξ^w	rank	n^w_{alg}	ϱ^w	ξ^w	rank	n^w_{alg}	ϱ^w	ξ^w	rank	n^w_{alg}	ϱ^w	ξ^w	rank	n^w_{alg}	ϱ^w	ξ^w	rank
$\mathcal{P}_{\mathcal{EEMACOMP}}$	56	119	70	1	34	59	52	1	36	38	39	1	9	30	29	1	4	24	23	1	6	20	20	1
$\mathcal{P}_{\mathcal{EEMACOMH}}$	0	0	0	5	0	0	0	5	0	0	0	5	0	0	0	4	0	0	0	4	0	0	0	4
$\mathcal{P}_{\mathcal{EEMMASMP}}$	61	0	2	2	13	0	2	2	3	0	0	3	6	0	0	2	5	0	0	3	1	0	0	3
$\mathcal{P}_{\mathcal{EEMMASMH}}$	2	1	1	4	6	1	1	3	1	1	1	2	3	0	1	3	6	0	1	2	4	0	0	2
$\mathcal{P}_{\mathcal{EEMACOMC}}$	0	0	0	5	0	0	5	4	0	0	0	5	0	0	0	4	0	0	0	4	0	0	0	4
$\mathcal{P}_{\mathcal{NSGA-II-MPA}}$	0	0	47	3	0	0	0	5	0	1	0	4	0	0	0	4	0	0	0	4	0	0	0	4

Table 7.26: Ranks for scenarios with $N_G = 100$, $R_g = 800$

	T_{sm}																							
	1				2				3				4				5				6			
$\mathcal{PF}$	n^w_{alg}	ϱ^w	ξ^w	rank	n^w_{alg}	ϱ^w	ξ^w	rank	n^w_{alg}	ϱ^w	ξ^w	rank	n^w_{alg}	ϱ^w	ξ^w	rank	n^w_{alg}	ϱ^w	ξ^w	rank	n^w_{alg}	ϱ^w	ξ^w	rank
$\mathcal{P}_{\mathcal{EEMACOMP}}$	63	0	4	3	57	9	0	1	40	8	0	1	30	12	0	1	23	16	0	1	19	13	0	1
$\mathcal{P}_{\mathcal{EEMACOMH}}$	0	0	0	4	0	0	0	4	0	0	0	4	0	0	0	4	0	0	0	5	0	0	0	5
$\mathcal{P}_{\mathcal{EEMMASMP}}$	0	0	0	4	0	0	0	4	0	0	0	4	0	0	0	4	0	0	0	5	0	0	0	5
$\mathcal{P}_{\mathcal{EEMMASMH}}$	0	0	0	4	0	0	0	4	0	0	0	4	0	0	0	4	1	1	0	4	1	2	0	4
$\mathcal{P}_{\mathcal{EEMACOMC}}$	55	0	67	2	1	0	60	2	0	0	40	2	0	0	30	2	0	0	24	2	0	0	20	2
$\mathcal{P}_{\mathcal{NSGA-II-MPA}}$	2	120	49	1	2	51	0	3	0	32	0	3	0	18	0	3	0	7	0	3	0	5	0	3

Table 7.27: Ranks for scenarios with $N_G = 300$, $R_g = 300$

	T_{sm}																							
	1				2				3				4				5				6			
$\mathcal{PF}$	n^w_{alg}	ϱ^w	ξ^w	rank	n^w_{alg}	ϱ^w	ξ^w	rank	n^w_{alg}	ϱ^w	ξ^w	rank	n^w_{alg}	ϱ^w	ξ^w	rank	n^w_{alg}	ϱ^w	ξ^w	rank	n^w_{alg}	ϱ^w	ξ^w	rank
$\mathcal{P}_{\mathcal{EEMACOMP}}$	118	114	0	1	60	57	0	1	39	39	0	1	29	27	0	1	24	23	0	1	15	18	0	1
$\mathcal{P}_{\mathcal{EEMACOMH}}$	0	0	0	6	0	0	0	5	0	0	0	5	0	0	0	5	0	0	0	4	0	0	0	6
$\mathcal{P}_{\mathcal{EEMMASMP}}$	0	3	0	3	0	0	0	5	0	0	0	5	0	2	0	3	0	0	0	4	2	0	0	4
$\mathcal{P}_{\mathcal{EEMMASMH}}$	1	0	0	5	0	2	0	3	1	0	0	3	0	2	0	3	0	0	0	4	2	1	0	3
$\mathcal{P}_{\mathcal{EEMACOMC}}$	0	1	120	2	0	0	60	2	0	0	40	2	0	0	30	2	0	0	24	2	0	0	20	2
$\mathcal{P}_{\mathcal{NSGA-II-MPA}}$	1	2	0	3	0	1	0	4	0	1	0	3	0	0	0	5	0	1	0	3	0	1	0	5

Table 7.28: Ranks for scenarios with $N_G = 300$, $R_g = 500$

	T_{sm}																							
	1				2				3				4				5				6			
$\mathcal{PF}$	n^w_{alg}	ϱ^w	ξ^w	rank	n^w_{alg}	ϱ^w	ξ^w	rank	n^w_{alg}	ϱ^w	ξ^w	rank	n^w_{alg}	ϱ^w	ξ^w	rank	n^w_{alg}	ϱ^w	ξ^w	rank	n^w_{alg}	ϱ^w	ξ^w	rank
$\mathcal{P}_{\mathcal{EEMACOMP}}$	119	118	0	1	59	58	0	1	39	39	0	1	29	29	0	1	23	23	0	1	19	19	0	1
$\mathcal{P}_{\mathcal{EEMACOMH}}$	0	0	0	5	0	0	0	5	0	0	0	4	0	0	0	4	0	0	0	4	0	0	0	4
$\mathcal{P}_{\mathcal{EEMMASMP}}$	0	1	0	4	0	1	0	4	0	0	0	4	0	0	0	4	0	0	0	4	0	0	0	4
$\mathcal{P}_{\mathcal{EEMMASMH}}$	1	1	0	3	1	1	0	3	1	1	0	3	1	1	0	3	1	1	0	3	1	1	0	3
$\mathcal{P}_{\mathcal{EEMACOMC}}$	0	0	0	5	0	0	0	5	0	0	0	4	0	0	0	4	0	0	0	4	0	0	0	4
$\mathcal{P}_{\mathcal{NSGA-II-MPA}}$	0	0	120	2	0	0	60	2	0	0	40	2	0	0	30	2	0	0	24	2	0	0	20	2

Table 7.29: Ranks for scenarios with $N_G = 300$, $R_g = 800$

	T_{sm}																							
	1				2				3				4				5				6			
$\mathcal{PF}$	n^w_{alg}	ϱ^w	ξ^w	rank	n^w_{alg}	ϱ^w	ξ^w	rank	n^w_{alg}	ϱ^w	ξ^w	rank	n^w_{alg}	ϱ^w	ξ^w	rank	n^w_{alg}	ϱ^w	ξ^w	rank	n^w_{alg}	ϱ^w	ξ^w	rank
$\mathcal{P}_{\mathcal{EEMACOMP}}$	0	5	0	2	2	3	0	2	35	18	0	2	28	18	0	1	21	17	0	1	18	17	0	1
$\mathcal{P}_{\mathcal{EEMACOMH}}$	0	0	0	4	0	0	0	4	0	0	0	5	0	0	0	4	0	0	0	4	0	0	0	6
$\mathcal{P}_{\mathcal{EEMMASMP}}$	0	0	0	4	0	1	0	3	1	7	0	3	1	1	0	3	2	4	0	3	0	2	0	3
$\mathcal{P}_{\mathcal{EEMMASMH}}$	0	2	0	3	0	0	0	4	1	0	0	4	0	0	0	4	0	0	0	4	1	1	0	3
$\mathcal{P}_{\mathcal{EEMACOMC}}$	0	0	0	4	0	0	0	4	0	0	0	5	0	0	0	4	0	0	0	4	1	0	0	5
$\mathcal{P}_{\mathcal{NSGA-II-MPA}}$	120	113	120	1	58	56	60	1	30	15	40	1	1	11	30	2	1	3	24	2	0	0	20	2

Table 7.30: Average rank of all algorithms with respect to all performances measures

$\mathcal{PF}$	rank
$\mathcal{P}_{\mathcal{EEMACOMP}}$	1.555 ± 1.040
$\mathcal{P}_{\mathcal{EEMACOMC}}$	2.833 ± 1.313
$\mathcal{P}_{\mathcal{EEMMASMH}}$	3.259 ± 0.850
$\mathcal{P}_{\mathcal{EEMMASMP}}$	3.481 ± 0.794
$\mathcal{P}_{\mathcal{NSGA-II-MPA}}$	3.259 ± 1.494
$\mathcal{P}_{\mathcal{EEMACOMH}}$	4.666 ± 0.824

7.4.8 Computational Complexity of the Algorithms

The runtime complexity of each algorithm can be analysed by investigating the runtime behavior of the sub-routines of the corresponding algorithm. The approximated worst case asymptotic complexity of each algorithm is estimated as follows:

- EEMACOMP algorithm

  The initialisation process has a worst case complexity of $O(c_1 n_o N_G^2)$, while the solution construction process has a worst case complexity of $O(c_2 n_o N_G^2)$. When checking whether to insert a new solution into the $\mathcal{PF}$, EEMACOMP performs a non-dominance check of worst case complexity $O(c_3 n_o P_{as})$. The worst case complexity for the crowding distance used in order to keep a bound on the archive size is $O(c_4 n_o P_{as}^2)$. The EEMACOMP global pheromone update has a worst case complexity of $O(c_5 n_o N_G P_{as})$ and the ApplyMobilityChanges procedure has a worst case complexity of $O(c_6 n_o P_{as} + c_7 n_o N_G^2)$. The pheromone conservation rule has a worst case complexity of $O(c_8 n_o N_G^2)$. The worst case complexity of EEMACOMP is $O(c_9 n_o P_{as} + c_{10} n_o P_{as}^2 + c_{11} n_o N_G P_{as} + c_{12} n_o N_G^2) = O(n_o N_G^2)$ where n_o is the number of objectives, P_{as} is the archive size, N_G is the number of nodes, and $c_1, c_2, ..., c_{12}$ are constants.

- EEMACOMH algorithm

  The EEMACOMH algorithm has a similar worst case complexity as EEMACOMP except for the global pheromone update, which has a worst case complexity of $O(c_5 N_G P_{as})$ and the pheromone conservation rule which has a worst case complexity of $O(c_8 N_G^2)$. The worst case complexity of EEMACOMH is $O(n_o N_G^2)$.

  Comparing EEMACOMP with EEMACOMH, the use of multiple pheromone ma-

trices requires an additional cost of $O(5c_5(n_o-1)N_G P_{as})$ due to the global pheromone update. EEMACOMP also requires an additional cost of $O(c_8(n_o-1)N_G^2)$ due to the pheromone conservation.

- EEMMASMP algorithm

  The EEMMASMP algorithm has a similar worst case complexity as EEMACOMP except for an additional processing for restricting the pheromones by an upper and lower limit in the order of $O(5c_{12}n_oN_G^2)$, where c_{12} is a constant. The worst case complexity of EEMMASMP is $O(n_oN_G^2)$.

- EEMMASMH algorithm

  The EEMMASMH algorithm has a similar worst case complexity as EEMACOMH except for additional processing in the order of $O(13c_{12}N_G^2)$ due to the restriction of the pheromones by an upper and lower limit, where c_{12} is a constant. The worst case complexity of EEMMASMH is $O(n_oN_G^2)$.

- EEMACOMC algorithm

  The EEMACOMC algorithm has a similar worst case complexity as EEMACOMP.

- NSGA-II-MPA has a worst case complexity $O(n_oN_G^2 + N_G\log(N_G) + k\log(k)) = O(n_oN_G^2)$ where $O(N_G\log(N_G) + k\log(k))$ is the worst case complexity of the k-shortest path algorithm.

The NSGA-II-MPA algorithm has the lowest worst case complexity because it does not require pheromone updates, and the complexity of the $k-$shortest path algorithm is less than the pheromone updates used in the ACO algorithms.

EEMMASMP has the highest worst case complexity because of the multi-pheromone processing and the restriction of pheromones by the highest and lowest limits. Also, EEMACOMP has a higher worst case complexity than EEMMASMH because of the multi-pheromone processing which occurs more frequently than the restriction of pheromones by the highest and lowest limits.

A fair ranking of the algorithms in terms of their worst case computational complexity is: NSGA-II-MPA $<$ EEMACOMH $<$ EEMMASMH $<$ EEMACOMC $\leq$ EEMACOMP $<$ EEMMASMP.

7.4.9 Overall Performance of Algorithms

Based on the analysis of the empirical results presented in Subsections 7.4.2-7.4.7, this subsection summarises the performance of the developed algorithms in terms of the $\bar{n}_{alg}$, $\bar{\varrho}$ and $\bar{\xi}$ metrics and the optimisation criteria.

A comparison of each algorithm for each scenario reveals the following conclusions:

- When change frequency, T_{sm}, decreased, all algorithms displayed lower values, and therefore good results for the spacing metric for most scenarios. The solutions are more uniformly distributed in the whole Pareto-optimal set, instead of gathering in a small region.
- When change severity, R_g, increased, the number of non-dominated solutions decreased as well and the value of the $\bar{\varrho}$ metric increased for all algorithms.
- All algorithms displayed a high value for $\bar{\xi}$ irrespective of T_{sm}, R_g, and N_G. High values of $\bar{\xi}$ show closeness of the solutions to the optimal Pareto set, and to some extent, the spread of the solutions across objective space.
- All algorithms displayed a very low value for the $\bar{\varrho}$ metric (below 0.3), showing that they produced uniformly distributed solutions.
- The EEMACOMH algorithm is affected the most when change severity increased to 800, producing a much smaller number of non-dominated solutions and a worst solution spread compared to the rest of the ACO algorithms.
- All ACO algorithms compared to the NSGA-II-MPA algorithm displayed a higher value for $\bar{n}_{alg}$ for 90% of the scenarios.
- A larger number of nodes combined with higher change severity negatively affected the performance of the ACO algorithms in terms of the number of non-dominated solutions and solution spread, even though the value of $\bar{\varrho}$ is still low and under 0.3.
- The EEMACOMP algorithm found the largest number of non-dominated solutions from EEMACOMH for all scenarios with $N_G > 30$ (66.6% of the scenarios). Also, EEMACOMP found the largest number of non-dominated solutions from EEMMASMP, EEMMASMH, and EEMACOMC for all scenarios with $N_G = 100$ and

$R_g = 800$ and scenarios with $N_G = 800$ (44.4% of the scenarios). The EEMACOMP algorithm produced a better solution spread than EEMACOMH for 82% of the scenarios, a better solution spread than EEMMASMP and EEMACOMC for 66% of the scenarios, a better solution spread than EEMMASMH for 77% of the scenarios, and better solution spread than NSGA-II-MPA for 88% of the scenarios.

- For all environment changes, the EEMACOMP algorithm found more non-dominated solutions than all the other algorithms and the NSGA-II-MPA found the least number of non-dominated solutions (refer to Figure 7.43).
- For all environment changes, the EEMACOMP algorithm had the best solution spread and the NSGA-II-MPA had the worst solution spread (refer to Figure 7.44).
- For all algorithms, there is a very small variation at each environment change in the values of the $\bar{n}_{alg}$, $\bar{\varrho}$, and $\bar{\xi}$ metrics, and the values of the EP, TNP, CP, and VNP objectives. This shows the robustness and adaptability of all the algorithms to the environment changes.
- The NSGA-II-MPA approach had a lower energy consumed per packet than all the ACO approaches and for all the scenarios.
- All ACO approaches are better than the NSGA-II-MPA approach with reference to the utilisation of the most heavily used link, TNP, objective for $N_G = 300$.
- The EEMACOMP, EEMMASMP, EEMMASMH, and EEMACOMC approaches are better than the NSGA-II-MPA approach with reference to the variance in node power levels, VNP, objective for all scenarios. The EEMACOMH approach is better than the NSGA-II-MPA approach with reference to the VNP objective for all scenarios except for scenarios with $R_g = 800$ and $N_G \in \{100, 300\}$.
- The NSGA-II-MPA approach had a lower cost per packet, CP, than all ACO approaches for all scenarios.
- The NSGA-II-MPA approach had a lower maximum node cost, MNC, than all ACO approaches for all scenarios except for scenarios with $N_G = 300$ and $R_g = 800$.

- EEMACOMP had the highest rank with reference to the performance criteria for most scenarios, and the highest average rank over all scenarios and performance criteria.
- EEMACOMH had the lowest average rank over all scenarios and performance criteria.
- If all objectives have the same importance it is recommended to use the EEMACOMP, EEMMASMP, EEMMASMH, or EEMACOMC ACO algorithms (especially the EEMACOMP), which provide more closeness to the true Pareto front and maintain better distribution of solutions in the Pareto front. If any of the EP, CP, or MNC objectives have a higher priority than the other objectives, it is recommended to use the NSGA-II-MPA algorithm.

7.5 Summary

This chapter presented an empirical study of the performance of the five ant multi-objective optimisation algorithms presented in this thesis and the role played by the various algorithmic features.

The experimental procedures and results of parameter tuning were given.

The five algorithms were compared with one another and with the NSGA-II, which was adapted in this thesis for the multi-objective, power-aware routing problem. Different scenarios were tested for each algorithm according to the values of different ACO and NSGA-II parameters and the Pareto fronts for each algorithm were obtained.

The experimental results showed that the five ACO algorithms, excluding the EEMACOMH algorithm, outperformed, on most scenarios, the NSGA-II-MPA algorithm in terms of the number of solutions and spacing metric. All algorithms produced similar results for the hypervolume metric for most of the scenarios. The NSGA-II-MPA approach had a lower energy consumed per packet, and lower cost per packet than all the ACO approaches and for all the scenarios. Also, the NSGA-II-MPA approach had a lower maximum node cost than all the ACO approaches for most scenarios. All ACO approaches had a lower utilisation of the most heavily used link than the NSGA-II-MPA for $N_G = 300$ and less variance in node power levels for most of the scenarios.

By minimising the five optimisation criteria for the power-aware routing problem,

the proposed ACO algorithms minimised the energy consumed per packet and spread the traffic over the network to make all nodes have similar amounts of consumed energy. Maximum energy consumption has been reduced which means that the lifetime of the first node to die is extended using the ACO approaches. Consequently, MANETS network lifetime was maximised and network partitioning was delayed.

In addition, the results demonstrated that EEMACOMP outperformed the other four ACO algorithms and the NSGA-II-MPA algorithm in terms of the number of solutions and spacing metric in most scenarios and produced the best rank. Therefore, in light of the results presented, the EEMACOMP approach is recommended by this study for the multi-objective, power-aware routing problem.

Chapter 8

Conclusion

8.1 Summary

As a special type of network, mobile ad hoc networks (MANETs) have increasingly been the focus of research in recent years. The network topology in MANETs usually changes with time. Therefore, as a result of the highly dynamic and distributed nature of MANETs, routing protocols are being presented with new challenges since traditional routing protocols may not be suitable for MANETs. In particular, energy efficient routing may be the most important design criterion for MANETs since mobile nodes are powered by batteries with limited capacity.

The main purpose of this thesis was to study ant algorithms as applied to the dynamic environment of mobile ad hoc networks and, specifically, to resolve the five power-aware metrics which were presented by Singh *et al.* [184]. These metrics aim to minimise the energy consumed per packet, maximise the time needed to network partition, minimise the variance in node power levels, minimise cost per packet, and minimise maximum node cost. Taking into consideration a realistic mobility model using an ant colony optimisation (ACO) approach, this thesis proposed to simultaneously optimise the five power-aware metrics for energy efficiency and maximising the lifetime of MANETs. A set of optimal solutions, the Pareto-optimal set, is found using ACO algorithms.

This thesis proposed five algorithms with which to solve the above multi-objective optimisation problem. The first two algorithms are the energy efficiency for mobile networks using multi-objective ant colony optimisation, multi-pheromone (EEMACOMP) algorithm and the energy efficiency for mobile networks using multi-objective ant colony optimisation, multi-heuristic (EEMACOMH) algorithm. These two algorithms are adaptations of multi-objective ant colony optimisation algorithms (MOACO) based on the ant colony system (ACS) algorithm.

The next two algorithms, namely, the energy efficiency for mobile networks using

multi-objective MAX-MIN ant system optimisation, multi-pheromone (EEMMASMP) algorithm and the energy efficiency for mobile networks using multi-objective MAX-MIN ant system optimisation, multi-heuristic (EEMMASMH) algorithm succeeded in solving the above multi-objective optimisation problem by using an adaptation of the MAX-MIN ant system optimisation algorithm.

The last algorithm implemented, namely, the energy efficiency for mobile networks using multi-objective ant colony optimisation, multi-colony (EEMACOMC) uses a multiple colony ACO algorithm.

In addition, this thesis used an adaptation of the NSGA-II algorithm called NSGA-II multi-objective power-aware algorithm (NSGA-II-MPA) to solve the multi-objective power-aware routing problem.

For each algorithm the following hypotheses or questions were investigated:

1. Is there a statistical significant difference in the performance of the algorithms?
2. Does performance deteriorate with increase in change frequency?
3. Does performance deteriorate with increase in change severity?
4. Are the algorithms scalable?
5. Is there an algorithm that is less affected by change frequency / change severity?
6. How is the performance of the algorithms over time?

The performance of each algorithm was tested under different scenarios for different change frequencies, change severities and number of nodes as outlined in Section 7.1.1. For each of the scenarios 30 simulations were executed and results were reported as averages over these simulations. Each estimated pareto front, $\mathcal{PF}$, produced by the EEMACOMP, EEMACOMH, EEMMASMP, EEMMASMH, EEMACOMC, and NSGA-II-MPA algorithms was evaluated using three performance metrics, namely the number of non-dominated solutions, $\bar{n}_{alg}$, the spread metric, $\bar{\varrho}$, and the hypervolume metric, $\bar{\xi}$ (refer to Section 7.1.3).

8.2 Conclusions

On the basis of the experimental results the final conclusions are summarised as follows:

- The EEMACOMP algorithm found a largest number of non-dominated solutions and produced a better solution spread compared to the rest of the algorithms, for high percentage of scenarios.
- All ACO algorithms compared to the NSGA-II-MPA algorithm displayed a higher value for $\bar{n}_{alg}$ for 90% of the scenarios and they produced a better solution spread for high percentage of scenarios.
- Performance for $\bar{n}_{alg}$ and $\bar{\varrho}$ metrics deteriorate with increase in change frequency, for all algorithms.
- Performance for $\bar{n}_{alg}$ and $\bar{\varrho}$ metrics deteriorate with increase in change severity, for all algorithms.
- The EEMACOMH algorithm is affected the most when change severity increased to 800, producing a much smaller number of non-dominated solutions and a worst solution spread compared to the rest of the ACO algorithms.
- A larger number of nodes combined with higher change severity negatively affected the performance of the ACO algorithms in terms of the number of non-dominated solutions and solution spread, even though the value of $\bar{\varrho}$ is still low and under 0.3.
- All the algorithms had a good performance over time. This shows the robustness and adaptability of all the algorithms to the environment changes.
- All algorithms displayed a high value for $\bar{\xi}$ irrespective of T_{sm}, R_g, and N_G. High values of $\bar{\xi}$ show closeness of the solutions to the optimal Pareto set, and to some extent, the spread of the solutions across objective space.
- EEMACOMP had the highest rank with reference to the performance criteria for most scenarios, and the highest average rank over all scenarios and performance criteria.

In summary, based on the simulations it can be concluded that using ant multi-objective optimisation to simultaneously optimise the five power-aware metrics is extremely beneficial because the traffic is spread over the network, thus forcing all nodes to have similar amounts of consumed energy. Maximum energy consumption has been reduced which means that the lifetime of the first node to die is extended using the ACO

approaches. Consequently, MANETS network lifetime was maximised and network partitioning was delayed.

This is the first time the power-aware routing multi-objective optimisation problem has been solved using an ant colony optimisation algorithm. All five algorithms presented in this thesis were shown to outperform the NSGA-II-MPA algorithm in terms of the performance metrics in most scenarios. Also, all the ACO approaches had a lower variance in node power levels and a lower utilisation of the most heavily used link than the NSGA-II-MPA approach. In addition, all ACO algorithms produced a very good solution distribution, high number of non-dominated solutions and dominated a high percentage of the objective space, showing closeness to the true Pareto front.

8.3 Future Work

Specific recommendations to develop and extend this work further and areas of future research include:

- Other mobility models such as the random waypoint mobility model can be studied in order to model different realistic situations of the movements of mobile nodes and study the behaviour of the proposed algorithms. Finally, these different mobility models may be compared in order to demonstrate their effects on the performance of the proposed ant routing algorithms.
- A detailed comparison of the performance of the ant-based algorithms with other meta-heuristics can be conducted.
- The influence of the control parameters on the ant-based algorithms under different number of nodes can be analysed.
- The influence of different weights for the objective parameters, λ_ψ, on the ant-based algorithms can be examined.
- The impact of the Pareto archive size on the performance of the ant-based algorithms can be analysed.
- Other performance metrics such as diversity in the objective space (DOM) proposed by Morrison and De Jong [150], and their application to the evaluation and

comparison of the developed multi-objective optimisation algorithms for the power aware routing problem can be investigated.